



HAL
open science

L'analyse de sensibilité globale sur matériaux composites vibroacoustiques avec la dépendance paramétrique

Wenqi Chai

► **To cite this version:**

Wenqi Chai. L'analyse de sensibilité globale sur matériaux composites vibroacoustiques avec la dépendance paramétrique. Other. Université de Lyon, 2018. English. NNT : 2018LYSEC037 . tel-02108453

HAL Id: tel-02108453

<https://theses.hal.science/tel-02108453>

Submitted on 24 Apr 2019

HAL is a multi-disciplinary open access archive for the deposit and dissemination of scientific research documents, whether they are published or not. The documents may come from teaching and research institutions in France or abroad, or from public or private research centers.

L'archive ouverte pluridisciplinaire **HAL**, est destinée au dépôt et à la diffusion de documents scientifiques de niveau recherche, publiés ou non, émanant des établissements d'enseignement et de recherche français ou étrangers, des laboratoires publics ou privés.

Numéro d'ordre NNT: 2018LYSEC037

Année: 2018

L'UNIVERSITÉ DE LYON
OPÉRÉE AU SEIN DE L'ÉCOLE CENTRALE DE LYON
ÉCOLE DOCTORALE MEGA
Mécanique, Energétique, Génie civil et Acoustique

T H E S I S

Global sensitivity analysis on vibro-acoustic composite materials with parametric dependency

defended on November 30, 2018 by

Wenqi CHAI

to obtain the title of

Doctor of École Centrale de Lyon

Specialty : ACOUSTICS

Jury members:

<i>Reviewers :</i>	Noureddine BOUHADDI	- Professor,	FEMTO-ST
	Alexandre KAWANO	- Professor,	USP
<i>Advisors :</i>	Mohamed ICHCHOU	- Professor,	ECL
	AbdelMalek ZINE	- Associate Professor,	ECL
<i>Examinators :</i>	Hervé RIOU	- Associate Professor,	ENS Cachan
	Marie-Annick GALLAND	- Professor,	ECL
	Oliver BAREILLE	- Associate Professor,	ECL

Ph.D. research project financed by China Scholarship Council.

Acknowledgements

To complete this piece of work, I received help from a lot of people in various ways.

At first, I would like to thank my thesis directors, colleagues and other collaborate researchers for their contribution of time and intelligence into this project, they are: Prof. Mohamed ICHCHOU, Dr. AbdelMalek ZINE; Dr. Olivier BAREILLE, Dr. Jean-Loup CHRISTEN, Dr. Olivier DESSOMBZ, Dr. Christophe DROZ, Dr. FAN Yu, Dr. Pascal FOSSAT, Mr. Nassardine GUENFOUD, Mr. LOU Mingyang, Dr. SUN Xiangkun, Dr. YI Kaijun, Dr. Zakaria ZERGOUNE; Prof. Stéphane DERRODE, Dr. DING Huaxiong, Ms. FU Zehua, Mr. LI Haoyu, Prof. Elisabeth MIRONESCU and Prof. Alexandre SAIDI. After countless discussions and meetings with everyone can we eventually accomplish such a complex task of multi-disciplinary research concerning vibro-acoustics, composite materials, statistics and data-mining.

Together I shall note the names of jury members who attended my thesis defence: Prof. Nouredine BOUHADDI, Prof. Marie-Annick GALLAND, Prof. Alexandre KAWANO and Dr. Hervé RIOU. Thank you for the efforts made during these months that finally get my research topic valorized with no regrets to my four years passed in France.

Secondly, as an international student whose hometown is ten thousand kilometers away from Ecully, I would like to express my gratitude to those who lead me to integrate into my student life in Centrale Lyon: Dr. DING Haohao, Ms. Francoise Leynaud, Dr. HUANG Xingrong, Mr. MURAMOTO Yuta, Ms. SUN Cheng, Dr. WANG Xiaofang and Dr. YANG Yifan. You opened up my window towards the vast land of France and Europe continent and taught me how to live a meaningful during these years.

Finally, I also must mention all my friends met during the coffee break, around the launch table or on the sports ground, especially my dearest classmates since almost ten years, the Ph.D. students from promotion 2009 of Centrale Pékin. Together we passed all the festivals, chinese or french, since we came here, like a family. You guys powered me up and gave me the ultimate courage to walk on the way of scientific research.

Moments with you will never fade out.

Abstract

With rapid development of mathematical models and simulation tools, the need of uncertainty quantification process has grown higher than ever before. Parametric uncertainties and overall decision stacks are nowadays the two main barriers in solving large scale systematic problem.

Global Sensitivity Analysis (GSA) is one reliable solution for uncertainty quantification which is capable to assess the uncertainty of model output on its inputs'. Among several GSA algorithms, Fourier Amplitude Sensitivity Test (FAST) is one of the most popular choices of researchers. Based on ANOVA-HDMR (ANalysis Of VAriance - High Dimensional Model Representation), it is both mathematically solid and computationally efficient.

One unfortunate fact is that the uniqueness of ANOVA-HDMR relies on the independency of input variables. It makes FAST unable to treat many industrial cases especially for those with only datasets but not distribution functions to be found. To answer the needs, two extended FAST methods with correlation design are proposed and further studied in this research. Among them FAST-c is distribution-based and FAST-orig is data-based.

As a frame of validation and application, a number of vibroacoustic problems are dealt with in this research. Vibroacoustic materials with substructures, are perfect test candidates for FAST-c and FAST-orig. Two application cases are presented in the first part of this thesis, following the literature review. The models chosen here are poroelastic material and sandwich composite structures, both having their mechanical properties hugely influenced by their microscopic and mesoscopic geometric parameters. Getting the original FAST method compared to the two with correlation design, many different features on materials' vibroacoustic performance are latter discovered.

Having got an answer for GSA on models with dependent variables, the second part of this thesis contains more extended researches related to FAST. It is taken into comparison with Random Forest, a well-known data-mining algorithm. The potential error of both algorithms are analyzed and the possibility of joint application is discussed. In the following chapters, more applications of FAST-series methods are reported. They are applied under various conditions where another improved version named FAST-pe is developed to treat a model of periodic structures with correlation among each units. Upon these FAST application cases, the design of preliminary process and the sampling strategies is the core part to be introduced.

Keywords: Global Sensitivity Analysis (GSA), Fourier Amplitude Sensitivity Test (FAST), vibro-acoustic materials, correlation and dependency

Résumé

Avec le développement rapide des modèles mathématiques et des outils de simulation, le besoin des processus de quantification des incertitudes a été bien augmenté. L'incertitude paramétrique et la grande quantité de décisions sont aujourd'hui les deux principales barrières dans la résolution des grands problèmes systématiques.

Capable de proportionner l'incertitude de la sortie sur celle des entrées, l'Analyse de Sensibilité Globale (GSA) est une solution fiable pour la quantification de l'incertitude. Parmi plusieurs algorithmes de GSA, l'Analyse de Sensibilité Globale par Amplitude de Fourier (FAST) est l'un des choix les plus populaires des chercheurs. Basé sur l'ANOVA-HDMR (ANalysis Of VAriance - High Dimensional Model Representation), il est solide en mathématique et efficace en calcul.

Malheureusement, la décomposition unique d'ANOVA-HDMR se dépend de l'indépendance des entrées. À cause de cela, il y a pas mal de cas industriels qui ne peuvent pas être traités par FAST, particulièrement pour ceux qui donnent uniquement des échantillons mais sans lois de distribution. Sous cette demande, deux méthodes extensives de FAST avec un design de corrélation sont proposées et étudiées dans la recherche. Parmi les deux méthodes, FAST-c s'est basé sur les distributions et FAST-orig s'est basé sur les échantillons.

Comme applications et validations, multiples problèmes vibroacoustiques se sont traités dans la recherche. Les matériaux acoustiques avec des sous-structures, sont des candidats parfaits pour tester FAST-c et FAST-orig. Deux applications sont présentées dans la première partie de la thèse, après l'état de l'art. Les modèles choisis sont un matériau poroélastique et des structures sandwich composite, dont les propriétés mécaniques sont toutes fortement influencées par les paramètres géométriques microscopiques ou mésoscopiques. D'avoir la méthode de FAST originale comparée avec les deux nouvelles, on trouve bien plus d'information sur la performance vibroacoustique de ces matériaux.

Déjà répondu à la demande de GSA sur les modèles avec les variables dépendantes, la deuxième partie de la thèse contient plus de recherches liées avec FAST. D'abord FAST est pris en comparaison avec Random Forest, un algorithme bien connu de data-mining. Leurs erreurs potentielles et la possibilité de fonctionner ensemble sont discutées. Et dans les chapitres suivants, plus d'applications de FAST sont présentées. Les méthodes sont appliquées sous plusieurs différentes conditions. Un modèle de structure périodique qui contient des corrélations parmi les unités nous a en plus forcé à développer une nouvelle FAST-pe méthode. Dans ces applications, les designs des processus préliminaires et les stratégies d'échantillonnage sont des éléments à présenter.

Mots-clés: Analyse de Sensibilité Globale (GSA), Fourier Amplitude Sensitivity Test (FAST), matériaux vibroacoustiques, corrélation et dépendance

Contents

General introduction	xix
Industrial Background	xix
Research Methodology	xx
Thesis Contribution	xxi
Thesis Outline	xxi
I Sensitivity Analysis on acoustic materials with correlation design	1
Part 1: Introduction	3
1 Literature Review	5
1.1 Global Sensitivity Analysis (GSA)	5
1.2 ANOVA	6
1.2.1 FAST	8
1.3 Correlation among variables	9
1.4 Algorithms compatible with correlated samples	10
1.4.1 Correlation Ratio Method (CRM)	10
1.5 Vibro-acoustic composite materials	10
2 GSA on porous elastic materials	13
2.1 Chapter introduction	13
2.2 JCA model	14
2.3 Micro-Macro model	15
2.4 FASTC	17
2.5 Identification of inputs' marginal distribution and of their correlation	18
2.5.1 3-parameter (3-p) micro-macro model	18
2.5.2 2-parameter (2-p) micro-macro model	19
2.6 Results comparison and discussion	20
2.6.1 Comparison of SA results with 3-parameter micro-macro model	20
2.6.2 Comparison of SA results with 2-parameter micro-macro model	23
2.7 Chapter conclusion	25
3 GSA on sandwich composite materials	29
3.1 Chapter introduction	29
3.2 Acoustic characteristics of sandwich panels	31
3.2.1 Mead's model	32
3.2.2 Renji's model	33
3.2.3 Coincidence frequency	33

3.2.4	Transition frequency	33
3.3	Homogenization of Meso-structures	34
3.3.1	Gibson-Ashby honeycomb structure and its extension	35
3.3.2	Gibson-Malek honeycomb structure and its deformation	36
3.4	Correlation and dependency discussion	37
3.5	FAST-orig	38
3.6	Identification of inputs' marginal distribution and of their correlation	40
3.6.1	Variables overview	40
3.6.2	Correlated variables	41
3.7	Results comparison and discussion	44
3.7.1	SA results on Mead's model	45
3.7.2	SA results on Renji's model	47
3.7.3	SA results on structures' transition frequencies	47
3.8	Chapter conclusion	48
Part 1: Conclusions		55
II Extended applications of GSA methods		57
Part 2: Introduction		59
4	When Global Sensitivity Analysis meets Random Forest	61
4.1	Chapter introduction	61
4.2	Special properties of Random Forest	63
4.2.1	Classification And Regression Trees	63
4.2.2	Out-Of-Bag validation and its variable importance selection	64
4.3	Experimental design	65
4.3.1	Acoustic transmission loss of sandwich panels	65
4.3.2	Choice between analytical models	65
4.4	Results comparison and discussion	66
4.4.1	Analytical model dataset	67
4.4.2	WFE model dataset	68
4.4.3	Discussion	69
4.5	Chapter conclusion	69
5	Extended FAST method for GSA on 1D-structural damper arrays	73
5.1	Chapter introduction	73
5.2	FAST-pe: multi-sampling curves design and parametric configurations	74
5.2.1	Basic structure of FAST-pe	74
5.2.2	Configurations of the raw algorithm	75
5.3	The occur of random characteristic frequency movement and its essentials	77
5.4	Studies into the problem	78
5.5	Chapter conclusion	81

6	Individual research case and representative FAST applications	83
6.1	Chapter introduction	83
6.2	Correction of biased RF estimations	84
6.2.1	Correction and comparison	85
6.2.2	Discussion	87
6.3	FAST sampling strategies in various research cases	88
6.3.1	Case 1: SA on multi-layer honeycomb structure optimization process	89
6.3.2	Case 2: SA on tilting pad journal bearing performance	92
6.4	Chapter conclusion	94
Part 2: Conclusions		97
Conclusions and perspectives		99
Publications during the thesis		103
A	Appendix A: Details of FAST post-proceeding based on FFT	105
B	Appendix B: Dataset reordering procedure for correlation design in FAST-pe algorithm	107
Bibliography		111

List of Figures

1	Identification and division of post normal science based on system uncertainties and decision stakes [Funtowicz 1990]	xix
1.1	Curse of dimensionality: a comparison of 3D and 2D spheres [Saltelli 2008]	6
1.2	Historical trend of publications concerning sensitivity analysis [Ferretti 2016]	6
1.3	Diagram presenting the basic mechanism of FAST [Cukier 1973]	8
2.1	2-parameter (a) and 3-parameter (b) micro-macro model	16
2.2	Marginal distribution of variables generated by 3-parameter micro-macro model and our approximation: (a): ϕ , (b): σ , (c): α_∞ , (d): Λ , (e): Λ'	18
2.3	Marginal distribution of variables generated by 2-parameter micro-macro model and our approximation: (a): ϕ , (b): σ , (c): α_∞ , (d): Λ , (e): Λ'	19
2.4	Statistics of the output set for JCA model with correlated inputs (3-parameter micro-macro model): (a): mean value \pm standard deviation; (b): normalized standard deviation. Thickness of material: 25mm	21
2.5	SA results for JCA model with correlated inputs (3-parameter micro-macro model) by different methods: FASTC, CRM with correlation design and original FAST, thickness of material: 25mm. (a): $SI(\phi)$, (b): $SI(\sigma)$, (c): $SA(\alpha_\infty)$, (d): $SI(\Lambda)$, (e): $SI(\Lambda')$	22
2.6	Statistics of the output set for JCA model with correlated inputs (3-parameter micro-macro model): (a): mean value \pm standard deviation; (b): normalized standard deviation. Thickness of material: 47mm	22
2.7	SA results for JCA model with correlated inputs (3-parameter micro-macro model) by different methods: FASTC, CRM with correlation design and original FAST, thickness of material: 47mm. (a): $SI(\phi)$, (b): $SI(\sigma)$, (c): $SA(\alpha_\infty)$, (d): $SI(\Lambda)$, (e): $SI(\Lambda')$	23
2.8	Statistics of the output set for JCA model with correlated inputs (2-parameter micro-macro model): (a): mean value and mean value \pm standard deviation; (b): normalized standard deviation. Thickness of material: 25mm	24
2.9	SA results for JCA model with correlated inputs (2-parameter micro-macro model) by different methods: FASTC, CRM with correlation design and original FAST, thickness of material: 25mm. (a): $SI(\phi)$, (b): $SI(\sigma)$, (c): $SA(\alpha_\infty)$, (d): $SI(\Lambda)$, (e): $SI(\Lambda')$	25

2.10	Statistics of the output set for JCA model with correlated inputs (2-parameter micro-macro model): (a): mean value and mean value \pm standard deviation; (b): normalized standard deviation. Thickness of material: 47mm	26
2.11	SA results for JCA model with correlated inputs (2-parameter micro-macro model) by different methods: FASTC, CRM with correlation design and original FAST, thickness of material: 47mm. (a): $SI(\phi)$, (b): $SI(\sigma)$, (c): $SA(\alpha_\infty)$, (d): $SI(\Lambda)$, (e): $SI(\Lambda')$	27
3.1	Geometric illustration for incident wave towards the face-plate	31
3.2	Meso-structure for the honeycomb sandwich panel with double vertical thickness	34
3.3	Meso-structures of different shapes: (a): double vertical thickness honeycomb, (b): triangle, (c): double vertical thickness rectangle and (d): rhombus	35
3.4	Original co-distribution of the 5 variables generated by 2-parameter micro-macro model	38
3.5	Co-distribution of the 5 variables generated by Iman's transform based on the original correlation matrix of 2-parameter micro-macro model	39
3.6	Marginal distribution of variables generated by Gibson-Ashby double vertical thickness hexagon model (yellow bars) and its mathematical approximation (magenta line)	41
3.7	Marginal distribution of variables generated by extended Gibson-Ashby triangle model (yellow bars) and its mathematical approximation (magenta line)	42
3.8	Marginal distribution of variables generated by Gibson-Malek double vertical thickness hexagon model (yellow bars) and its mathematical approximation (magenta line)	42
3.9	Marginal distribution of variables generated by deformed Gibson-Malek double vertical thickness rectangle model (yellow bars) and its mathematical approximation (magenta line)	43
3.10	Marginal distribution of variables generated by deformed Gibson-Malek rhombus model (yellow bars) and its mathematical approximation (magenta line)	43
3.11	Transmission loss estimated by Mead's model with correlated inputs (similar for all meso-structures). Left: mean value \pm standard deviation and transition frequency; right: normalized standard deviation.	45
3.12	SA results for Mead's model with correlated inputs (Gibson-Ashby double vertical thickness hexagon model) by different methods.	45
3.13	SA results for Mead's model with correlated inputs (extended Gibson-Ashby triangle model) by different methods.	46
3.14	SA results for Mead's model with correlated inputs (Gibson-Malek double vertical thickness hexagon model) by different methods.	47

3.15	SA results for Mead’s model with correlated inputs (deformed Gibson-Malek double vertical thickness rectangle model) by different methods.	48
3.16	SA results for Mead’s model with correlated inputs (deformed Gibson-Malek rhombus model) by different methods.	49
3.17	SA results for Renji’s model with correlated inputs (Gibson-Ashby double vertical thickness hexagon model) by different methods. . . .	50
3.18	SA results for Renji’s model with correlated inputs (extended Gibson-Ashby triangle model) by different methods.	51
3.19	SA results for Renji’s model with correlated inputs (Gibson-Malek double vertical thickness hexagon model) by different methods. . . .	51
3.20	SA results for Renji’s model with correlated inputs (deformed Gibson-Malek double vertical thickness rectangle model) by different methods.	52
3.21	SA results for Renji’s model with correlated inputs (deformed Gibson-Malek rhombus model) by different methods.	52
3.22	SA results of transition frequency with correlated inputs by different methods. Left: triangle meso-structure, right: other meso-structures.	53
4.1	A simple illustration of Random Forest given by Wang et al. [Wang 2015].	63
4.2	Sensitivity indices obtained by FAST, samples from analytical model.	67
4.3	Variable importance sorted by RF OOB validation and normalized with the results of FAST, samples from analytical model.	67
4.4	Sensitivity indices obtained by FAST, samples from WFE model. . .	69
4.5	Variable importance sorted by RF OOB validation and normalized with the results of FAST, samples from WFE model.	70
4.6	A mapping of estimated values (y values) on original sampling values (x values).	71
4.7	An example of how RF mistreat the function discontinuity.	72
5.1	Uniform periodic sampling curve for traditional FAST method. . . .	74
5.2	Multiple uniform periodic sampling curves for FAST-pe method. . .	75
5.3	Multiple uniform periodic sampling curves for FAST-pe method under different dephasing restrictions.	76
5.4	Stop band created by the array of resonators.	77
5.5	Fourier amplitude given by FAST algorithm.	78
5.6	Fourier amplitude given by FAST-pe algorithm.	79
5.7	SA results of ten simulations accounting the frequencies 10Hz and 32Hz.	80
5.8	FAST-pe test results with different dephasing limits.	81
6.1	Estimated value mapping of RF results based on regression decision trees.	85
6.2	RF estimated value mapping along frequency axe.	86

6.3	OOB error of RF estimation at 550Hz of vibro-acoustic model, before correction.	87
6.4	OOB error of RF estimation at 550Hz of vibro-acoustic model, after correction.	88
6.5	Corrected RF estimated value mapping along frequency axe.	89
6.6	OOB error of RF estimation on the whole frequency band of vibro-acoustic model.	90
6.7	OOB error of RF estimation on the whole frequency band of vibro-acoustic model, after correction.	91
6.8	A photo of a double-layer sandwich sample made by 3D-printing. . .	92
6.9	Photo of a single bearing pad (left) and the illustration of complete 5-pad bearing system (right).	93
6.10	Five geometrical parameters of the tilting pad journal to be studied: (a): r the shaft radius, (b): R the pad internal radius, (c): R_p the pivot radius, (d): β the pivot location, (e): α the pad extent angle. .	94

List of Tables

2.1	Sampling bounds for inputs of micro-macro models	17
3.1	Sensitivity analysis methods	40
3.2	Table of variables and their values	40
3.3	Table of variables' bounds chosen for different meso-structures	41
4.1	Table of variables and their values	66
5.1	Table of variables and their corresponding sensitivity indices	78
5.2	Table of some most observed spectrums with input frequencies with $\omega_1=11\text{Hz}$ and $\omega_2=21\text{Hz}$	79

General introduction

Contents

Industrial Background	xix
Research Methodology	xx
Thesis Contribution	xxi
Thesis Outline	xxi

Industrial background

Uncertainty is an essential existence in the dynamic universe, from nanoscopic movements to megascopic observations. In the aspect of scientific research, according to Figure 1, uncertainty is an important measurements for the development of science. With more and more extremely fast computational processors being

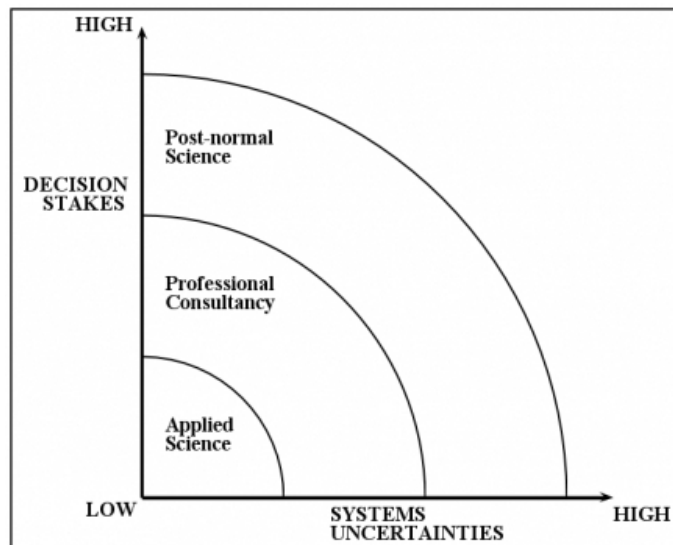


Figure 1: Identification and division of post normal science based on system uncertainties and decision stakes [Funtowicz 1990]

invented in recent decades, we can afford to construct and maintain models and systems with more and more complexities. Concerning the butterfly effect, in a huge model, small changes at input values could possibly result in enormous shock at model outputs. Thus, uncertainty identification and quantification is becoming a great issue and can no longer be ignored and approximated. For most of industrial and scientific objectives in systematic input-output analysis, such as optimization,

model reduction or meta-model extraction, the corresponding parametric tools can hardly work well without a solid preliminary study using uncertainty quantification tools.

Composite materials and structures is a category of mechanical systems that grew up with the increase of productivity. In the domain of vibro-acoustic applications, composite materials have a dominant role compared to traditional materials, particularly in case of anti-noise designs for various vehicles. Obeying the mass law of acoustic theories, the main purpose of composite materials are to maintain the best possible rigidity and damping properties and at the same time to avoid the structural resonance around its working frequency. After over a century of development, the design of composite structures has become extremely delicate, into microscale, and can now be realized by countless fabrication process, including many new technics like 3-D printing. Thus these materials are nowadays under urgent need of uncertainty control, especially in the design process of some conceptional structures.

Concerning the approaches for systematic input-output analysis, some characteristic properties of these variables must be studied. Several basic benchmarks such as marginal distribution rules can be easily evaluated and get directly used in uncertainty quantification algorithms. While some high dimensional statistical information such as dependency among variables have rarely been considered in published applications.

Research Methodology

The main methods that we preferred in this thesis are FAST(Fourier Amplitude Sensitivity Test)-series global sensitivity analysis (GSA) algorithms. FAST is a non-parametric algorithm that can quantitatively estimate the proportion of uncertainty for a certain output upon its inputs'. Based on FFT (Fast Fourier Transform), the biggest advantage of FAST is its temporal efficiency, for its computational intensity on sampling phase is rather lower than other algorithms. The only problem is that ANOVA-HDMR (ANalysis Of VAriance - High Dimensional Model Representation), the theoretic basis of FAST, is no longer unique under parametric dependency. Without the uniqueness of decomposition, error will occur when using traditional FAST to estimate sensitivity indices, and it's hard to tell how great the error is. Thus the main content of this thesis will be how to get FAST compatible with models containing parametric dependency.

In order to verify the accuracy and robustness of these modified FAST algorithms, several other methods are chosen as references in sensitivity analysis. CRM (Correlation Ratio Method) is a distribution-based ANOVA sensitivity

analysis algorithm, with a history over 2 decades. Its accuracy and stability has been proven but its computational cost is so great that its nearly impossible to get it applied on industrial cases. And another referential method is Random Forest (RF), which is a popular data-mining algorithm, at least much more popular than FAST. RF is originally a meta-modelling algorithm with an internal function of input evaluation, so it's totally under another system of data analysis. Concerning its increasing popularity, a comparison is made to discover the advantages and disadvantages of FAST and RF compared to each other.

Thesis Contribution

As mentioned before, FAST conventionally does not support dependent inputs, which greatly limited its applications. The main purpose is to improve FAST to get it compatible with such kind of sampling conditions, specifically observed in our vibro-acoustic models. During the research, some other model constraints are found and need to be treated with extra technics, and the error caused by the non unique ANOVA decomposition is also estimated. Several improved FAST-series algorithms are proposed under different conditions.

ANOVA-based GSA methods are mostly distribution-based algorithms, while the currently most popular IO-analysis methods such as Random Forest are mostly data-based. A deeper study between these two algorithms shows that in the aspect of uncertainty quantification, they have quite comparable results, both able to make self evaluation. Comparisons are also made upon their compatibility, additional functions, efficiency and theoretical basis, and some constructive conclusion finally get drawn for further developments of GSA.

As testing cases for developed FAST algorithms, their mathematical complexities are not very high and can be treated with a steady process of preliminary study - sampling - post-treatment - results. While in more common case like cooperation with other laboratory members, we can always encounter some special constraints in phases of sampling and model evaluation. Some experience on how to choose a proper GSA algorithms and to correctly make them work towards the expectation of model designers are drawn through two small projects with my colleagues.

Thesis Outline

This thesis contains in total 6 chapters, divided into the first half part and the second half part. Part 1 mainly focuses on the efforts of improving FAST algorithms under the needs of GSA with dependent input variables. Part 2 is a relatively loose part composed by three unrelated chapters where each of them discussed an

interesting topic related to FAST.

In part 1, the first chapter is conventionally the literature review, which leads up the next two chapters. Chapter 2 presented a first application of a newly developed FAST-c algorithm on a mathematical model of porous elastic material with correlated inputs. Chapter 3 follows the perspective of chapter 2 and proposed another FAST-orig algorithm to estimated the potential error of FAST-c on sandwich composite materials.

The part 2 begins with chapter 4 comparing the performance of FAST and RF in uncertainty quantification. Chapter 5 is an unfinished research on proposing a new FAST-pe algorithms for another kind of correlation among multiple units of periodic structures. Chapter 6 combines all other small pieces of my laboratory work, including some interesting RF investigation and two cooperation cases with my colleagues.

Part I

Sensitivity Analysis on acoustic materials with correlation design

Part 1: Introduction

For decades, both global sensitivity analysis algorithms and acoustic composite materials have always been rapidly developing. For them, one represents a comparably accurate and stable uncertainty quantification method and the other represents some of the most high-powered and structurally delicate industrial designs. Basically the global sensitivity analysis algorithms are mostly statistical methods, thus there's very little cases of application in traditional mechanical or material domain, until the very fast computer processors makes the large amount and large scale simulations possible for scientific research facilities.

My thesis is part of continuous work began by our colleagues who wisely chose the comparatively efficient FAST (Fourier Amplitude Sensitivity Test) algorithm to apply on periodic acoustic materials. At that time, it was a great success to get the mechanical uncertainties proportioned to structural geometrical parameters and thus met the agreements of empirical theories. But still, ANOVA (ANalysis Of VAriance) is a set of systematic theories with lot of statistical conceptions. Some of them can be easily compatible with simple mathematical tools, such as parametric marginal distributions, variance and expectations; but some don't quite get along with mechanical intuitions, such as the hypothesis of parametric independency for the ANOVA based HDMR (High Dimension Model Representation). The study of parametric dependency is not commonly necessary for vibro-acoustic researches and the dependency itself can largely vary under different context.

Years before the main direction of research in global sensitivity analysis is on its computational efficiency, limited by the calculation resources at that time. While during the passed 20 years, thanks to high power processurs, publications concerning ANOVA-based GSA applications have increased more than 100 times. For many research cases, the parametric independency hypothesis were obvious barriers for their expansion on industrial scale. Based on two typical models of acoustic materials, the main objective of these two pieces of work is to develop the FAST algorithm under particular needs of parametric dependency and to find a proper way for its applicationsa.

The two periodic acoustic material models are, namely, a porous elastic material model and a sandwich honeycomb material model. Both as materials with (approximately) periodic structures, they have a common point that their macroscopic physical properties are partially determined by geometrical sub-structures. Such particularity makes them like models with two systematic levels in the aspect of sensitivity analysis. The SA algorithms are applied on the first level of identifying the influence of input physical parameters on the output acoustic properties, while these physical parameters themselves are outputs of the second level model with its

microscopic geometric inputs. Such facts makes us unable to avoid the parametric dependency or correlation properties and have to discover the potentials of FAST algorithm.

The chapter of literature review will include some basic conceptions and theories of GSA, of FAST and of the acoustic materials being studied. Then two chapters will separately be given to the FAST applications on porous elastic materials and sandwich composite materials. A continuous clue of improvements on FAST algorithm will be present in throughout these chapters. Some general conclusions will be drawn after all these three chapters.

Literature Review

Contents

1.1	Global Sensitivity Analysis (GSA)	5
1.2	ANOVA	6
1.2.1	FAST	8
1.3	Correlation among variables	9
1.4	Algorithms compatible with correlated samples	10
1.4.1	Correlation Ratio Method (CRM)	10
1.5	Vibro-acoustic composite materials	10

1.1 Global Sensitivity Analysis (GSA)

Sensitivity analysis is *the study of how uncertainty in the output of a model (numerical or otherwise) can be apportioned to different sources of uncertainty in the model input* (Saltelli, 2004), yet is an advanced conception of uncertainty quantification. Under the general objective of quantifying the uncertainty of input-output systems, actually many approaches, including various deviational and regression algorithms, can be categorized as SA methods. Most of them work with the methodology of fixing all other variables to analyze the influence of a certain input on the output. Thus, as these methods mainly focus on a fixed point and its nearby space, they are commonly called Local Sensitivity Analysis (LSA). While in this thesis we would rather recommend another kind of SA methods, called Global Sensitivity Analysis (GSA). Easy to understand from its name, GSA aims at evaluating the influence of every inputs at the same time by browsing the whole sampling space.

The main reason of proposing GSA in modern model analysis is to avoid the curse of dimensionality, briefly presented in Figure 1.1: In this illustration, the sphere represents the sampling space of LSA compared to the hypercube representing GSA sampling. In low dimensions, meaning with few inputs, their volume of sampling space are still comparable, but when the number of inputs is above 5, the samples in the hyper sphere can no longer well represent the whole sampling space, thus its SA results might be misled by some local space features.

Decades ago when computer processors were not strong enough, it's quite difficult to make a complete space sampling for GSA. At that time many GSA algorithms have their theoretical basis elaborated but can not actually get implemented. LSA,

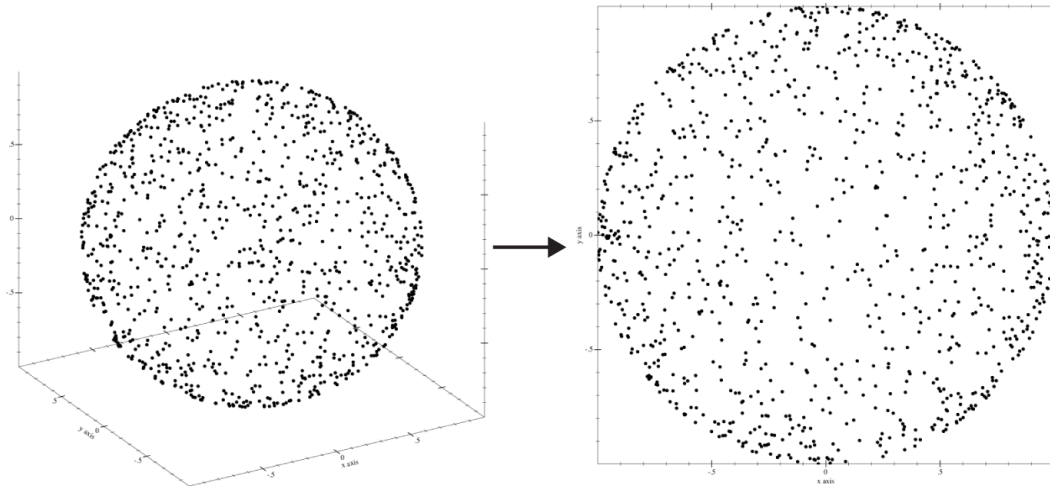


Figure 1.1: Curse of dimensionality: a comparison of 3D and 2D spheres [Saltelli 2008]

with its advantage of easy implementation and easy explanation to public, dominates the world of scientific research til today. This situation keeps until recent years, coming together with the era of big data, there is an obvious increase of researches using GSA methods. A report shows that during the last decade more enthusiasm was observed in the application of GSA methods than in LSA ones.

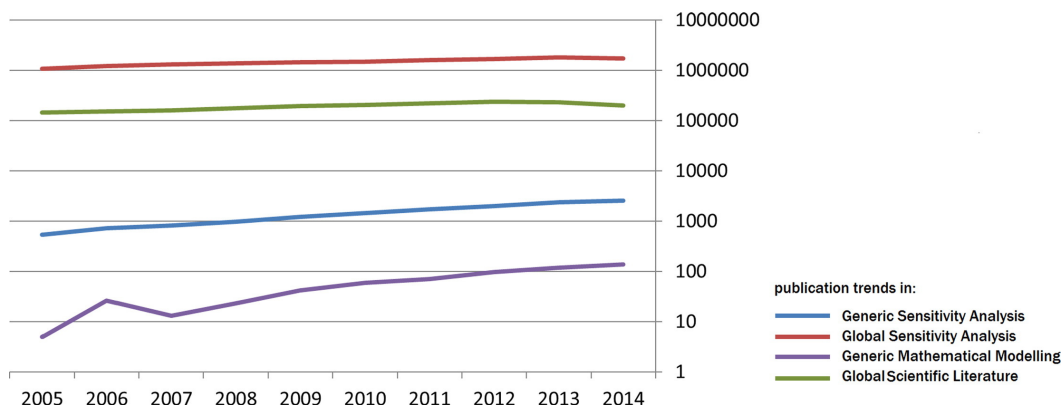


Figure 1.2: Historical trend of publications concerning sensitivity analysis [Ferretti 2016]

1.2 ANOVA

During more than 50 years of development, numerous GSA methods have been proposed, among which many widely used ones, belong to the ANOVA (ANalysis Of VAriance) class. ANOVA is a traditional statistic tool firstly given at 19th century and later well developed at the beginning of 20th centry [Fisher 1918]. Nowadays

ANOVA has grown into a big system of general parametric correlation estimation solution, and the ANOVA-based GSA algorithms are developed on the One-Way-ANOVA, where only one output vector is being analyzed. It denotes a group of SA methods based on a same system of sensitivity indices S . Usually S is a real positive value, indicating the strength of sensitivity for one or several inputs upon the model output. Only under some special definitions the sensitivity indices can be negative.

For a model $Y = f(x_1, x_2, \dots, x_n)$ with $f : \mathbb{R}^n \rightarrow \mathbb{R}$, it has been proved by Sobol' [Sobol' 1990] that the total variance of the output $V(Y)$ can be uniquely decomposed into the sum of conditional variances as following under several conditions, calling ANOVA-HDMR (High Dimension Mathematical Representation):

$$V(Y) = \sum_i V_i(x_i) + \sum_i \sum_{j>i} V_{ij}(x_i, x_j) + \sum_i \sum_{j>i} \sum_{l>j} V_{ijl}(\dots) + \dots + V_{123\dots n}(x_1, \dots, x_n), \quad (1.1)$$

and the sensitivity indexes are defined as $S_u = V_u/V(Y)$, $u \subseteq \{1, \dots, n\}$, which means

$$1 = \sum_i S_i + \sum_i \sum_{j>i} S_{ij} + \sum_i \sum_{j>i} \sum_{l>j} S_{ijl} + \dots + S_{123\dots n}. \quad (1.2)$$

A more compact definition of the first order sensitivity index is given by:

$$S_i = \frac{V_{X_i}(E_{X_{\sim i}}(Y|X_i))}{V(Y)} = \frac{V_i}{V(Y)}, \quad i = 1, 2, \dots, n, \quad (1.3)$$

where $X_{\sim i}$ means all the inputs except X_i . The index S_i represents the ratio of variance of the output Y explained by the input X_i . Its statistical meaning is the expectation of variance that can be reduced when fixing x_i somewhere in the sampling space. Based on the Equation 1.2, for systems with uncorrelated inputs, $\sum S_i \leq 1$ is always true. And when $\sum S_i = 1$, the system is called an additive system.

Besides, the high order terms of sensitivity indices can also have an analytical expression in recursive form:

$$V_{ij} = V_{X_i, X_j}(E_{X_{\sim i, j}}(Y|X_i, X_j)) - V_i - V_j, \quad (1.4)$$

$$S_{ij} = \frac{V_{ij}}{V(Y)} = \frac{V_{X_i, X_j}(E_{X_{\sim i, j}}(Y|X_i, X_j))}{V(Y)} - S_i - S_j. \quad (1.5)$$

These higher order sensitivity indexes represent the pure co-influence of several inputs on the output.

And when summing up all the terms related to a certain input, named as S_{Ti} , for example:

$$S_{T1} = S_1 + S_{12} + S_{13} + S_{123}. \quad (1.6)$$

This term is called the total sensitivity index, which shows the maximum possible influence of a variable, by measuring the portion of uncertainty that would be left out if all the other inputs are fixed. Its analytical expression is:

$$S_{Ti} = 1 - \frac{V_{X_{\sim i}}(E_{X_i}(Y|X_{\sim i}))}{V(Y)} = \frac{E_{X_{\sim i}}(V_{X_i}(Y|X_{\sim i}))}{V(Y)}. \quad (1.7)$$

1.2.1 FAST

FAST is one of the best accepted ANOVA-based GSA methods, being granted by its smart design using periodic sampling curves and FFT as variance estimator. Figure 1.3 is a brief diagram showing the essential elements of algorithm design.

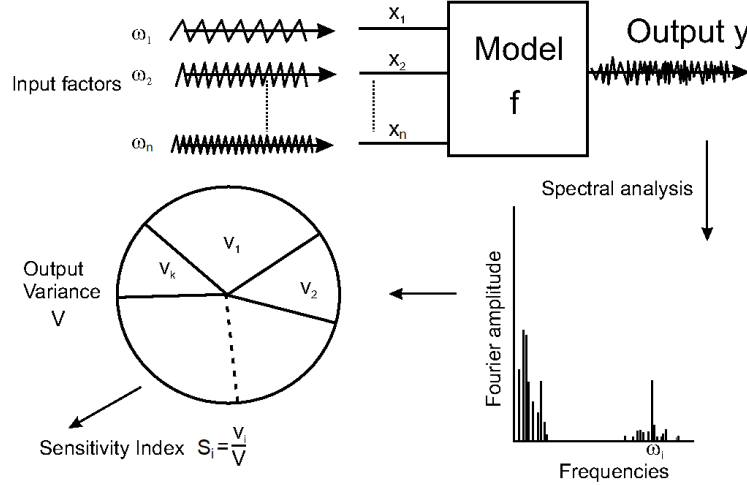


Figure 1.3: Diagram presenting the basic mechanism of FAST [Cukier 1973]

Since firstly computed by McRae et al. [McRae 1982], FAST has always been regarded as one of the most efficient methods in the area of global sensitivity analysis in benchmarks [Gatelli 2009]. With the order M defined as the minimum interference order (usually equal to 4), the total variance $V(Y)$ is approximated using the Fourier coefficient A_j, B_j :

$$V(Y) \approx 2 \sum_{j=1}^{(N-1)/2} (A_j^2 + B_j^2), \quad (1.8)$$

where N is the total sampling number chosen according to the value of M and

$$A_j = \frac{1}{2\pi} \int_{-\pi}^{\pi} f(x_1, x_2, \dots, x_n) \cos(js) ds,$$

$$B_j = \frac{1}{2\pi} \int_{-\pi}^{\pi} f(x_1, x_2, \dots, x_n) \sin(js) ds.$$

In FAST, the discrete sampling vector \mathbf{X}_i is generated by

$$x_i^{(j)} = \frac{1}{2} + \frac{1}{\pi} \arcsin(\sin(\omega_i s^{(j)} + \phi_i)), \quad (1.9)$$

where ω_i is the characteristic frequency particularly chosen for each \mathbf{X}_i , depending on the value of M . ϕ is a set of random numbers generated for this quasi-random sampling process. Then the V_i used for the estimation of S_i is approximated by:

$$V_i \approx 2 \sum_{j=1}^M (A_{j\omega_i}^2 + B_{j\omega_i}^2). \quad (1.10)$$

The modern FAST algorithm is nowadays designed by Saltelli and Bolado [Saltelli 1998] with a mix of traditional FAST [Cukier 1973] and some other ANOVA-based methods. It has been applied to different cases such as forest planning [Pacala 1996], nuclear waste treatment [Jacques 2006] and system reliability verification [Borgonovo 2003]. Such implementations proved its effectiveness and robustness in multi disciplinary cases.

1.3 Correlation among variables

As an important assumption, the whole structure of ANOVA is based on independent variables, but this is not the common case in industrial applications. There are several reasons why variables become correlated, while the most important one is that these variables themselves are outputs of another model. There are several classical measures of correlation between variables, among which one can cite Pearson's and Spearman's coefficients.

Pearson's correlation coefficient ρ^p uses the covariance function $\text{cov}(x_i, x_j)$, and is defined as:

$$\rho_{ij}^p = \frac{\text{cov}(x_i, x_j)}{\sigma_{x_i} \sigma_{x_j}}, \quad (1.11)$$

where σ_x is the standard deviation of x . This coefficient measures the linear dependence between two variables.

Spearman's correlation coefficient is defined as:

$$\rho_{ij}^s = 1 - \frac{6 \sum_{k=1}^N (\text{rank}(x_i^k) - \text{rank}(x_j^k))^2}{N(N^2 - 1)}, \quad (1.12)$$

where $\text{rank}(x)$ is an operator allowing to obtain the position of each element after sorting them in increasing order. Spearman's correlation coefficient indicates the monotonic relationship between variables.

There are some similarities between these two correlation coefficients. Both of them have values between -1 and 1, where -1 means strictly negative correlation, 1 means strictly positive correlation and 0 means uncorrelated. They both have the properties that $\rho_{ij} = \rho_{ji}$ and $\rho_{ii} = 1$. In most industrial cases, the correlation matrix, which is composed of these coefficient values, is symmetric and positive definite. This is an important property for the correlation design of an advanced FAST algorithm.

The difference between Pearson's and Spearman's correlation coefficient is that Pearson's represents the linear correlation while Spearman's represents the monotonic correlation, making it more suitable for non-linear systems. Because of its use of the $\text{rank}(\cdot)$ function, Spearman's correlation coefficient (resp. matrix) is also called rank correlation coefficient.

Strictly speaking, the expression (1.1) of ANOVA can no longer be used on a model with correlated variables because its decomposition is no longer unique [Chastaing 2012]. Although the first order sensitivity indexes S_i can still be calculated by formula (1.3), their sum can greatly exceed 1.

1.4 Algorithms compatible with correlated samples

Several sensitivity analysis methods have been developed to handle correlation between variables. Among them, let's mention Kucherenko's advanced Monte-Carlo (MC) estimators [Kucherenko 2012] which are based on the classic Sobol'-Jensen estimator [Saltelli 2010], Mara's sensitivity estimator [Mara 2015] based on Rosenblatt transformation, and Chastaing's newly developed covariance based sensitivity index [Chastaing 2012]. They are not preferred for various reasons, some of them can only work in strict conditions, and some others are not based on ANOVA-HDMR so incomparable with FAST design.

1.4.1 Correlation Ratio Method (CRM)

Correlation Ratio Method (CRM) is a common referential algorithm for correlation design of GSA algorithms. CRM was firstly proposed by McKay et al. [McKay 1997] as an alternative method to Sobol's method for non-orthogonal cases. The specificity of this algorithm is that it used a r-LHS (replicated Latin Hypercube Sampling), corresponding to the estimators developed by Ratto and Tarantola [Saltelli 2004, Saltelli 2001]. In detail, supposing that the r-LHS is executed r times with N points each time, then \mathbf{Y} is a $N \times r$ matrix of evaluation results. In \mathbf{Y} , for a given l as replication index, $y_i^{(lj)} = f(\mathbf{X})$, \mathbf{X} being the input vector in the r-LHS sampling whose i^{th} component x_i lies in the interval $[\frac{j-1}{N}, \frac{j}{N}]$. The total and the first order conditional variances are calculated in this way:

$$V(Y) = \frac{1}{Nr} \sum_{j=1}^N \sum_{l=1}^r (y_i^{(lj)} - \bar{y})^2, i = 1, 2, \dots, n, \quad (1.13)$$

and

$$V_i = \frac{1}{N} \sum_{j=1}^N (\bar{y}_i^{(j)} - \bar{y})^2, \quad (1.14)$$

where

$$\bar{y}_i^{(j)} = \frac{1}{r} \sum_{l=1}^r y_i^{(lj)}.$$

The disadvantage of r-LHS is its computational cost. For instance, with five inputs, CRM requires almost ten times more samples than FAST, which makes it less practical despite its better accuracy.

1.5 Vibro-acoustic composite materials

Noise control is an eternal topic in both civil and industrial engineering. It can be regarded in different aspects: isolation, absorption, resonance and many other passive or active technics. Porous materials and sandwich composite materials are separately the most popular choices in sound absorption and isolation.

A common index for sound absorption measurement is the sound absorption coefficient, noting the proportion of acoustic power getting absorbed after reflection. Mathematical models such as Johnson-Allard, simplified Lafarge and Champoux-Allard (JCA) model [Allard 2009] and Biot-Allard model [Biot 1956] are developed to better estimate the performance of porous material backed by a rigid wall. But it should be mentioned that for many kinds of porous materials used in sound absorption, their airpore substructure can greatly influence the overall mass and their acoustic performance in medium and high frequencies. The relation between their microstructures and macroscopic mechanical properties is a key point in sensitivity analysis.

Transmission Loss (TL) and thus the critical frequency, are very important indicators to estimate the structural sound isolation capacities and its proper working frequency band. During long time of research, their analytical estimations in isotropic panels have become accurate enough. While with the development of material science, more and more composite materials, sandwich composite structures, for example, are applied in engineering cases, replacing traditional materials. While granted for its high stiffness-to-mass ratio, the reduction in the overall structural density may actually harm its sound isolation properties. In open publications, several approaches have been made to estimate the acoustic characteristic properties of homogenized sandwich panels: pure analytical solutions [Mead 1969, Renji 2005] or with the help of Finite Element methods [Yang 2017]. If the meso-structures of the core layer need to be considered, the Gibson-Ashby model [Gibson 1997] and its improved version can also be applied together as a sandwich panel model with core layer homogenization.

GSA on porous elastic materials

Contents

2.1	Chapter introduction	13
2.2	JCA model	14
2.3	Micro-Macro model	15
2.4	FASTC	17
2.5	Identification of inputs' marginal distribution and of their correlation	18
2.5.1	3-parameter (3-p) micro-macro model	18
2.5.2	2-parameter (2-p) micro-macro model	19
2.6	Results comparison and discussion	20
2.6.1	Comparison of SA results with 3-parameter micro-macro model	20
2.6.2	Comparison of SA results with 2-parameter micro-macro model	23
2.7	Chapter conclusion	25

2.1 Chapter introduction

Porous materials have historically become one of the most successful solutions in sound absorption problems, and we already have several models to estimate their sound absorption efficiency based on their macroscopic physical characteristics. While as the micro structure of porous material can strongly vary under different fabrication conditions, their physical properties may contain larger uncertainty than classical materials. This explains the growing interest in sensitivity analysis for noise control applications. Specifically, in the study of Ouisse et al. [Ouisse 2012] the issue of sensitivity analysis of absorption indicators is dealt with. Christen et al. [Christen 2016] considered the transmission loss through layered composite panels as an indicator for the sensitivity analysis. In both cases, some interesting trends with regards to the more influential material parameters were provided.

However, in these works, the variables are mostly supposed to be independent and uniformly or normally distributed. While actually, concerning porous materials, a micro-macro semi-empirical model, recently proposed by Doutres et al. [Doutres 2011], shows that the variables studied in the JCA model may have correlation among them. Other works on acoustic foam's microstructures are also

reviewed, such as Zielinski et al. [Zielinski 2015], which present similar acoustic properties, while the correlation was not clearly pointed out.

As mentioned before, ANOVA-HDMR actually fails for correlated inputs and the traditional FAST can not work correctly with correlation, thus some improvements are needed. In this piece of work, the FAST method with Correlation design (named FASTC in this paper) which is considered further was proposed by Xu and Gertner [Xu 2008]. The advantage of FASTC is that it requires only the knowledge of correlation matrix, which is more accessible than conditional distribution density function in industrial cases. It's like a lighter version of algorithms based on full input datasets.

One of the main objectives of this work is to find out how correlated the variables of the JCA model are, and to estimate the impact of the correlation on SA estimations. This will be achieved through the micro-macro model and by observing their effects on the SA results. These statistics may help to better understand how to handle uncertainties in manufacturing and filtering phase for materials with complex microstructures. Also, this study can be regarded as a first test of the FASTC method's effectiveness and reliability on vibroacoustic applications.

2.2 JCA model

The JCA model is used to estimate the acoustic absorption coefficient of porous material sample whose frame remains rigid when backed by an impervious rigid wall. It has only one output, the absorption coefficient α , with five inputs, also called non-acoustic parameters, namely the porosity ϕ , the flow resistivity σ , the tortuosity α_∞ , and the characteristic viscous and thermal lengths Λ and Λ' . This model also implies a non-material parameter ω representing the acoustic angular frequency.

The effective density ρ_e , including viscous and inertial effects, can be calculated by:

$$\rho_e(\omega) = \rho_0 \left(\alpha_\infty + \frac{\nu_0 \phi}{j\omega q_0} G(\omega) \right), \quad (2.1)$$

with $\nu_0 = \eta/\rho_0$, η being the dynamic viscosity, ρ_0 being the air density, $q_0 = \eta/\sigma$ being the static viscous permeability, $j = \sqrt{-1}$, and:

$$G(\omega) = \sqrt{1 + \left(\frac{2\alpha_\infty q_0}{\phi \Lambda} \right)^2 \frac{j\omega}{\nu_0}}. \quad (2.2)$$

The bulk modulus related to thermal effects K is given by the simplified Lafarge model:

$$K(\omega) = \frac{\gamma P_0}{\gamma - \frac{\nu' \phi}{1 + \frac{\nu' \phi}{j\omega q_0} G'(\omega)}}, \quad (2.3)$$

where P_0 is the static pressure, γ is the heat ratio, $\nu' = \nu_0/\text{Pr}$, Pr being the Prandtl

number, q'_0 is the static thermal permeability and

$$G'(\omega) = \sqrt{1 + \left(\frac{2q'_0}{\phi\Lambda'}\right)^2 \frac{j\omega}{\nu'}}. \quad (2.4)$$

With the Champoux-Allard approximation:

$$q'_0 = \frac{\phi\Lambda'^2}{8}, \quad (2.5)$$

it leaves only six variables required for the calculation, including the angular frequency ω . With these presented formulas, the characteristic impedance Z_c , the surface impedance Z_s and the wave number k can be calculated as below:

$$k(\omega) = \omega \sqrt{\frac{\rho_e(\omega)}{K(\omega)}}, \quad (2.6)$$

$$Z_c(\omega) = \sqrt{\rho_e(\omega)K(\omega)}, \quad (2.7)$$

$$Z_s(\omega) = -\frac{1}{\phi} j Z_c(\omega) \cot(k(\omega)e), \quad (2.8)$$

where e is the thickness of the material sample. Finally the sound absorption coefficient α is presented as

$$\alpha(\omega) = 1 - \left| \frac{Z_s(\omega) - Z_0}{Z_s(\omega) + Z_0} \right|^2, \quad (2.9)$$

where $Z_0 = \rho_0 c_0$ and c_0 being the speed of sound.

2.3 Micro-Macro model

In view of micro-structuration of acoustic foams, a semi-empirical micro-macro model was recently proposed by Doutres et al. [Doutres 2011]. The latter was considered mainly for polyurethane (PU) foams. One of the most important assumptions is that the foams are nearly or totally homogeneous, because their characteristic dimension is far larger than the size of inhomogeneities. Another assumption is that the micro structure of foams are approximated as a periodic stacking of Kelvin cells, or tetrakaidecahedral cells, which is the basis of parameter estimation. At last all the foams with a degree of anisotropy larger than 1.25 are rejected because the model can only work on at least quasi-isotropic PU foams.

This model has five outputs, which are the material parameters of the JCA model, and 3 input parameters. These parameters are the strut length l , the strut thickness t and the reticulation rate R_w . A simplification for high porosity cases, with ϕ lying between 0.97 and 0.99, can reduce these parameters to only 2, expressing l and t as a function of the cell size C_s . The inputs are measured from the Kelvin cell as shown in Figure 2.1, extracted from the works of Doutres et al..

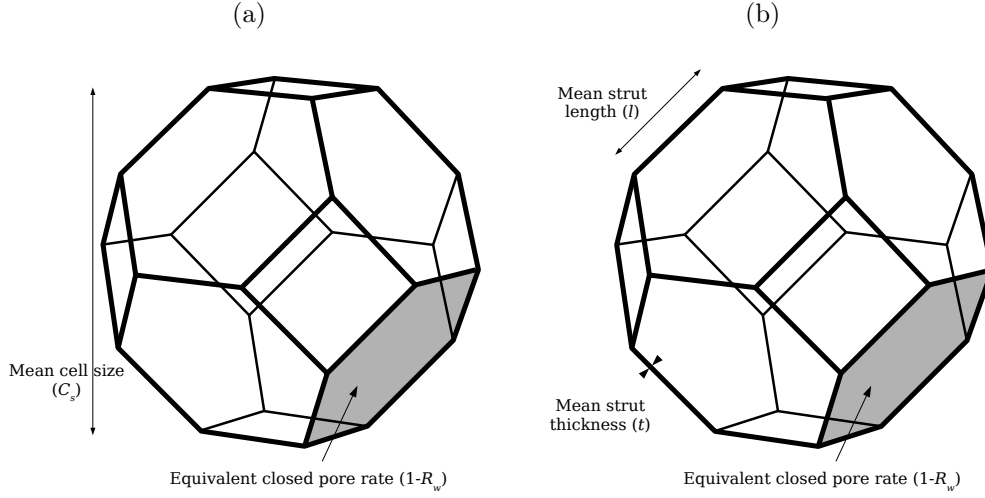


Figure 2.1: 2-parameter (a) and 3-parameter (b) micro-macro model

In practice, l , t and C_s can be measured by optical micrograph, but R_w can only be measured with a Scanning Electron Microscope (SEM). When expressed mathematically, the 3-parameter model and the 2-parameter model use exactly the same formulas with the variables l , t and R_w :

$$\phi = \frac{V_f}{V_t} = 1 - C_t^\rho \left(\frac{t}{l}\right)^2, \quad (2.10)$$

with V_f being the fluid volume within the cell, V_t being the total cell volume and $C_t^\rho = (2\sqrt{3} - \pi)/\sqrt{2}$;

$$\alpha_\infty = 1.05 \left(\frac{1}{R_w}\right)^{-0.6763}, \quad (2.11)$$

$$\sigma = C^\beta (C_r^\rho \frac{t}{l^2})^2 \left(\frac{1}{R_w}\right)^{1.1166}, \quad (2.12)$$

with $C_r^\rho = 3\pi/8\sqrt{2}$, $C^\beta = 128\eta$, and η being the dynamic fluid viscosity taken equal to 1.85×10^{-5} Pa.s;

$$\Lambda' = \frac{2V_f}{A_t} = \frac{8l\sqrt{2}}{3} \frac{1 - \frac{t^2(2\sqrt{3}-\pi)}{l^2\sqrt{2}}}{1 + 2\sqrt{3} - R_w(1 + 2\sqrt{3} - \frac{4\pi t}{l\sqrt{3}})}, \quad (2.13)$$

with A_t being the surface of the frame in contact with the saturation fluid;

$$\Lambda = \frac{\Lambda'}{n} = \frac{\Lambda'}{1.55} \left(\frac{1}{R_w}\right)^{-0.6763}, \quad (2.14)$$

where the coefficient 1.55 is obtained empirically for fully reticulated foams.

The 2-parameter simplification is obtained by assuming that the ratios $A = C_s/l\sqrt{2}$ and $B = l/t$ are constant. However, these ratios are provided with rather

wide error margins, so they are considered as independent parameters in the present study. Supposing that no experimental statistics is given, all micro structure quantities are uniformly sampled as default, with their bounds listed in Table 2.1:

Table 2.1: Sampling bounds for inputs of micro-macro models

Parameter	Variable	Lower bound	Upper bound
<i>Common parameter</i>			
Reticulation rate	$R_w(\%)$	5	100
<i>3 – parameter model</i>			
Strut length	$l(\mu\text{m})$	141	530
Strut thickness	$t(\mu\text{m})$	36	160
<i>2 – parameter model</i>			
Cell size	$C_s(\mu\text{m})$	500	1 500
Empirical parameter A	$A(-)$	1.97	2.69
Empirical parameter B	$B(-)$	3.25	4.31

It can be seen that this model generates five outputs with only three or four inputs, which means that there must be some correlation among these physical quantities.

2.4 FASTC

It should be noticed that the correlated case is not often considered in SA research, as ANOVA actually fails in case of correlated variables. In the limited literature survey, the FASTC method proposed by Xu and Gertner [Xu 2008] seems to be an implementable and efficient method for models with limited a priori knowledge.

The core of FASTC’s correlation design is Iman’s transform [Iman 1982], which allows to create a set of correlated samples by reordering existing ones. Its principle is simple: for a sampling matrix \mathbf{X} containing uncorrelated row vectors and a positive definite and symmetric correlation matrix \mathbf{C} , let $\mathbf{C} = \mathbf{P}\mathbf{P}'$ by Cholesky factorization, then $\mathbf{X}_b = \mathbf{X}\mathbf{P}'$ has exactly the same correlation matrix as the objective correlation matrix \mathbf{C} . For the objective correlation matrix, both Pearson and Spearman correlation matrices can be used, but Spearman’s matrix is preferred. Noticing that \mathbf{X}_b doesn’t contain the same elements as \mathbf{X} , Iman’s solution is to reorder all elements in \mathbf{X} to ensure that it has the same rank as \mathbf{X}_b . The error in the correlation matrix caused by using \mathbf{X} instead of \mathbf{X}_b is limited when there are enough samples. What should be paid attention to is that this method can only be applied to normalized samples with mean value equal to 0 and standard deviation equal to 1.

After the denormalization, a correlated sampling matrix \mathbf{X} is finally obtained, but with only the first column containing periodic sampling data. So when applying FFT on the output dataset $\mathbf{Y} = \mathbf{f}(\mathbf{X})$, only S_1 can be correctly calculated. In order to properly estimate other first-order sensitivity indices S_i , \mathbf{Y} must also be reordered

each time correspond to the original periodicity of x_i . As for another algorithm taken as referential in this research, the CRM (Correlation Ratio Method), also uses Iman's transform for the generation of correlated datasets. But as it takes a different mechanism of SI estimation specifically designed for r-LHS, there is no problem of separate SA estimation.

2.5 Identification of inputs' marginal distribution and of their correlation

In order to apply these SA methods, the first step is to study the original datasets for some necessary information such as each variable's marginal distribution and their correlation coefficients. All the samples are generated by MC sampling of the micro-macro model.

2.5.1 3-parameter (3-p) micro-macro model

In figure 2.2, the yellow bars represent the original marginal distributions from samples generated by Micro-Macro model and the magenta line is the closest uniform, exponential or lognormal approximate.

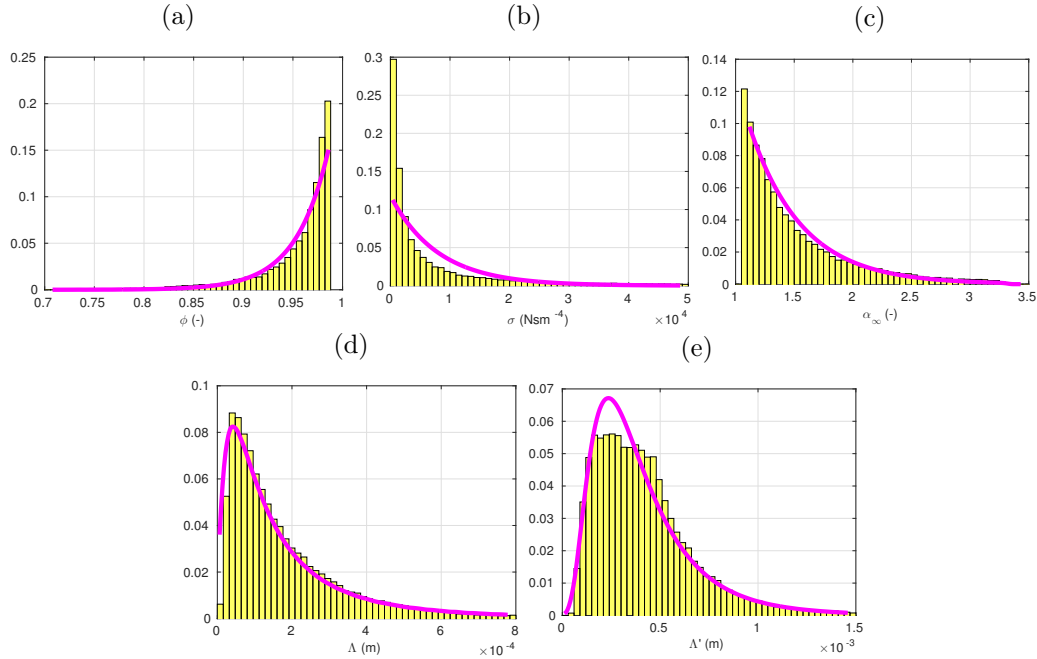


Figure 2.2: Marginal distribution of variables generated by 3-parameter micro-macro model and our approximation: (a): ϕ , (b): σ , (c): α_∞ , (d): Λ , (e): Λ'

The first three parameters (ϕ , σ , α_∞) seem to be correctly represented by an exponential trend. Meanwhile, the viscous and the thermal lengths can be approximated by lognormal distribution. The rank correlation matrix of this dataset is also

obtained:

$$\begin{array}{c}
 \phi \\
 \sigma \\
 \alpha_\infty \\
 \Lambda \\
 \Lambda'
 \end{array}
 \begin{bmatrix}
 \phi & \sigma & \alpha_\infty & \Lambda & \Lambda' \\
 1 & -0.85 & 0.00 & 0.53 & 0.77 \\
 -0.85 & 1 & 0.39 & -0.87 & -0.95 \\
 0.00 & 0.39 & 1 & -0.73 & -0.33 \\
 0.53 & -0.87 & -0.73 & 1 & 0.86 \\
 0.77 & -0.95 & -0.33 & 0.86 & 1
 \end{bmatrix}
 \quad (2.15)$$

It shows that most of these variables are strongly correlated to each other, especially for the characteristic lengths. Indeed, they both have similar correlation properties: positively correlated to the porosity ϕ and negatively correlated to the air flow resistivity σ and the tortuosity α_∞ . No correlation between the porosity ϕ and the tortuosity α_∞ is observed. Indeed the last four parameters σ , α_∞ , Λ and Λ' all depend exponentially on the reticulation rate R_w in the mathematical expression of the model. Combined with the empirical correlation between Λ and Λ' (nearly linear in fully reticulated case[Doutres 2011]), the 4 variables become closely correlated as shown in Eq. 2.15.

2.5.2 2-parameter (2-p) micro-macro model

Just as for the 3-p model, the comparison of marginal distributions are shown in the Figure 2.3:

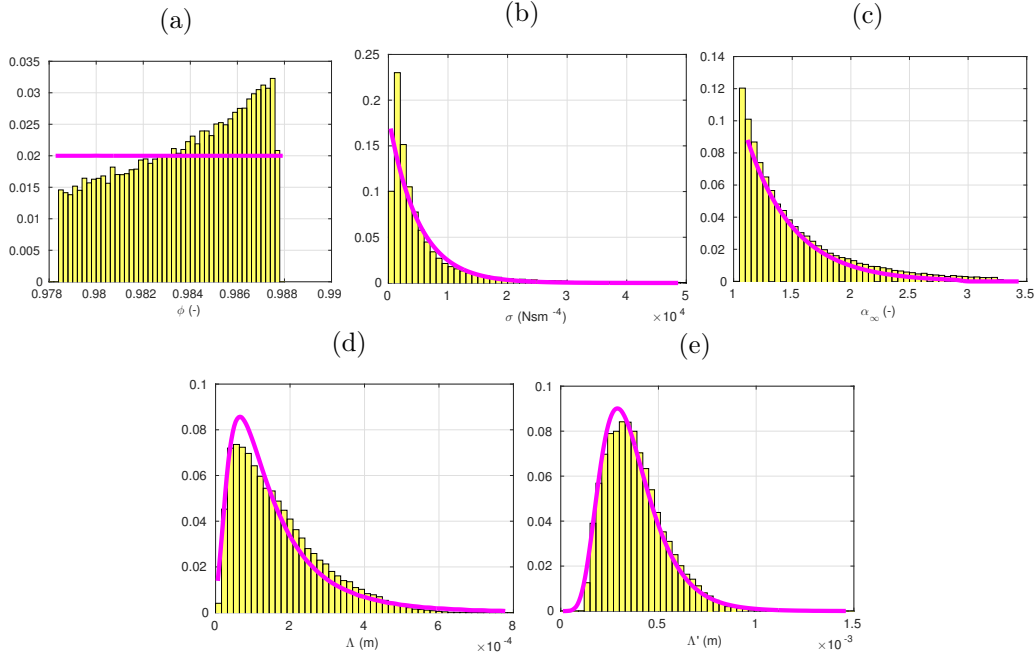


Figure 2.3: Marginal distribution of variables generated by 2-parameter micro-macro model and our approximation: (a): ϕ , (b): σ , (c): α_∞ , (d): Λ , (e): Λ'

In this approximation the porosity ϕ is considered uniformly distributed, since the model is valid only for a narrow range of porosity, and no clear trend emerge for a

distribution. Similarly to the 3-p model, σ and α_∞ are approximated by exponential functions and the characteristic lengths Λ , Λ' by lognormal functions. Finally the rank correlation matrix is shown to be:

$$\begin{array}{c} \phi \\ \sigma \\ \alpha_\infty \\ \Lambda \\ \Lambda' \end{array} \begin{bmatrix} \phi & \sigma & \alpha_\infty & \Lambda & \Lambda' \\ 1 & -0.16 & 0.00 & 0.05 & 0.08 \\ -0.16 & 1 & 0.71 & -0.94 & -0.94 \\ 0.00 & 0.71 & 1 & -0.90 & -0.57 \\ 0.05 & -0.94 & -0.90 & 1 & 0.86 \\ 0.08 & -0.94 & -0.57 & 0.86 & 1 \end{bmatrix} \quad (2.16)$$

The main difference with the 3-p case is the absence of correlation between the porosity ϕ and any other variables, whereas it was strongly negatively correlated to the flow resistivity in the former case. This can be explained as in the 2-parameter micro-macro model, the expression of the porosity ϕ depends only on the cell size and not on the reticulation rate R_w , while the latter has been observed to have a dominant effect by Doutres et al. [Doutres 2014] in the micro-macro models in most cases.

2.6 Results comparison and discussion

2.6.1 Comparison of SA results with 3-parameter micro-macro model

The SA algorithms are applied on the five non-acoustic parameters of the JCA model, to determine which among them have the most influence on the output α . The correlation properties are induced by 3-parameter model and 2-parameter model with the micro structural variables uniformly sampled as in Table 2.1. For the SA estimation parameters, 2 different thickness of 25mm (1 in.) and 47mm ($\simeq 2$ in.) are tested using all three SA methods on the frequency range of 100Hz - 2500Hz. The two different thicknesses and the frequency range are chosen to be identical to those in the study of Ouisse et al. [Ouisse 2012]. So the analysis results represent an overall view of the JCA model's uncertainty under a wide range of microstructure and environment conditions uncertainties.

The SA results are presented as a set of curves of first order sensitivity indexes estimated by FASTC, CRM and FAST method along the frequency band. The two FAST methods require 5000 samples each while 50000 samples are used in CRM method. According to our experience, the value of sensitivity indexes in the lowest part of the frequency band is not very reliable due to the low value of absorption in this region. However, the most interesting results are the trends in mid and high frequencies. The mean value \pm standard deviation and the Normalized Standard Deviation (NSD) of absorption are plotted in order to visualize the variability of the model output with frequency. Generally, the greater these values, the more useful and more valuable will the SA tests be.

2.6.1.1 SA results of 1 in. (25mm) thickness samples

In the case of 25mm thick samples with a wide range of reticulation rate, the SA results are shown in Figure 2.5 and the output variability shown in Figure 2.4:

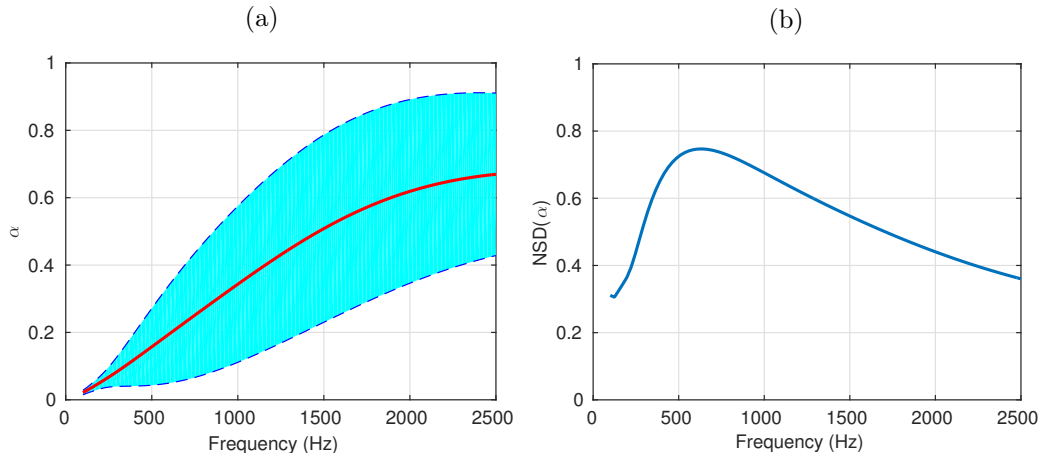


Figure 2.4: Statistics of the output set for JCA model with correlated inputs (3-parameter micro-macro model): (a): mean value \pm standard deviation; (b): normalized standard deviation. Thickness of material: 25mm

Looking at Figure 2.4, several frequency zones can be identified: mean absorption as well as standard deviations increase steeply up to 2000Hz, and more slowly between 2000 and 2500 Hz. The maximum value of $NSD(\alpha)$ lies between 500 and 1000Hz, with a moderate and increasing mean value of α . It imposes a focus on sensitivity indexes around 1000Hz.

The curves in Figure 2.5 illustrate the importance of taking correlation into account. Huge estimation gaps are observed between the SA results of uncorrelated FAST and the two correlated methods FASTC and CRM, who give close results to each other. As expected, FASTC always slightly underestimates the S_i , but the negligible error compared to CRM indirectly demonstrates the robustness of these 2 SA methods. According to the graphs, Λ appears to be the dominant parameter, except at very low frequency. Its steady influence at mid-high frequency makes it the most interesting variable to control.

Also as expected, ϕ appears to have the least influence on the output. This is due to the mechanism of micro-macro model in which ϕ does not depend on R_w , which has been proven in [Doutres 2014] to be very influential. The strong correlation shown in the correlation matrix not only results in similar trends for the S_i of the correlated variables but these trends are very different to any of those in the uncorrelated case. Empirically, at low frequency, Λ' is observed to be dominant, while Λ has no influence, as shown also by the results of FAST. But also with the highly recognized correlation among them, a transfer point appears on the curve of Λ at low frequency while $S_{\Lambda'}$ keeps a significant value at high frequency. Finally, it should be mentioned that the SA results of FAST shown in the graphs differ

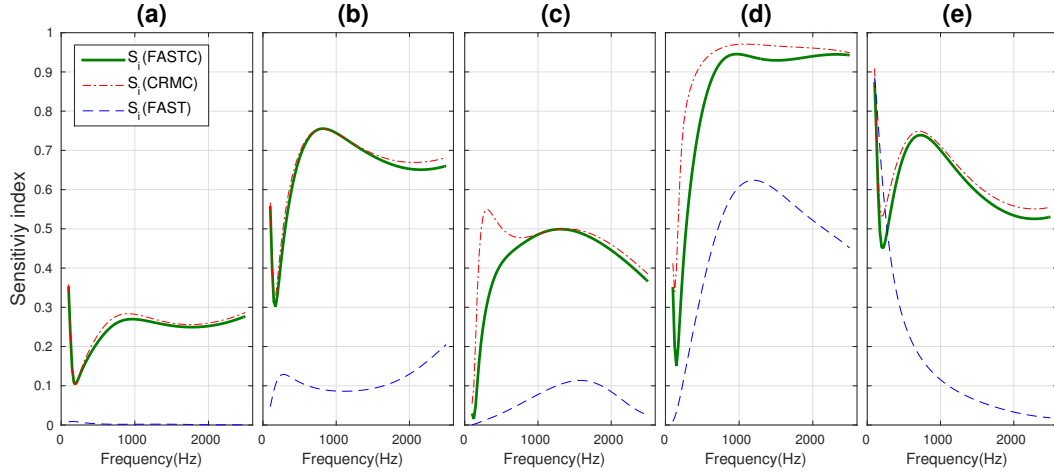


Figure 2.5: SA results for JCA model with correlated inputs (3-parameter micro-macro model) by different methods: FASTC, CRM with correlation design and original FAST, thickness of material: 25mm. (a): $SI(\phi)$, (b): $SI(\sigma)$, (c): $SA(\alpha_\infty)$, (d): $SI(\Lambda)$, (e): $SI(\Lambda')$

from the results of Ouisse et al. [Ouisse 2012], highlighting the effect of distribution change.

2.6.1.2 SA results of 2 in. ($\approx 47\text{mm}$) thickness samples

In the case of 47mm thick samples with a wide range of reticulation rate, the SA results are shown in Figure 2.7 and the output variability shown in Figure 2.6:

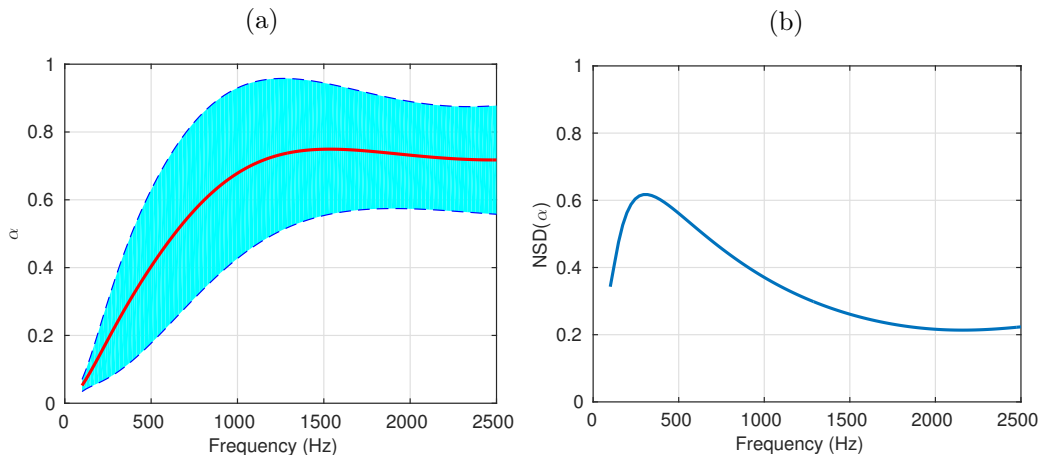


Figure 2.6: Statistics of the output set for JCA model with correlated inputs (3-parameter micro-macro model): (a): mean value \pm standard deviation; (b): normalized standard deviation. Thickness of material: 47mm

As can be imagined, with a greater thickness, the absorption coefficient increase more rapidly than with 25mm thickness. Its mean value reaches its maximum in

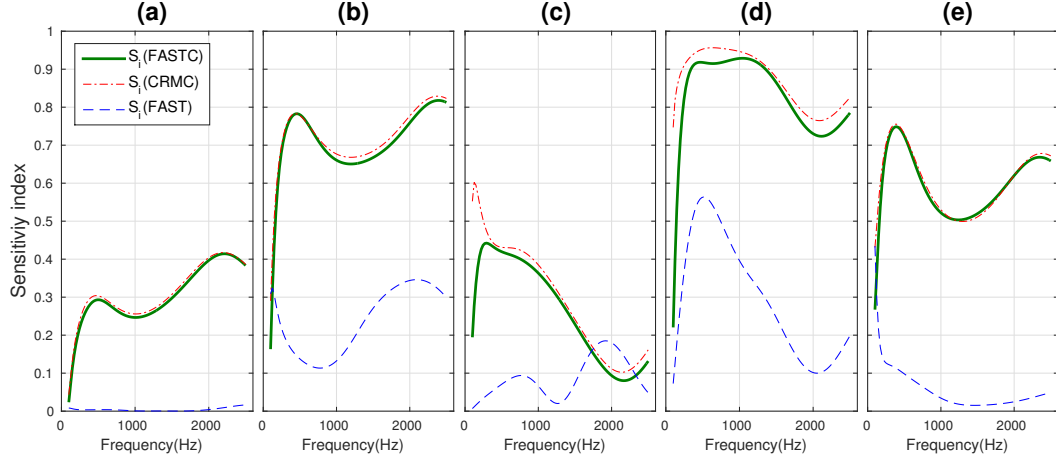


Figure 2.7: SA results for JCA model with correlated inputs (3-parameter micro-macro model) by different methods: FASTC, CRM with correlation design and original FAST, thickness of material: 47mm. (a): $SI(\phi)$, (b): $SI(\sigma)$, (c): $SA(\alpha_\infty)$, (d): $SI(\Lambda)$, (e): $SI(\Lambda')$

the mid-frequency band between 1000 and 1500Hz, while the standard deviation gradually decreases when the frequency increases. Similarly, the NSD curve also shows that the low-mid frequency band should be concentrated on while the study on high frequency can be less valuable.

Similarly to the NSD curve, the S_i curves of FASTC all reach their first peak at about 500Hz while the curves of uncorrelated FAST do not follow this trend. In Figure 2.5, the sensitivity indexes estimated by FASTC are all much greater than those estimated by FAST. However in Figure 2.7, we observe that S_{α_∞} estimated by FASTC is even smaller than the one of original FAST at around 2000Hz. Though σ and α_∞ have similar correlations with other variables, they have totally different effects on these two variables' uncertainties. This shows that the impact of correlation coefficients on the sensitivity indexes can hardly be predicted. The curves of 47mm samples have similar trends to the 25mm samples, with Λ still being the most influential variable at low-mid frequency while sharing dominant position with σ in the high frequency band. Finally, the sensitivity indexes vary faster in this case than with 25mm samples, owing to the shift towards lower frequencies of the first absorption maximum and phenomena occurring after it.

2.6.2 Comparison of SA results with 2-parameter micro-macro model

2.6.2.1 SA results of 1 in. (25mm) thickness samples

In case of 25mm thick highly reticulated samples, the SA results are shown in Figure 2.9 and the output variability shown in Figure 2.8:

Regarding Figure 2.8, though the NSD curve has slightly shifted, the trends are

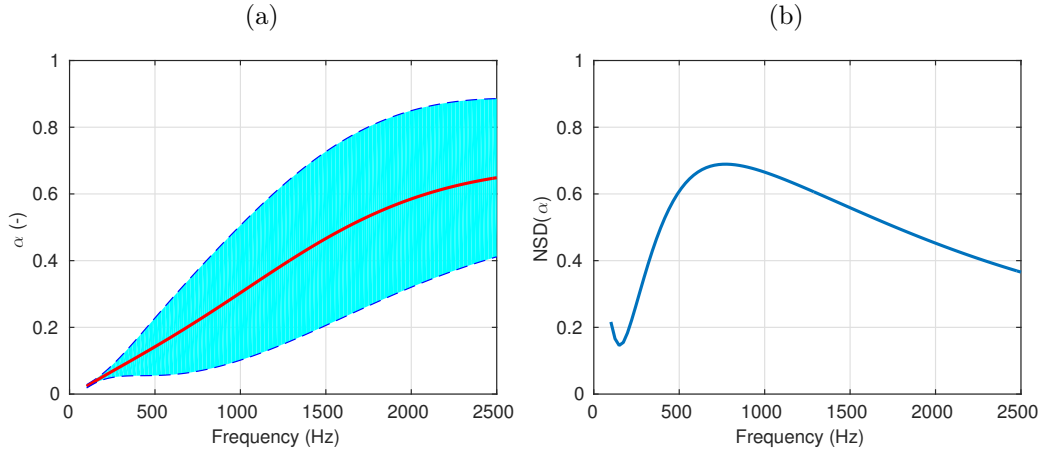


Figure 2.8: Statistics of the output set for JCA model with correlated inputs (2-parameter micro-macro model): (a): mean value and mean value \pm standard deviation; (b): normalized standard deviation. Thickness of material: 25mm

exactly the same as in Figure 2.4. As expected from the 3-p results, improving the knowledge of the porosity cannot really reduce the variability in the absorption coefficient, and the uncertainty in the "constants" A and B lead to close marginal distributions and correlation matrices.

As for the S_i curves, though their forms seem different from the 3-p ones, the frequencies where the extrema occur remain the same. The main differences concern the porosity and the tortuosity. The sensitivity index relative to ϕ always remains very low. Comparing S_ϕ between 3-p and 2-p model, it can be seen that when correlation with other variables no longer exists (Eq.2.16), its sensitivity index decrease to almost 0, just as in the uncorrelated FAST. So in case of ϕ , the correlation properties explain about 0.3 to 0.4 the absolute value of its sensitivity index, which can be a reference for other variables. On the other hand, α_∞ , whose value depends only on R_w , show more influence on the output than in case of 3-p model. This basically highlights the influence on absorption of the reticulation rate, to which all influential macroscopic parameters are correlated. Such results has also been shown in [Doutres 2014].

2.6.2.2 SA results of 2 in. (≈ 47 mm) thickness samples

In case of 47mm thick highly reticulated samples, the output variability are shown in Figure 2.10 and the SA results in Figure 2.11. It can be seen that they are remarkably close to those of the 3-p model of Figures 2.6 and 2.7.

After comparing the four sets of results, we can draw the conclusion that the 2-parameter model has little impact on the sensitivity of absorption to non-acoustic parameters. On the one hand, reducing the number of parameters may appear as reducing uncertainty, but this is compensated by the wide variability range of the cell size C_s considered in this study. A previous study [Doutres 2015] showed

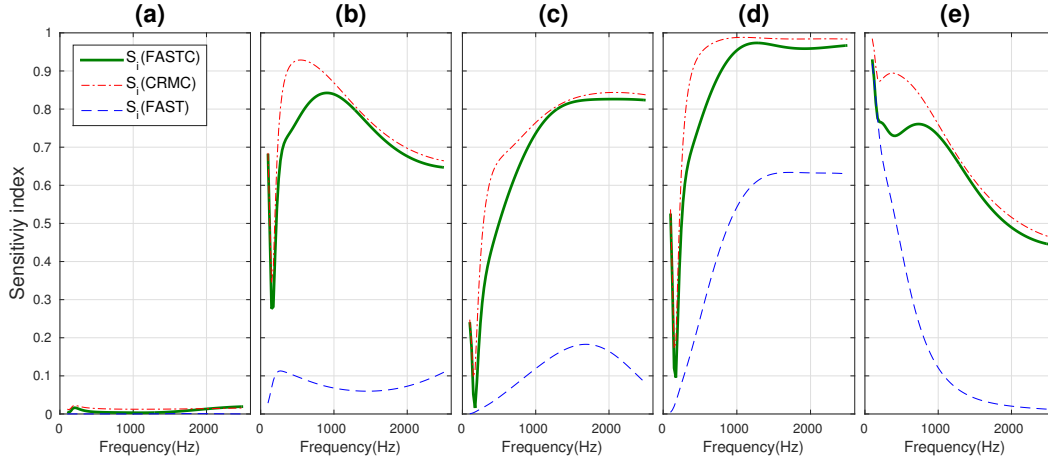


Figure 2.9: SA results for JCA model with correlated inputs (2-parameter micro-macro model) by different methods: FASTC, CRM with correlation design and original FAST, thickness of material: 25mm. (a): $SI(\phi)$, (b): $SI(\sigma)$, (c): $SA(\alpha_\infty)$, (d): $SI(\Lambda)$, (e): $SI(\Lambda')$

that the rather wide uncertainty on the "constants" A and B have little influence on the variability of the non-acoustic parameters, except on the porosity. Since the latter has little influence on the acoustic absorption, this uncertainty has little consequence. The main difference between the two models is in the correlation between the porosity and the other parameters, rather strong with 3 parameters and absent in the 2-p model. This leads to very different values for the porosity's sensitivity index, although it remains the least influential of the five non-acoustic parameters considered.

2.7 Chapter conclusion

In this paper, the effect of uncertainties and correlations among parameters of the sound absorption Johnson-Champoux-Allard model was studied. Sensitivity analysis methods considering the correlation among the inputs of JCA model generated by a secondary micro-macro empirical model were considered in depth. In order to deal with this problem, a FASTC method based on Iman's transform is specially chosen for correlated variables. The novelty of the approach lies in the account taken of correlation.

Concerning the inputs' joint distribution, two main observations can be made from the micro-macro model used in this study. First, every parameter's marginal distribution is strongly biased and usually far from the commonly used normal or uniform distributions. The shape of the distribution is an important factor on uncertainty assessment. Secondly, the correlations among variables are much stronger than expected, and questions the frequent hypothesis that the parameters are independent. The only previously well-established correlation was that between the

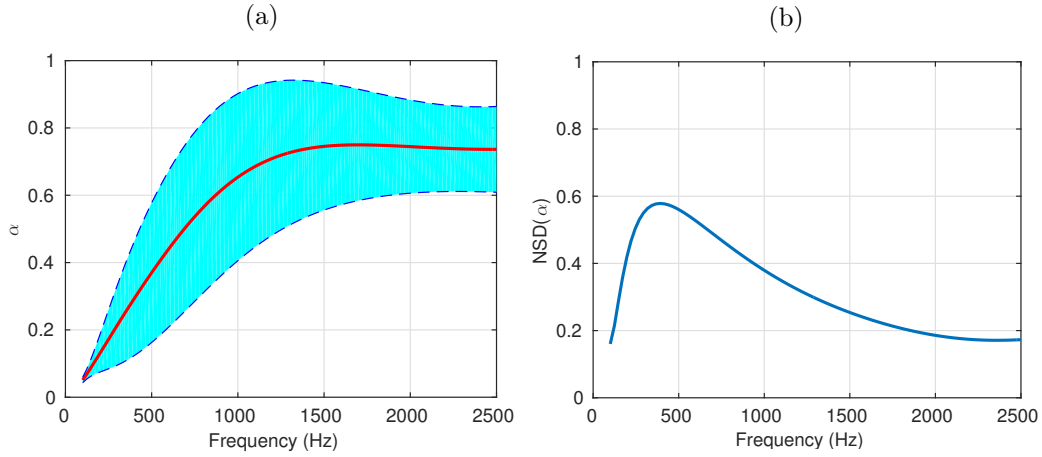


Figure 2.10: Statistics of the output set for JCA model with correlated inputs (2-parameter micro-macro model): (a): mean value and mean value \pm standard deviation; (b): normalized standard deviation. Thickness of material: 47mm

viscous and thermal characteristic lengths, where the latter is commonly estimated as twice the former [Allard 2009]. In this paper, we show that the correlation among other variables are generally equivalent or even stronger than the one between Λ and Λ' . Among these five variables, the only one which is kept almost independent from others is the porosity ϕ .

The SA results taking correlation effects into account are different from the ones in former studies. While the sensitivity index of ϕ keeps a negligible value, the other variables all have a noticeable effect (compared to SA results without correlation) with first-order sensitivity indexes ranging from 0.5 up to 0.99. This phenomenon is especially remarkable in the high frequency band, which is the main working condition of acoustic foams. Different behaviors are also observed under different micro-macro assumptions and sample thicknesses. Such results show that the pre-determined reticulation rate and sample thickness also have impact on forms of S_i curves.

The physical meaning of this SA is that if one wants to control the uncertainty of porous material's absorption coefficient, filtering the products with their viscous length can be the most effective way. While in case of 47mm thickness porous material samples, the parameter to be filtered should be better chosen under knowledge of its working frequency, because its SA results varies brutally in medium and high frequency band. Of course this conclusion depends on the micro-macro model and on the hypothesis that no extra control in production is applied.

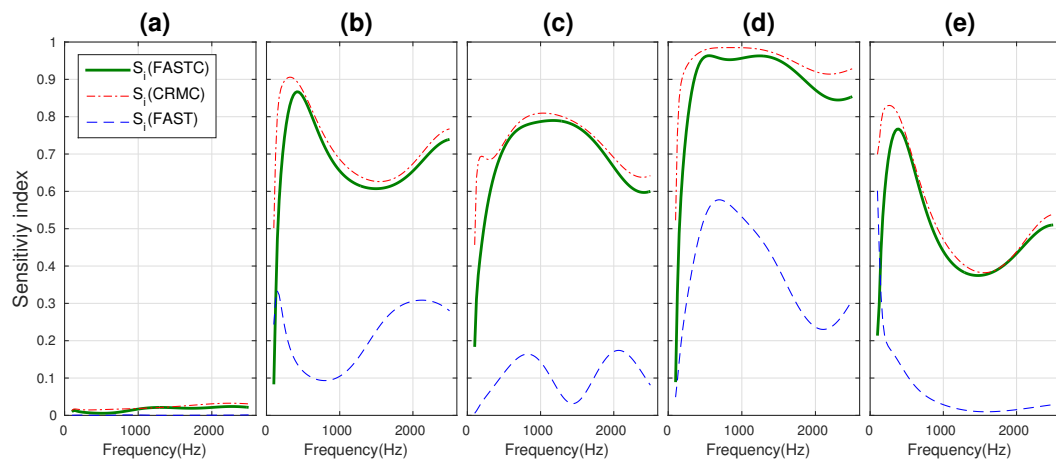


Figure 2.11: SA results for JCA model with correlated inputs (2-parameter micro-macro model) by different methods: FASTC, CRM with correlation design and original FAST, thickness of material: 47mm. (a): $SI(\phi)$, (b): $SI(\sigma)$, (c): $SA(\alpha_\infty)$, (d): $SI(\Lambda)$, (e): $SI(\Lambda')$

GSA on sandwich composite materials

Contents

3.1 Chapter introduction	29
3.2 Acoustic characteristics of sandwich panels	31
3.2.1 Mead's model	32
3.2.2 Renji's model	33
3.2.3 Coincidence frequency	33
3.2.4 Transition frequency	33
3.3 Homogenization of Meso-structures	34
3.3.1 Gibson-Ashby honeycomb structure and its extension	35
3.3.2 Gibson-Malek honeycomb structure and its deformation	36
3.4 Correlation and dependency discussion	37
3.5 FAST-orig	38
3.6 Identification of inputs' marginal distribution and of their correlation	40
3.6.1 Variables overview	40
3.6.2 Correlated variables	41
3.7 Results comparison and discussion	44
3.7.1 SA results on Mead's model	45
3.7.2 SA results on Renji's model	47
3.7.3 SA results on structures' transition frequencies	47
3.8 Chapter conclusion	48

3.1 Chapter introduction

Different from simple plate structures, composite structures could contain more uncertainties on their macroscopic mechanic properties. These uncertainties can be accumulated throughout the procedures of manufacturing: a bit of error allowed for the core meso-structure, a bit of error allowed for the combination of layers, etc.. These observed variation of the structural mechanical parameters will finally result in the variation of the objective characteristic property: acoustic properties. In the

process of structural optimization, the reduction of uncertainties at the system output is one necessary issue. Already acknowledged the uncertainty of the structural mechanical parameters, variable filtering is the first step of setting up optimization algorithms. Which parameters are more influential to the output and which are not?

To answer the question of variable filtering, quite a lot of methods have been proposed. The classical maximum entropy principle was applied to estimate the confidence intervals for the TL of rigid walls [Reynders 2014]. A stochastic boundary element method (BEM) was proposed for the calculation of industrial structural acoustic property variation [Amico 2013]. A review of uncertainty assessment methods in vibroacoustics [Ohayon 2014] can also be referred, including the popular hybrid FE-SEA method [Cicirello 2013]. Among the literatures, the best solution for the uncertainty proportion problem probably is the Global Sensitivity Analysis, which is able to describe the influence of each parameters on the variability of the output. Rapidly developed after the 1990s, more and more ANOVA(Analysis of Variance)-based GSA algorithms have been applied in vibroacoustics. As one of the most computational costless algorithm, the Fourier Amplitude Sensitivity Test (FAST) was preferred in acoustic composite material analysis: the study on elastic porous materials and their micro-structures [Ouisse 2012, Doutres 2014] and the study on isotropic single or sandwich panels [Christen 2016]. The first-order sensitivity indices and the total sensitivity indices, together, helped to better identify the most and the least influential inputs on the output uncertainty.

But, as mentioned, the sandwich composite sample, can not be completely treated as the combination of three isotropic layers. Though the optimization and the uncertainty assessment are always imposed on the macroscopic, the meso-structures are extra contents that should must be considered. Quite often when sandwich composite materials are studied, their mechanical parameters are supposed to be normally or uniformly distributed. But with the meso-structures considered, not only the variables' marginal distribution rules can be customized, but also the correlation or dependency can be involved. An advanced FAST algorithm called FASTC (S-FAST), which can take the correlation into consideration, has been tested in a previous publication [Chai 2017]. That piece of work was about sound absorption capacities of elastic porous material with specific micro-structure. Compared to the traditional FAST method, FASTC presents more information on variables' correlation properties and that makes the GSA results more adaptable to real industrial case. But also, that investigation has shown some limitation of using correlation matrix as the only indicator of variable dependency. So another FAST-orig method will be proposed in this piece of work and to be compared with former ones.

The main objective of this work is to take an overall sensitivity analysis to identify the mechanical parameters which have the most contribution on material's acoustic performance uncertainties within different frequency bounds. For the purpose of an intense comparison, multiple core meso-structures and sound transmission models are involved. Including FAST-orig, FASTC and the classical FAST, three

SA methods are applied to ten cases of composite structure models for the uncertainty assessment of three acoustic indicators: TL, transition frequency and critical frequency.

3.2 Acoustic characteristics of sandwich panels

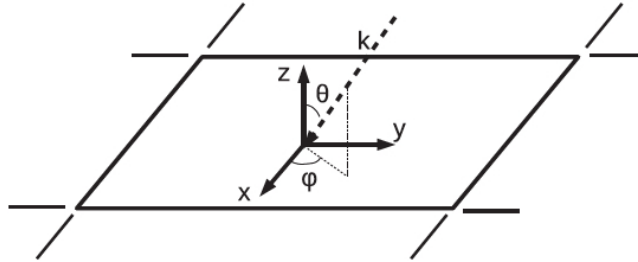


Figure 3.1: Geometric illustration for incident wave towards the face-plate

Concerning the sound transmission properties in sandwich structures, some characteristic indicators should be paid attention on with preference. The sound Transmission Loss (TL) is the most important direct measure of the structural sound isolation capacity, so is preferred as in first order. Then the structural coincidence frequency, it tells the proper working frequency band of this kind of material. And at last, the transition frequency is a meaningful indicator to be estimated for scientific research, which is a direct reference for the choice of vibroacoustical analysis tools.

Mead's model [Mead 1969, Clarkson 1983], Renji's model [Renji 2005] and Guillaumie's model [Guillaumie 2015], are preferred in this work, to estimate the TL, the coincidence frequency and the transition frequency. They are valid in this research case when the two face-plates of the sandwich structure have the same isotropic mechanical properties. Meanwhile, the Guillaumie's model requests that the core layer should also be isotropic, which is not always true under certain meso-structure choices. So for the purpose of precision, Baho's model [Baho 2016] could be more accurate. But in this work Guillaumie's model is finally chosen as an approximation because this model has generally the same inputs as Mead's and Renji's models. This makes the study on variables' correlation characteristics easier.

The input parameters of the three models are: the Young's modulus of the face plate E , the core layer's shear modulus G_{xz} and G_{yz} , the mass per surface area m of the sandwich structure and the damping factor η of the whole structure. Among these inputs, E and η are variables with preset intervals, and m is calculated with the following expression:

$$m = 2\rho_s h_s + \rho_c^{eq} h_c,$$

in which h_s and ρ_s represent respectively the face plate thickness and density, h_c and ρ_c^{eq} represent the core layer thickness and density. Among these variables, ρ_s ,

h_s and h_c are all fixed with preset values while ρ_c^{eq} needs to be calculated along with G_{xz} and G_{yz} depending on which meso-structure is chosen in test.

3.2.1 Mead's model

With a resultant sound wave pressure loading on the panel defined as p , equation of motion in this structure is firstly given by Mead and Markus [Mead 1969] as a beam theory and later developed by Clarkson and Ranky [Clarkson 1983] with several corrections [Mead 1972] and assumptions:

1. The core bending stresses are negligible compared with the face plate direct stresses.
2. The panel motion in the transverse direction for all the three layers is the same.
3. The shear strains in the face-plates in planes perpendicular to the plane of the plate are negligible.

After eliminated the terms above, the equation can be reduced to this form:

$$D_f \nabla^6 w - g'(D_f + D) \nabla^4 w + m\omega^2 \nabla^2 w - mg' \omega^2 w = \nabla^2 p - g' p, \quad (3.1)$$

with ω being the sound wave angular frequency. In the equation, core shear parameter $g' = g(1 + i\eta)(1 - \nu^2)$, $g = 2G/Eh_s h_c$, with the core storage shear modulus usually approximated by $G = \sqrt{G_{xz} G_{yz}}$. $D_f = Eh_s^3/6(1 - \nu^2)$ represents the double face-plate bending stiffness and $D = Eh_s(h_s + h_c)^2/2$ represents the structural bending stiffness.

This equation of motion finally gives this expression of the structural impedance Z equivalent to the one proposed by Narayanan and Shanbhag [Narayanan 1982]:

$$Z(\omega) = \frac{(1 + i\eta)D_f k^6 + (1 + i\eta)g(D_f + D)k^4 - m\omega^2 k^2 - m\omega^2 g(1 - \nu^2)}{i\omega(k^2 + g)}, \quad (3.2)$$

in which the wavenumber is noted as k . Finally the transmission loss is obtained as following:

$$\tau = \left| \frac{P_T}{P_I} \right|^2 = \left| \left(\frac{Z \cos \theta}{2Z_0} + 1 \right)^{-1} \right|^2, \quad Z_0 = \rho_0 c_0, \quad (3.3)$$

$$\text{TL} = -10 \log_{10} \tau. \quad (3.4)$$

Same as in the definition of the wavenumber

$$k = \frac{\omega}{c_0} \sin \theta,$$

θ indicates the angle of incident sound wave respect to the normal direction of the face-plate, shown in Figure 3.1.

3.2.2 Renji's model

This model indicates that it considers especially the shear deformation of the traverse plane due to the traverse shear stresses, and the form of its equation of motion is [Renji 2005]:

$$N\nabla^4 w - m\omega^2 \nabla^2 w + mg\omega^2 + gc\omega = gp, \quad (3.5)$$

with the shear rigidity $N = gD$. Ignoring the imaginary part of D the expression of the structural impedance is given as [Christen 2016]:

$$Z(\omega, \theta) = im\omega \left[1 + \left(\frac{D}{Nc_0^2} \sin^2 \theta - \frac{D}{mc_0^4} (1 + i\eta) \sin^4 \theta \right) \omega^2 \right]. \quad (3.6)$$

It should be mentioned that in equation (3.5) the notation c represents the structural damping coefficient, who has a linear correlation with η . But as the term is later ignored, the damping factor is mainly considered in the shear rigidity N .

3.2.3 Coincidence frequency

Based on Renji's model and his simplification on TL expressions, he provides an analytical formula [Renji 2005] to estimate the coincidence frequencies for sandwich composite panels. This estimation of coincidence frequency takes assumption that no dissipation exists in the panel, which means the damping factor η will not be involved. The formula is given as:

$$f_{c,t}^2 = \frac{c_0^4 m}{4\pi^2 D}, \quad (3.7)$$

where $f_{c,t}$ is an estimation of panel's critical frequency without considering its traverse deformation. And the corrected coincidence frequency f_c is further calculated by:

$$f_c^2 = \frac{f_{c,t}^2}{\left[1 - \frac{c_0^2 m}{N \sin^2 \theta} \right] \sin^4 \theta}. \quad (3.8)$$

But it should be mentioned that this estimation shows quite great error for both Renji's and Mead's model, so in this research the final coincidence frequency value is actually directly obtained from the TL curve.

3.2.4 Transition frequency

In order to make the algorithm of estimating the TF compatible to the inputs mentioned above, the Guillaumie's formula [Guillaumie 2015] is preferred. It supposes that the equivalent core material piece is isotropic, which is not really true in this case of honeycomb structure. Recent research [Baho 2016] shows that in case of

highly orthotropic structure, the error of Guillaumie's formula is about 15%. The expression of TF is:

$$f_t^G = \frac{N}{4\pi} \sqrt{\frac{1}{mD}}. \quad (3.9)$$

The definition of this transition frequency is based on the structural modal density, representing the intersection frequency between the asymptotical pure bending modal density and the pure shear modal density.

3.3 Homogenization of Meso-structures

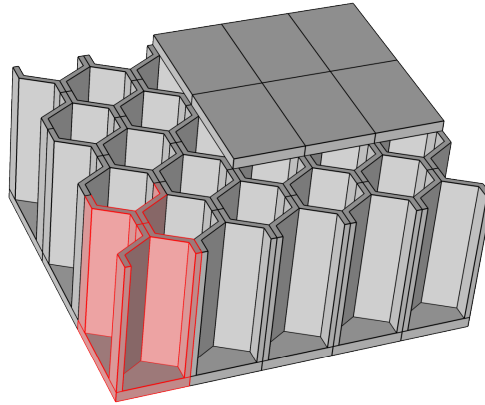


Figure 3.2: Meso-structure for the honeycomb sandwich panel with double vertical thickness

As is indicated before, sandwich composite materials are very preferred in industrial applications for their high rigidity-to-mass ratio. The core layer of a sandwich panel can be filled with porous material or with different kind of 2D, 3D meso-structures in order to maintain its bending stiffness while decreasing the overall mass. Honeycomb is among most popular meso-structures with high space efficiency and mature industrial production procedures. And based on the honeycomb structure, various meso-structures such as triangle, rectangle or rhombus periodic structures can also be easily evaluated via simple deformation.

Required by Mead's and Renji's model, the estimation of equivalent core layer physical and mechanical parameters are necessary. Gibson-Ashby (G-A) model [Gibson 1997] is a classical model with its simple methodology which can be applied on meso-structures with different shapes. And recently, the Gibson-Malek (G-M) model [Malek 2015] is proposed as a correction of Gibson-Ashby for honeycomb meso-structures.

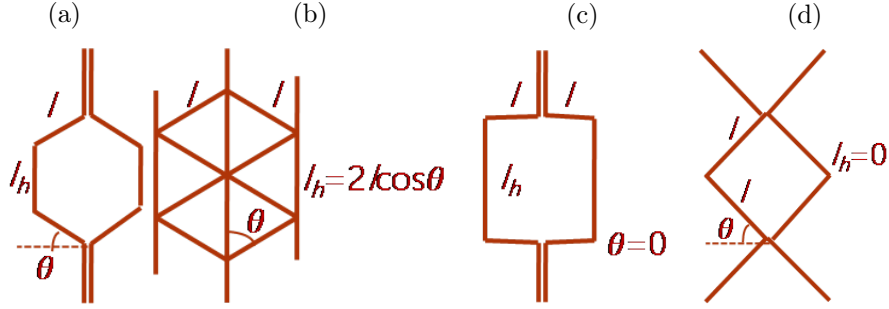


Figure 3.3: Meso-structures of different shapes: (a): double vertical thickness honeycomb, (b): triangle, (c): double vertical thickness rectangle and (d): rhombus

3.3.1 Gibson-Ashby honeycomb structure and its extension

With the Gibson-Ashby model, the equivalent shear modulus, Young's modulus and density per unit surface can be analytically estimated. In this research, the estimation of the shear modulus in 2 directions G_{xz} , G_{yz} and the density m is necessary for further calculation in Mead's and Renji's model. This estimation requires the physical parameters of core material such as the density ρ_c and the isotropic shear modulus G_c , but also several geometric parameters: l , l_h and θ , as presented in Figure 3.3. Exceptionally, the wall thickness of meso-structures is noted t and has a fixed value of 0.2mm in this work.

Supposing that the surface of cross section is a constant value under slight bending or compression deformation, the equivalent density of the honeycomb structure can be easily obtained with some geometric approximations:

$$\frac{\rho_c^{eq}}{\rho_c} = \left(\frac{t}{l}\right) \frac{l + l_h}{(l \sin \theta + l_h) \cos \theta}. \quad (3.10)$$

And the directional shear modulus G_{xz} and G_{yz} are estimated based on these two relationships. When dividing one unit of the meso-structure into several pieces of walls with each the shear strain γ_i , the shear stress τ_i and the pure wall volume V_i :

$$G_{xz} \gamma_{xz}^2 V \leq \sum_i (G_c \gamma_i^2 V_i), \quad (3.11)$$

$$\frac{\tau_{xz}^2}{G_{xz}} V \leq \sum_i \left(\frac{\tau_i^2}{G_c V_i} \right). \quad (3.12)$$

In the equations V represents the total volume of the unit including the pore space. It should be mentioned that the values of γ_i , τ_i and V_i all depend on how the structure is divided, while γ_i and τ_i need to be recalculated for each direction (x-z plane or y-z plane). In the algorithms, G_c is given by $E_c/(1 + \nu_c)$.

Precising the expressions above, it can be obtained that:

$$\frac{G_{xz}}{G_c} = \left(\frac{t}{l}\right) \frac{\cos \theta}{l_h/l + \sin \theta}. \quad (3.13)$$

While for G_{yz} :

$$\begin{aligned}\frac{G_{yz}}{G_c} &\leq \left(\frac{t}{l}\right) \frac{h/l + 2 \sin^2 \theta}{2(l_h/l + \sin \theta) \cos \theta}, \\ \frac{G_{yz}}{G_c} &\geq \left(\frac{t}{l}\right) \frac{l_h/l + \sin \theta}{(1 + 2l_h/l) \cos \theta},\end{aligned}$$

there is an interval of possible values. After several finite elements simulations, one empirical formula is concluded

$$G_{yz} = G_{yz_{lower}} + \frac{0.787}{h_c/l} (G_{yz_{upper}} - G_{yz_{lower}}), \quad (3.14)$$

where the term (h_c/l) should be a value between 1 and 10.

3.3.1.1 Triangle meso-structure

As the last pattern presented in Figure 3.3, all the units are supposed to be equilateral triangles with common walls in y-axis. The definition of the structural geometric parameters are a bit different from the ones of honeycomb structures. Thus the expressions for the equivalent physical parameters are also modified.

$$\frac{\rho_c^{eq}}{\rho_c} = \left(\frac{t}{l}\right) \frac{2(1 + \cos \theta)}{\sin \theta \cos \theta}. \quad (3.15)$$

For the shear modulus, the same process is applied:

$$\frac{G_{xz}}{G_c} = \left(\frac{t}{l}\right) \tan \theta. \quad (3.16)$$

Similarly, an interval is obtained for the value of G_{yz} :

$$\begin{aligned}\frac{G_{yz}}{G_c} &\leq \left(\frac{t}{l}\right) \frac{1 + \cos \theta}{\sin \theta}, \\ \frac{G_{yz}}{G_c} &\geq \left(\frac{t}{l}\right) \frac{4 \cos \theta}{\sin \theta(1 + \cos \theta)}.\end{aligned}$$

As the triangle structure can be simply regarded as a division of the hexagonal structure, the same empirical relationship (3.14) can be applied.

3.3.2 Gibson-Malek honeycomb structure and its deformation

This model is an improvement of Gibson-Ashby model considering some complex elastic deformations at the nodes, the notations are kept as the same in Gibson-Ashby model.

$$\frac{\rho_c^{eq}}{\rho_c} = 1 - \frac{l \cos \theta (l_{h_b} + l \sin \theta)}{(l \cos \theta + t)(h + l \sin \theta)}, \quad (3.17)$$

$$\frac{G_{xz}}{G_c} = \frac{t/l}{(l_h/l + \sin \theta)(\cos \theta + t/l)} \left[\cos^2 \theta \left(\frac{l_b}{l}\right) + 2 \left(\frac{t}{l}\right) \tan \left(\frac{\pi}{4} - \frac{\theta}{2}\right) \right], \quad (3.18)$$

$$\frac{G_{yz}}{G_c} = \frac{t/l}{(l_h/l + \sin \theta)(\cos \theta + t/l)} \left[\sin^2 \theta \left(\frac{l_b}{l} \right) + \frac{l_h}{l} + \left(\frac{t}{l} \right) \tan \left(\frac{\pi}{4} - \frac{\theta}{2} \right) \right], \quad (3.19)$$

in which some specified notations are used:

$$l_b = l - t \tan \left(\frac{\pi}{4} - \frac{\theta}{2} \right); l_{hb} = l_h - t \tan \left(\frac{\pi}{4} - \frac{\theta}{2} \right).$$

3.3.2.1 Double vertical thickness rectangle and rhombus deformation

The estimation of the shear modulus of rectangle and rhombus meso-structures can be simply done by modifying the geometric inputs in Gibson-Malek model, without constructing a new model. For double vertical thickness rectangle meso-structure, the characteristic angle θ is set to be 0, while for rhombus meso-structure, the vertical direction wall length l_h is set to be t . l_h can not be set directly to 0 because L_{hb} will become a negative value.

3.4 Correlation and dependency discussion

Both FASTC and CRM rely on Iman's transform to introduce correlation among samples. This process is known to introduce errors in the obtained correlation coefficients, compared to the objective correlation matrix, especially if the number of samples is too low. Because FASTC requires fewer samples than CRM, the error in the sampling reordering phase may be more important. In our cases, the error on each coefficient is always less than 10%, but the difference could reach 20% with fewer samples. The minimum number of samples is discussed in Iman et al. [Iman 1982]'s work. Secondly, Iman's transform requires only the knowledge of the inputs' marginal distributions and their correlation matrix. This is generally not sufficient to define an n-dimensional co-distribution function. Kucherenko et al. indicated in their paper [Kucherenko 2012] that the definition of a certain copula is needed. In fact, without this copula, the sensitivity index S_i value is often not uniquely defined. As presented in Figure 3.4 and Figure 3.5, the original co-distribution and the approximated one have large discrepancies, although they have similar correlation matrices. This is especially the case for the porosity ϕ , which is not correlated with the other variables in the 2-p micro-macro model. For these parameters, Iman's transform does not provide a good approximation of the original co-distribution, which is used by FASTC.

In authors' former studies, errors have actually already been observed due to Iman's transform. In that case, for a correlated model with 8 inputs, when the inputs' entry positions are changed, their expected SA values get also changed, particularly for these highly correlated parameters. Such phenomenon can not occur in traditional FAST algorithm, so only Iman's transform and its post-treatment can explain these biased SA results. One question is that among these SA results obtained under different conditions, we can't tell which approaches better the theoretic

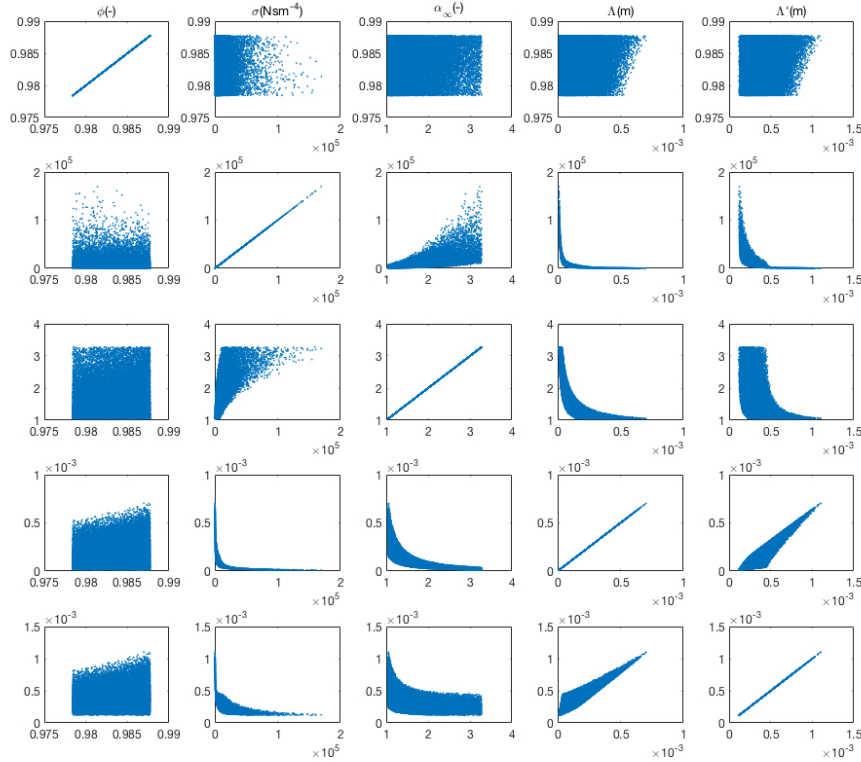


Figure 3.4: Original co-distribution of the 5 variables generated by 2-parameter micro-macro model

one. Errors can be recognized but not be evaluated, which is the major hindrance to the application of FASTC.

A quantification of the error induced by incomplete information can hardly be evaluated only by analyzing the internal mechanism of the algorithm, FASTC, etc.. One way to evaluate it would be to make a direct comparison of the original samples and the reconstructed samples, as presented by Figure 3.4 and Figure 3.5, in a more quantitative way. But this may not be easily feasible for the estimation of SA errors indirectly caused by Iman's transform. The greatest problem is that few of the popular ANOVA-based SA methods use existing samples for sensitivity indexes estimation. Unlike classical Sobol's estimator, neither CRM nor FASTC can be used with MC sampling phase, since it cannot satisfy periodicity or LHS requirements.

3.5 FAST-orig

It has been noticed that the correlated case is not often considered in SA research, as ANOVA actually fails in case of correlated variables. In some limited litera-

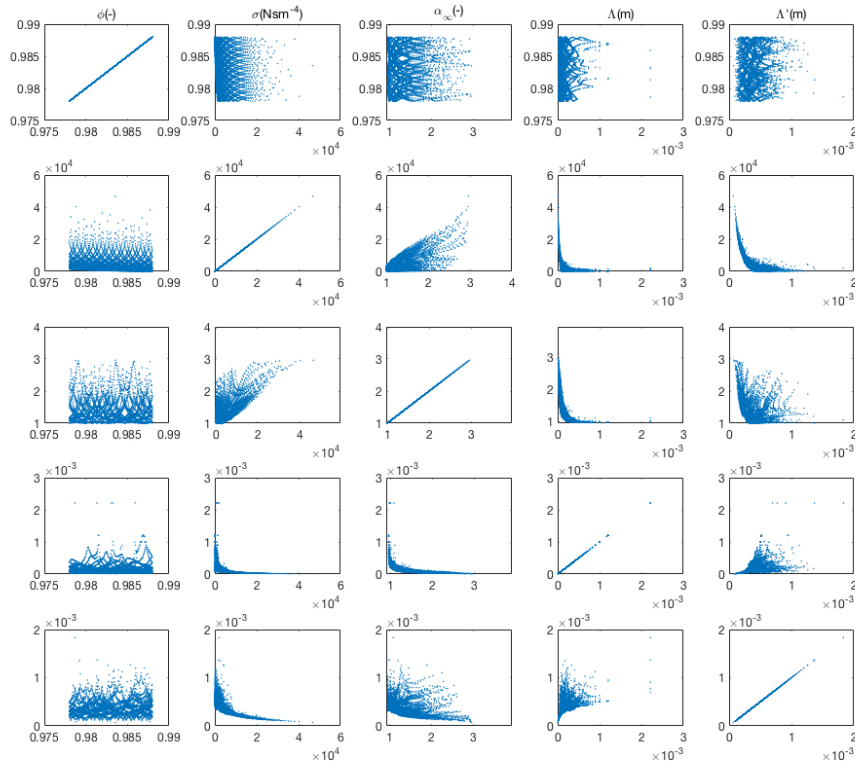


Figure 3.5: Co-distribution of the 5 variables generated by Iman’s transform based on the original correlation matrix of 2-parameter micro-macro model

tures, the FASTC method proposed by Xu and Gertner seems to be an implementable and efficient method for models with limited a priori knowledge. See example [Zheng 2015, Gaspar 2014]

FASTC relies on Iman’s transform [Iman 1982] to construct a set of correlated samples with a certain correlation matrix provided. The conventional FAST procedures are then executed on these correlated samples. Different from the FAST method, the estimation of each sensitivity index requires a reordering of output dataset before the Fourier Transform, which slightly increased the calculation complexity.

In a previous research, some potential error induced by Iman’s transform in FASTC algorithm has been discovered [Chai 2017]. Theoretically, such error represents indeed the difference between dependent variables and correlated variables. As this error can not be self-estimated by FASTC itself, a corrected FASTC algorithm, called FAST-orig, using original samples as datasets, is taken into account for a comparison with FASTC.

Table 3.1: Sensitivity analysis methods

Algorithm	Sampling method	Estimator
FASTC-orig	Original datasets	FFT
FASTC	Periodic sampling + Iman's transform	FFT
FAST	Periodic sampling	FFT

3.6 Identification of inputs' marginal distribution and of their correlation

3.6.1 Variables overview

For these meso-structure models, their inputs samples can be freely defined and the outputs will be used in sensibility analysis upon Mead's and Renji's models. Referring to previous studies [Christen 2016, Baho 2016], several geometric parameters are set to be constant while others are set to be uniformly distributed regarding to certain characteristic indicators. For the uncertainty of inputs, their bounds of variation are uniformly set as $\delta = 20\%$. See Table 5.1 and Table 3.3

Table 3.2: Table of variables and their values

Notation	Variable	Value(variance bounds)	Unit
c_0	Sound speed in air	343.2	m/s
E	Face-plate Young's modulus	$70(\pm\delta)$	GPa
E_c	Core material Young's modulus	see Table 3.3	GPa
h_c	Core layer thickness	20	mm
h_s	Face-plate thickness	1	mm
l	Non-vertical meso-structural length	see Table 3.3	mm
l_h	Vertical meso-structural length	see Table 3.3	mm
t	Meso-structural wall thickness	$0.2(\pm\delta)$	mm
η	Structural damping factor	0.005	-
θ	Meso-structural angle	see Table 3.3	rad
ν	Face-plate Poisson's ratio	0.1	-
ν_c	Core material Poisson's ratio	$0.34(\pm\delta)$	-
ρ_0	Air density	1.27	kg/m ³
ρ_c	Core material density	$2700(\pm\delta)$	kg/m ³
ρ_s	Face-plate density	3050	kg/m ³

Some constraints are applied to E_c , l , l_h and θ to specify the meso-structures and to unify the equivalent structural mass and stiffness.

Though the variables defined in Table 5.1 and Table 3.3 are all uniformly distributed, the outputs of the meso-structure homogenization model, same as the inputs of sandwich panel sound transmission model, the G_{xz} , G_{yz} and m may not be generated with uniform distribution. So with five different meso-structures, their

Table 3.3: Table of variables' bounds chosen for different meso-structures

Variable	G-A	Triangle	G-M	Rectangle	Rhombus	Indicator
E_c (GPa)	$18 \pm \delta$	$37 \pm \delta$	$17 \pm \delta$	$17 \pm \delta$	$17 \pm \delta$	$G_{xz} + G_{yz} = 0.8 \text{GPa}$
l (mm)	$2.45 \pm \delta$	$6.05 \pm \delta$	$2.6 \pm \delta$	$2.5 \pm \delta$	$3.4 \pm \delta$	$\bar{m} = 12 \text{kg/m}^3$
l_h (mm)	$2.45 \pm \delta$	-	$2.6 \pm \delta$	$5.4 \pm \delta$	$0.2 \pm \delta$	depends on the shape
θ (rad)	$\pi/6 \pm \delta$	$\pi/3 \pm \delta$	$\pi/6 \pm \delta$	0	$\pi/4 \pm \delta$	depends on the shape

probability density functions (pdf) as well as their correlation properties should be measured separately. Such information is not only useful for deeper investigation into meso-structure models, but also necessary for the application of FAST series SA methods.

3.6.2 Correlated variables

In this section the marginal distribution details and the correlation properties of the homogenized physical parameters G_{xz} , G_{yz} , m , etc. are separately presented in order of different core layer meso-structures: Gibson-Ashby honeycomb, Figure 3.6 and Matrix (3.20); Gibson-Ashby triangle, Figure 3.7 and Matrix (3.21); Gibson-Malek honeycomb, Figure 3.8 and Matrix (3.22); Gibson-Malek rectangle, Figure 3.9 and Matrix (3.23); Gibson-Malek rhombus, Figure 3.10 and Matrix (3.24).

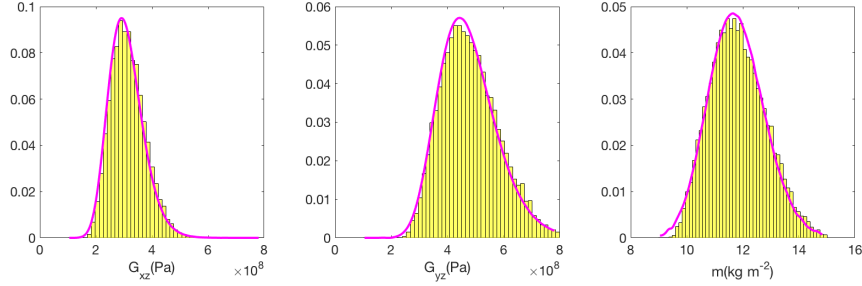


Figure 3.6: Marginal distribution of variables generated by Gibson-Ashby double vertical thickness hexagon model (yellow bars) and its mathematical approximation (magenta line)

$$\begin{matrix} & E & G_{xz} & G_{yz} & m & \eta \\ \begin{matrix} E \\ G_{xz} \\ G_{yz} \\ m \\ \eta \end{matrix} & \left[\begin{array}{ccccc} 1 & 0.01 & 0.00 & 0.00 & -0.01 \\ 0.01 & 1 & 0.58 & 0.44 & -0.00 \\ 0.00 & 0.58 & 1 & 0.57 & -0.01 \\ 0.00 & 0.44 & 0.57 & 1 & -0.01 \\ -0.01 & -0.00 & -0.01 & -0.01 & 1 \end{array} \right] & & & & \end{matrix} \quad (3.20)$$

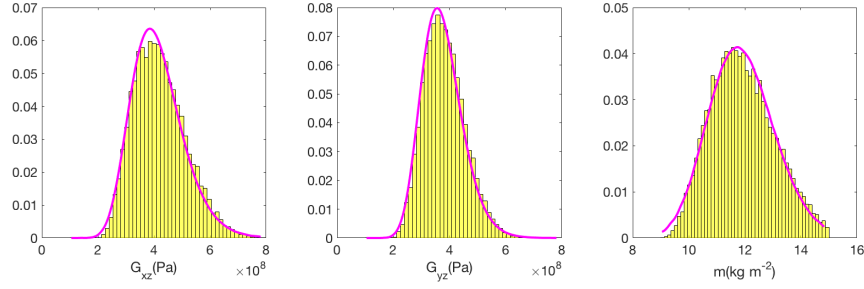


Figure 3.7: Marginal distribution of variables generated by extended Gibson-Ashby triangle model (yellow bars) and its mathematical approximation (magenta line)

$$\begin{array}{c} E \\ G_{xz} \\ G_{yz} \\ m \\ \eta \end{array} \begin{bmatrix} E & G_{xz} & G_{yz} & m & \eta \\ 1 & 0.01 & 0.01 & 0.01 & 0.00 \\ 0.01 & 1 & -0.15 & 0.65 & 0.00 \\ 0.01 & -0.15 & 1 & 0.16 & -0.00 \\ 0.01 & 0.65 & 0.16 & 1 & -0.01 \\ 0.00 & 0.00 & -0.00 & -0.01 & 1 \end{bmatrix} \quad (3.21)$$

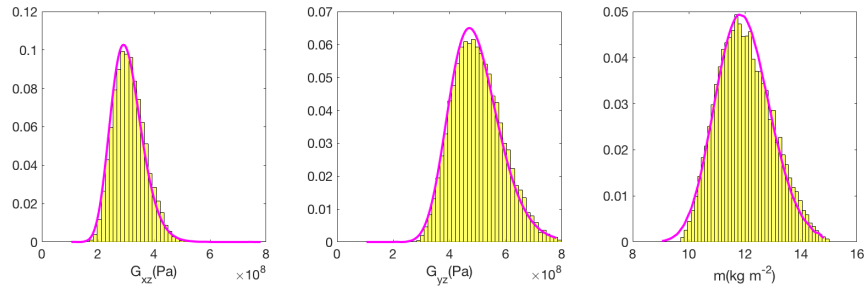


Figure 3.8: Marginal distribution of variables generated by Gibson-Malek double vertical thickness hexagon model (yellow bars) and its mathematical approximation (magenta line)

$$\begin{array}{c} eta \\ G_{xz} \\ G_{yz} \\ m \\ \eta \end{array} \begin{bmatrix} E & G_{xz} & G_{yz} & m & \eta \\ 1 & -0.00 & -0.00 & 0.01 & -0.00 \\ -0.00 & 1 & 0.68 & 0.51 & 0.02 \\ -0.00 & 0.68 & 1 & 0.61 & 0.01 \\ 0.01 & 0.51 & 0.61 & 1 & 0.01 \\ -0.00 & 0.02 & 0.01 & 0.01 & 1 \end{bmatrix} \quad (3.22)$$

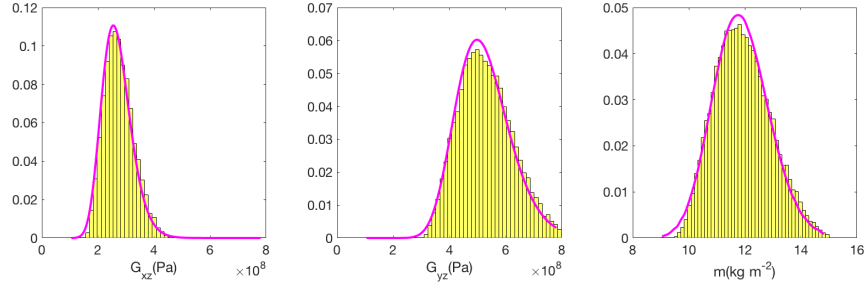


Figure 3.9: Marginal distribution of variables generated by deformed Gibson-Malek double vertical thickness rectangle model (yellow bars) and its mathematical approximation (magenta line)

$$\begin{matrix} & E & G_{xz} & G_{yz} & m & \eta \\ \begin{matrix} E \\ G_{xz} \\ G_{yz} \\ m \\ \eta \end{matrix} & \begin{bmatrix} 1 & -0.00 & 0.00 & 0.00 & -0.01 \\ -0.00 & 1 & 0.66 & 0.53 & -0.00 \\ 0.00 & 0.66 & 1 & 0.63 & -0.01 \\ 0.01 & 0.53 & 0.63 & 1 & -0.01 \\ -0.01 & -0.00 & -0.01 & -0.01 & 1 \end{bmatrix} \end{matrix} \quad (3.23)$$

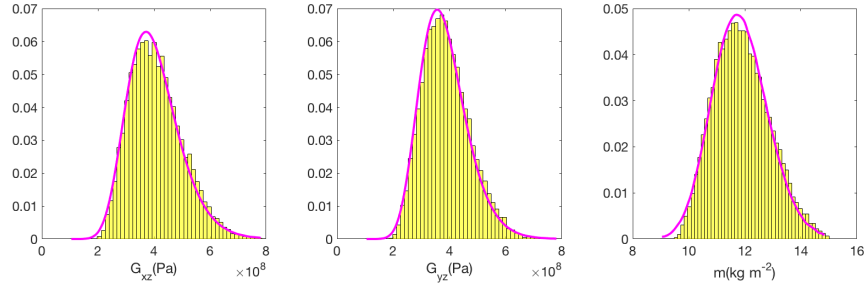


Figure 3.10: Marginal distribution of variables generated by deformed Gibson-Malek rhombus model (yellow bars) and its mathematical approximation (magenta line)

$$\begin{matrix} & E & G_{xz} & G_{yz} & m & \eta \\ \begin{matrix} E \\ G_{xz} \\ G_{yz} \\ m \\ \eta \end{matrix} & \begin{bmatrix} 1 & 0.00 & -0.00 & 0.01 & 0.01 \\ 0.00 & 1 & 0.15 & 0.51 & 0.00 \\ -0.00 & 0.15 & 1 & 0.47 & 0.01 \\ 0.01 & 0.51 & 0.47 & 1 & 0.00 \\ 0.01 & 0.00 & 0.01 & 0.00 & 1 \end{bmatrix} \end{matrix} \quad (3.24)$$

Referring to figures and correlation matrices, some interesting details can be found for these meso-structures. Comparing the marginal distributions graphs of G_{xz} , G_{yz} and m , two pattern of distributions can be recognized. One pattern is presented by the double vertical thickness hexagon and rectangle meso-structures,

with obvious different mean values for G_{xz} and G_{yz} . The other pattern by the triangle and rhombus meso-structure, with similar G_{xz} and G_{yz} value and distribution rules. Such difference shows clearly that the double vertical thickness industrial design can greatly increase the value of G_{yz} and increase the level of orthotropy in a macroscopic view.

Interestingly, the correlation properties among these variables seems to have similar relations with the meso-structures. Firstly, the structural density m is always strongly correlated to the shear modulus G_{xz} and G_{yz} . It can easily be understood as the rigidity is generally related to the compactness for a same piece of material. Secondly, the correlation index between the two shear modulus depends on whether the meso-structure has double vertical thickness wall or not. If so, the shear modulus are strongly correlated, which means the structural stiffness are generally equally enforced in each directions, while the pore shape seems to be less important. If not, the shear modulus are weakly (rhombus) or even negatively (triangle) correlated, which shows the importance of pore shape deformation on the overall structural physical properties.

As in preset, the face-plate Young's modulus E and the structural damping factor η are uniformly distributed, so there's no need to study their marginal distribution properties.

3.7 Results comparison and discussion

As the mean value of the homogenized sandwich panel physical parameters are controlled to be the same for each case, only one evaluation on the overall sound transmission performance is enough. The Figure 3.11 has also shown the coincidence frequency at about 600Hz and the transition frequency at about 1050Hz. At the coincidence frequency, the minimum transmission loss is down to 10dB with a relative high normalized standard deviation, which indicates the necessity of executing uncertainty analysis around this frequency.

As introduced before, two sound transmission models combined with five different meso-macrostructures form in total 10 cases. The 10 sets of SA results are divided into two sections based on the sound transmission models. Generally similar trends of transmission loss curve can be recognized in each section.

For each variable of these 10 models, three SI curves are given by FAST, FSATC and FAST-orig, representing GSA results with different levels of parametric dependency acknowledgements: FAST means the ignorance of dependency; FSATC means a rough estimation with only the correlation coefficients considered; FAST-orig means taking full consideration of parametric dependency. Computationally FAST is the most efficient while theoretically FAST-orig should give the nearest estimation of analytical sensitivity indices. Thus the comparison of GSA results in this section will be focused on balancing their efficiency and accuracy and to discuss the compatibility of each algorithm.

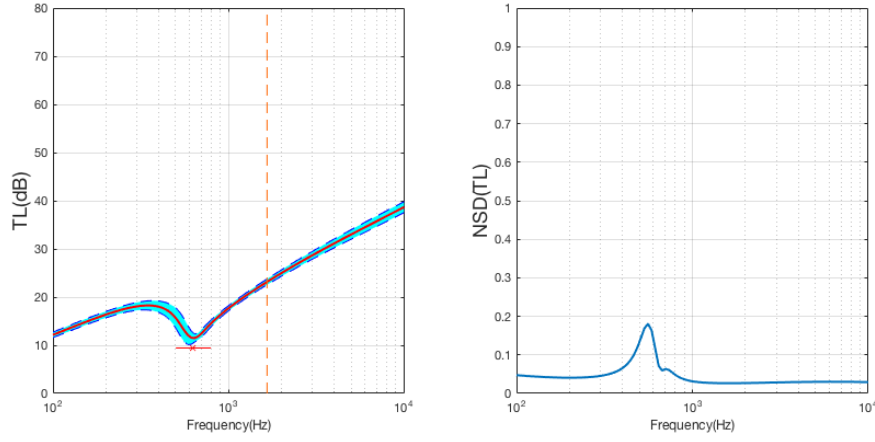


Figure 3.11: Transmission loss estimated by Mead’s model with correlated inputs (similar for all meso-structures). Left: mean value \pm standard deviation and transition frequency; right: normalized standard deviation.

3.7.1 SA results on Mead’s model

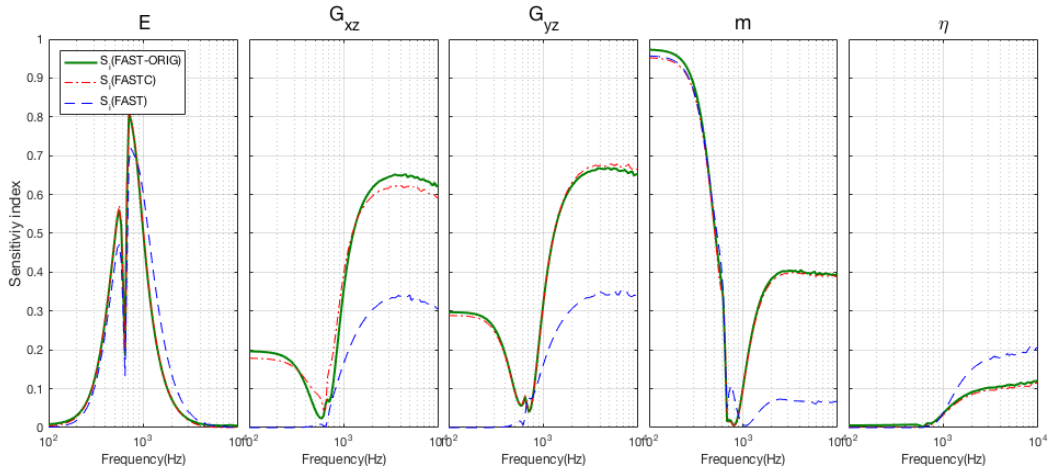


Figure 3.12: SA results for Mead’s model with correlated inputs (Gibson-Ashby double vertical thickness hexagon model) by different methods.

Regarding the SA curves for each variables, the first point that to be mentioned is the particular evolution trend of SI curve for E the Young’s modulus. This is the only variable that has an important influence on the output around the coincidence frequency. With or without correlation, at the coincidence frequency, the sum of the first-order SI is far lower than 1, which means quite complex high-order interaction effects are hidden behind the mechanism.

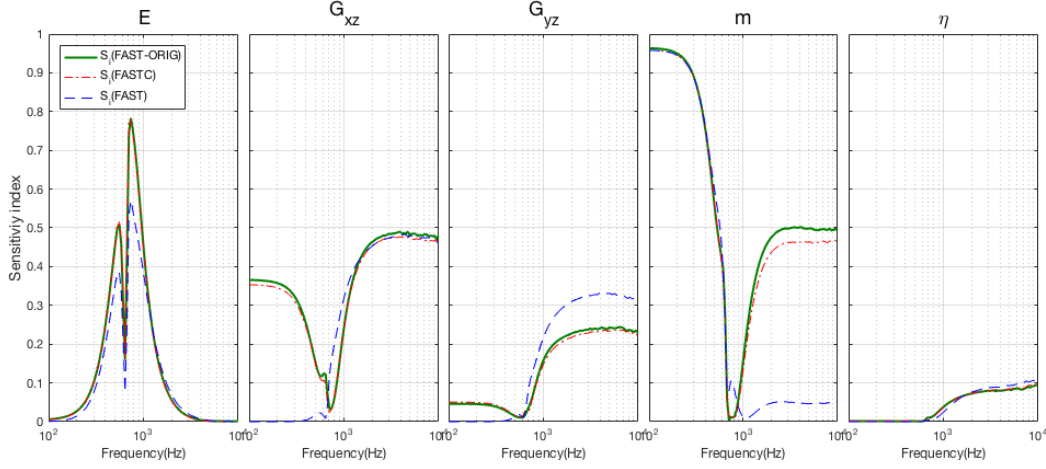


Figure 3.13: SA results for Mead's model with correlated inputs (extended Gibson-Ashby triangle model) by different methods.

With the correlation effect involved, the SA curves for G_{xz} , G_{yz} and m all have a "V" shape, which present their solid influence on TL in the frequency bands before and after the coincidence frequency. The importance of the three inputs are quite different for different meso-structures, one could be more important on certain frequency band but less important on another band. The only common point is that m the density keeps to be the dominant factor at low frequency band, which has a good agreement with the basic theory of mass law.

Regarding the curves obtained by the classic FAST method, it can be seen that with the correlation effect, the value of these sensitivity indices have been greatly changed. Noticed that both positive and negative correlation exists among the variables, their effects reflected on the SA curves can also be positive or negative. But the correspondence is not absolute, positive correlation can result to decrease of sensitivity index or even no change at all. And relatively, when looking at the SA curve of η the damping factor, its SA curves are obviously compressed when the correlation among other variables are taken is into consideration.

A bit different from other meso-structures, only in case of the Gibson-Ashby triangle model the two shear modulus G_{xz} and G_{yz} have apparent different value in the whole frequency interval. Similarly, only in this meso-structure G_{xz} has a non-negligible importance on the structural coincidence frequency. Such special properties may be caused by the fixed rigid walls in y-axis of the triangle meso-structure, which has a major contribution to the overall structural rigidity.

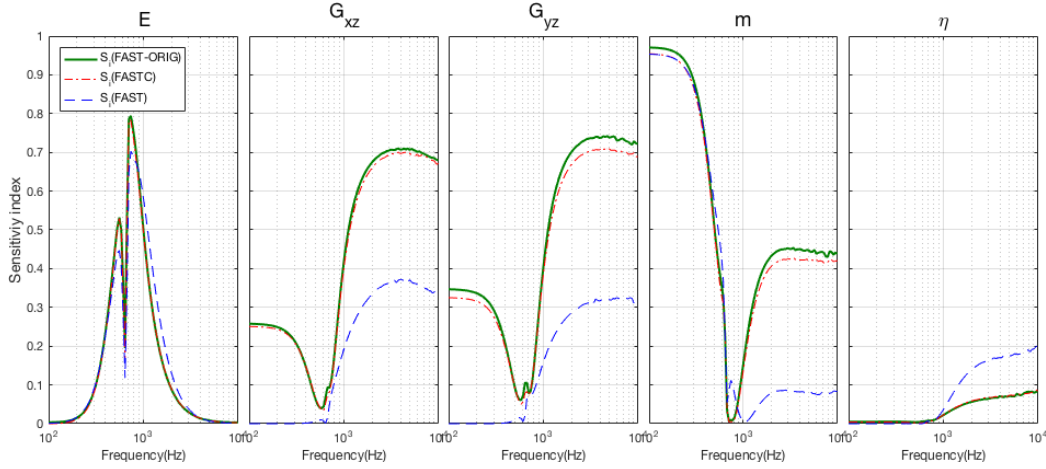


Figure 3.14: SA results for Mead's model with correlated inputs (Gibson-Malek double vertical thickness hexagon model) by different methods.

3.7.2 SA results on Renji's model

Compared with Mead's model, the charts obtained by Renji's model seems to be quite different, in many aspects.

As for the SA curves of the five inputs, compare to the ones of Mead's model, only few similar features can be recognized in the curves of E and η . In most cases even the basic forms of the curves are totally different. Especially for the SA curves of the shear modulus G_{xz} and G_{yz} , they have both an "W" shape curve, with one extreme at the coincidence frequency and another at around the transition frequency. For Mead's model, the SI curve become relatively stable when above the transition frequency, while for Renji's model, no similar features can be observed.

For the sensitivity indices estimated with Mead's model, the correlation properties among variables mainly increase their value, while for Renji's model, FASTC and FAST-orig methods always give a lower SI estimation than FAST. Such phenomenon indicates again the unpredictable effects caused by the correlation properties.

Other points conveyed by these charts, including the NSD properties, SA results of coincidence frequencies and specialty of the triangle meso-structure, are similar to the ones described in Mead's model.

3.7.3 SA results on structures' transition frequencies

For a sandwich panel, in the structural aspect, the rigidity-to-mass property is always the most important quality criteria. Here the rigidity includes not only the compression rigidity, but also the shear rigidity, which reflects mainly on the

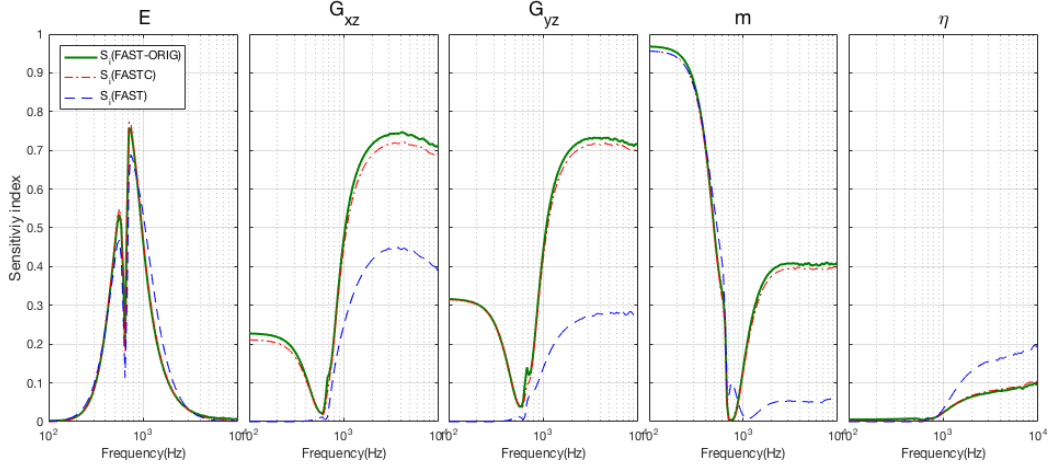


Figure 3.15: SA results for Mead's model with correlated inputs (deformed Gibson-Malek double vertical thickness rectangle model) by different methods.

transition frequency of the vibroacoustic material. This frequency is adjusted to be a fixed value for comparison purpose in this piece of work. But still if considering its uncertainty, as shown in Figure 3.22, the value of transition frequency is shown to be quite sensitive to G_{yz} the shear modulus in x-axis for the uncorrelated case, except for the rhombus meso-structure. Such results are pretty easy to understand as the hexagon and rectangle meso-structures both have double vertical thickness design while the triangle structure has fixed vertical walls as basic shape.

But when the correlation is considered, it can be seen that actually the shear modulus G_{xz} has also great potential influence on the transition frequency, as the correlation between these 2 shear modulus objectively exists in most cases. Here the only exception is the triangle meso-structure, where the correlation amplified mainly the importance of m the density but not G_{xz} . Such facts indicate the possibility that for such meso-structure based on vertical walls, the thickness of the walls, rather than the deformation of substructures, has greater influence on the structural shear rigidity.

3.8 Chapter conclusion

This chapter presents an investigation of two ANOVA-based GSA algorithms: FASTC and FAST-orig, on vibroacoustic models with internally correlated inputs. The purpose is to find out how the variables' correlation and dependency properties can influence the GSA results, and to make a comparison between the two algorithms.

The correlated samples for the sound transmission models, are firstly generated by two different core layer homogenization models. These samples, with their

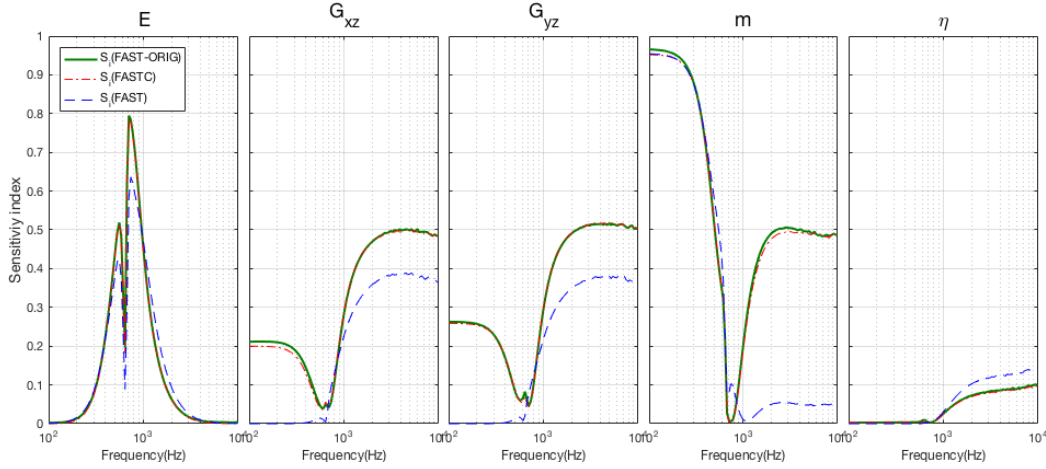


Figure 3.16: SA results for Mead's model with correlated inputs (deformed Gibson-Malek rhombus model) by different methods.

marginal distribution and correlation properties well retrieved, are then thrown into sensitivity analysis. In this piece of work, five different meso-structures and two different sound transmission models are studied so finally in total 20 sets of sensitivity analysis results are obtained.

Under a general view of the GSA results, the face-plate rigidity and the structural density both are the most critical factors for the sandwich panel's transmission loss and coincidence frequency. While for the transition frequency, the two directional shear modulus own dominant roles, especially with the correlation and dependency properties counted. Such results means that in most cases these are the variables that should firstly be controlled in order to limit the output's uncertainty. The core meso-structures do have affects on the panel's SA results, though may not as great as those caused by different sound transmission models. The variables' marginal density functions and correlation matrices finally turn into relative floating variation features on their SA curves. This phenomenon is especially obvious for the sensitivity indices values of the shear modulus. It confirms the necessity of distribution and correlation study before the execution of GSA.

For the comparison between Mead's and Renji's model, the SA results indicate that they are two wholly different models. Not only their SA curves have different patterns, their average TL curves can not even match each other, for a same piece of material. Their differences are mainly represented at the estimation of coincidence frequency and the TL curve trend at mid-high frequency. Further numerical simulation or experiments are required to tell the accuracy of these two models.

As for the comparison among GSA algorithms under condition of parametric dependency, FAST, FASTC and FAST-orig are compared in the aspects of accuracy and acomputational efficiency. Quite obviously FAST is not suitable for correlated variables as its SI estimations are far from the ones obtained by the other two algorithms. While for FASTC and FAST-orig, theoretically FAST-orig can give the most

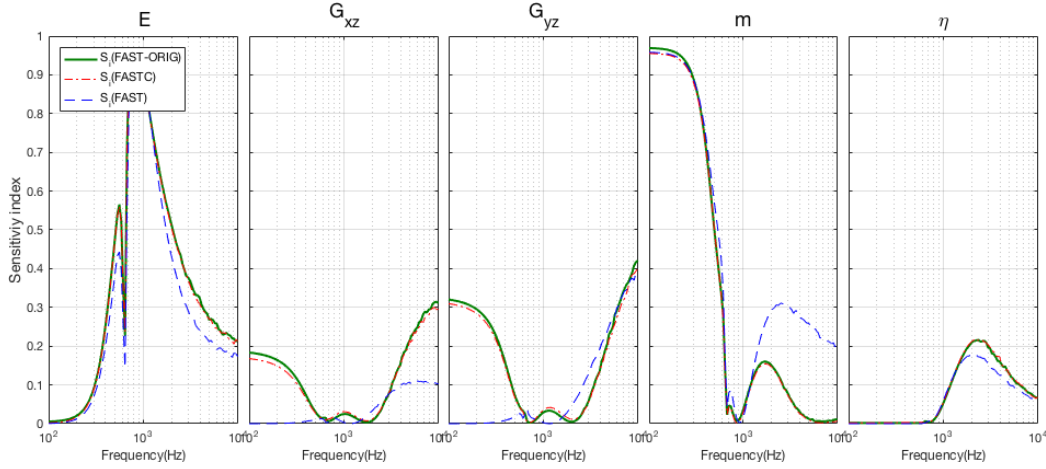


Figure 3.17: SA results for Renji's model with correlated inputs (Gibson-Ashby double vertical thickness hexagon model) by different methods.

accurate estimation and FASTC can only give one of the solutions for non-unique ANOVA-HDMR. It is almost impossible to self-evaluate the results of FASTC, thus this set of SI could be coincidentally the correct one or more possibly not very exact ones. Shown in the cases studied in this chapter, FASTC and FAST-orig gave very similar results, which means at least in this model of vibroacoustic sandwich panel, SIs calculated by FASTC are totally acceptable. Thus the preference between FASTC and FAST-orig mostly depends on their compatibility. For tests with full datasets given, FAST-orig is the theoretical best solution with an extremely high calculation efficiency, and for others with limited information, FASTC is an acceptable solution which can be easily applied on various cases.

Still there are concerns left to be reviewed. The most important one, is the core meso-structure, which is becoming more and more complex with the development of manufacturing technologies. More and more structures can no longer be analytically evaluated to obtain their homogenized mechanical parameters. Thus, finite element methods are more and more required, which can easily exceed the calculation capacity of personal computers using these ANOVA-based GSA algorithms. The solution of the calculation efficiency problem requires efforts in different domains.

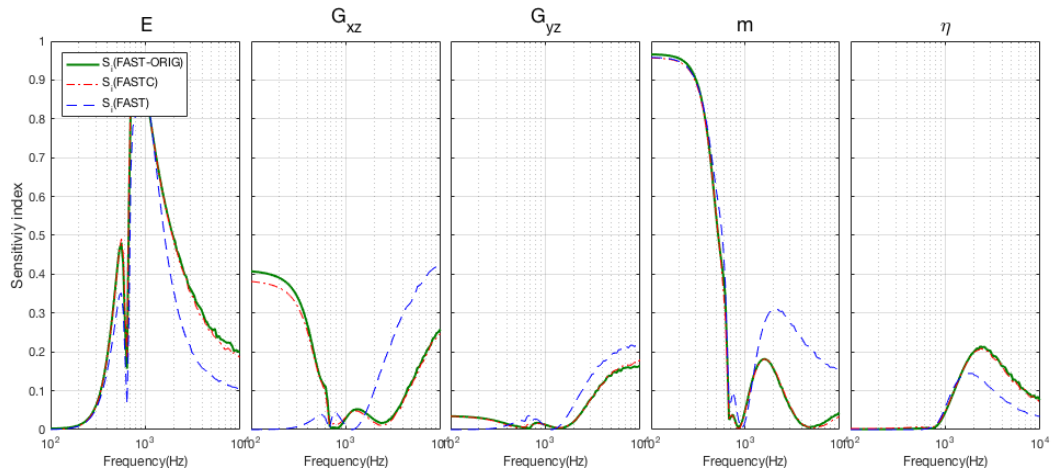


Figure 3.18: SA results for Renji's model with correlated inputs (extended Gibson-Ashby triangle model) by different methods.

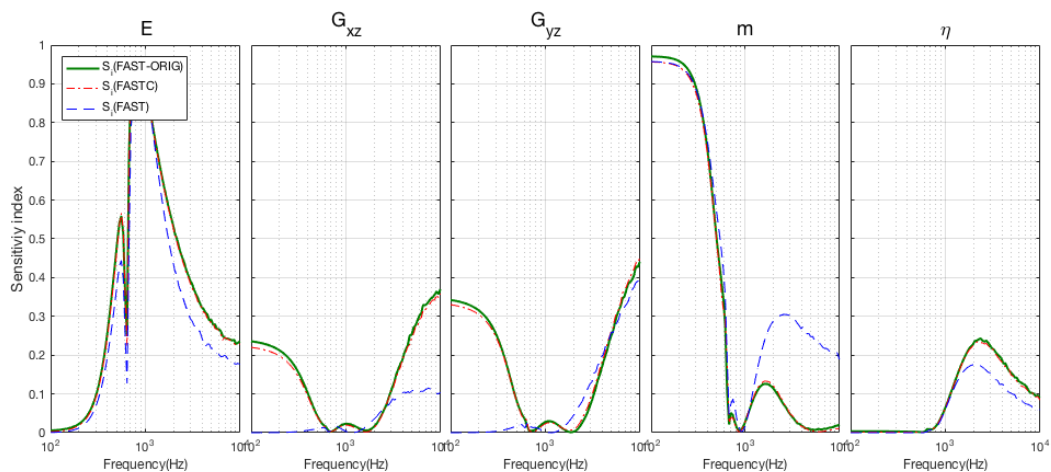


Figure 3.19: SA results for Renji's model with correlated inputs (Gibson-Malek double vertical thickness hexagon model) by different methods.

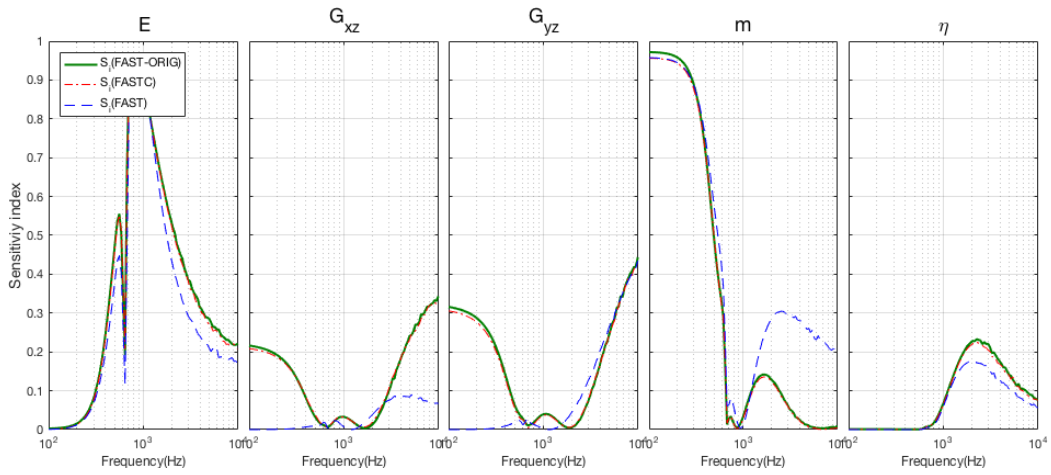


Figure 3.20: SA results for Renji's model with correlated inputs (deformed Gibson-Malek double vertical thickness rectangle model) by different methods.

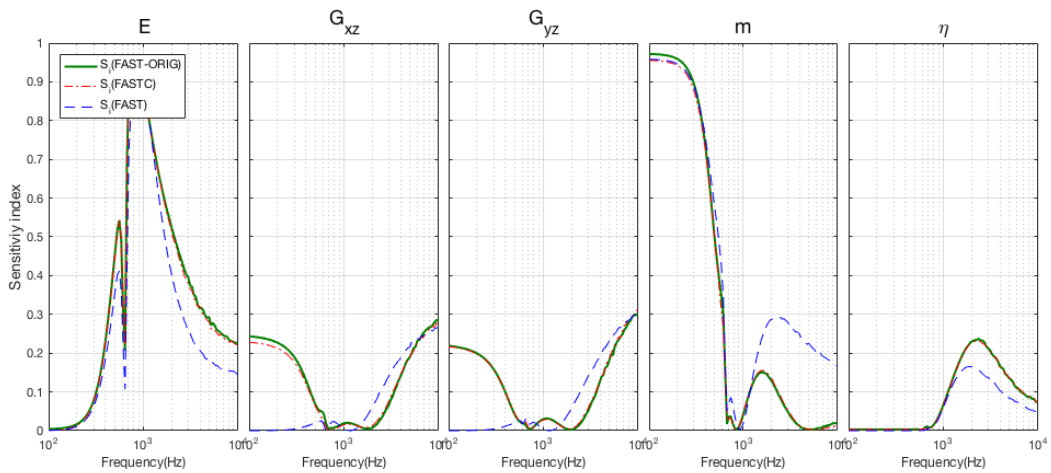


Figure 3.21: SA results for Renji's model with correlated inputs (deformed Gibson-Malek rhombus model) by different methods.

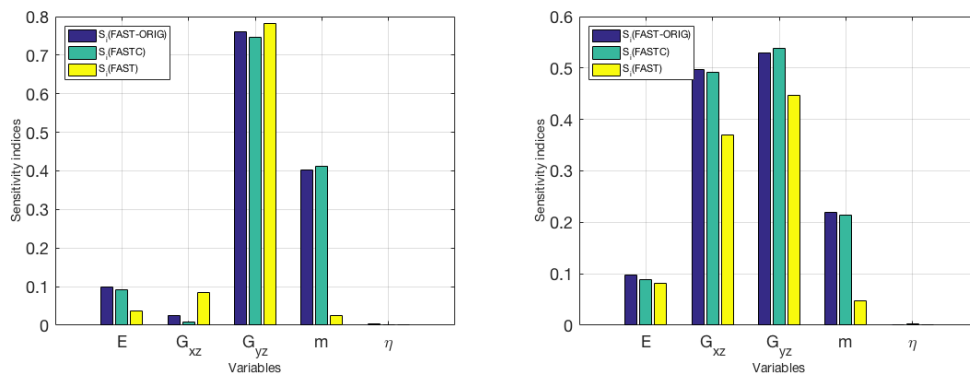


Figure 3.22: SA results of transition frequency with correlated inputs by different methods. Left: triangle meso-structure, right: other meso-structures.

Part 1: Conclusions

Though chapter 2 and chapter 3 are all named 'Global sensitivity analysis on XXX materials', the actual main roles of Part 1 are these FAST series sensitivity analysis algorithms. The two models taken into analysis are both simplified analytical models of acoustic materials that already exists for decades. Together, they constructed a platform where we have some primitive constraints on sampling strategies and these advanced FAST algorithms with correlation design can then be tested and compared.

All the ANOVA-based sensitivity analysis algorithms mentioned in this chapter are CRM, FAST, FAST-c and FAST-orig, among which CRM and FAST are traditional algorithms, FAST-c is a recently proposed one and FAST-orig is actually original. These algorithms perfectly present the evolution of ANOVA-based GSA algorithms: from FAST which can only treat periodic datasets without correlation, to CRM which firstly used Iman's transform to construct correlated samples and successfully calculated the sensitivity indices, then FAST-c combined their essence of Fourier amplitude test and Iman's transform, finally FAST-orig completed FAST-c by fixing the bug of correlation and dependency.

The saying that the FAST series algorithms are the main roles of this first part doesn't mean that the results of sensitivity analysis are of no use. In opposition, applications of GSA methods on models with preliminary acknowledgements are totally reasonable. Same as in the domain of deep learning, the statistical results obtained by these various algorithms can only become scientific when they are analyzed together with analytical or empirical evidence. Such examples can be widely found in the development of AI algorithms, where the most valuable final step is always a competition or a test executed by human-beings. Thus, as a kind of statistical method that has not yet been very commonly used, it's somehow necessary to use two traditional cases for its self-proof, and moreover, these FAST algorithms do provide some interesting new details.

Apart from all these definitions and theories and formulas, this part of thesis established the basic structure of GSA applications on structural dynamics. Some key steps are: preliminary study and parameter configurations; correlation design and the generation of sampling curves; parallel calculation and efficiency evaluations; statistical post-treatment and SA results comparisons. For a complete research using GSA algorithms, these steps are absolutely necessary and are the basis of any potential improvements.

Part II

Extended applications of GSA methods

Part 2: Introduction

Originality is always considered as a premium factor in scientific researches. In chapter 2 of part 1, we have an analytical physical model and a newly developed but not original algorithm, and their first met is reported. It's like organizing a date for two opponents and the originality is the occurrence of first date for those who have never met each other before. While in the next chapter, a new opponent comes and with its preference we make a new hairstyle for the FAST-c algorithm, the positive effect of this new hairstyle is the main originality of this chapter. In this part of work, the main direction will not change but to organizing more dates between GSA methods and structural dynamic systems, but more originalities must be discovered.

In the previous part, with two examples of application, the main structure of our scientific research procedures has been presented in four steps. There are preliminary studies of the model and the methods, which have occupied quite long text before, while in this part of work more attention will be paid on the interactions between physical models and GSA methods. Deeper investigations into some certain steps of GSA applications will be the main theme of this part of thesis.

In the previous part, actually quite a lot of background information have been given, concerning GSA, FAST, periodic acoustic structures, etc.. Based on these information, several questions may worth a discussion. For example, GSA as an uncertainty quantification tool, though under a rapid increasing trend, can still only occupy 1% of all publications in the category of sensitivity analysis, while some other data based methods such as data mining algorithms has grown into incredible popularity in recent decades, what makes the difference between them? This question could be very difficult to answer in global view, but some microscopic comparison could possibly be made, in some specific domains. And also for our DySCo group in LTDS, various periodical or non-periodical structures are under the study of tens of researchers, thus in the aspect of technical supporter, how should these GSA algorithms be properly chosen and configured for different models with different needs? Should some new functions be developed for some specific structures? With the basic acknowledgements of GSA applications in part 1, these details do worth a discussion.

Already mentioned above, this part of thesis will be written in a less organized way where no common thread can be found among the chapters, they are like side branches which enrich the whole thesis. Taking the fast boat of machine learning, chapter 4 will present a comparison between FAST and Random Forest (RF), their pros and cons in case of uncertainty quantification will be discussed. Chapter 5 will introduce an incomplete original FAST series algorithms specifically designed for

periodical structures, many details of FAST algorithm are re-designed. And lastly the chapter 6, which is an assemble of all other small pieces of works in laboratory, represents the view of various physical models in the aspect of a data analyst.

When Global Sensitivity Analysis meets Random Forest

Contents

4.1 Chapter introduction	61
4.2 Special properties of Random Forest	63
4.2.1 Classification And Regression Trees	63
4.2.2 Out-Of-Bag validation and its variable importance selection	64
4.3 Experimental design	65
4.3.1 Acoustic transmission loss of sandwich panels	65
4.3.2 Choice between analytical models	65
4.4 Results comparison and discussion	66
4.4.1 Analytical model dataset	67
4.4.2 WFE model dataset	68
4.4.3 Discussion	69
4.5 Chapter conclusion	69

4.1 Chapter introduction

The trend of increasing complexity of mathematical models in various domains has resulted increased uncertainties both in model parameters and model structures. Whereas the uncertainty in inputs may often reflect directly on the output, the need for model uncertainty quantification has been so far highly raised. Concentrated on analytical expressions, Sensitivity Analysis (SA) is a traditional way to get the uncertainty of output explained by the uncertainties of inputs. Fixing all variables except one certain to observe its influence on the output, which is exactly the spirit of Local Sensitivity Analysis (LSA), has already been performed by scientists and engineers through thousands of years along the history. Later entering the electronic era, with the support of computational calculation capacity, some more stochastic algorithms and data-based algorithms have been developed and have got apparent advantage towards old LSA methods.

Global Sensitivity Analysis (GSA), namely being distinguished as the opposite conception of Local Sensitivity Analysis, is a category of advanced SA methods. The

key point of GSA is to vary all the inputs together and to study their sensibility at the same time using the same datasets. Such kind of approach makes it possible to estimate the interaction effect among variables [Sobol 2001] and to avoid the curse of dimensionality [Bellman 1957]. Literally, GSA methods can be applied on no matter what mathematical models with quantitative inputs and outputs. Beginning by some applications in chemistry [Saltelli 2005], GSA has been proved effective in civil engineering [Gaspar 2014], climate change [Zheng 2015], safety measurements [Borgonovo 2003], etc. Fourier Amplitude Sensitivity Test (FAST) algorithm, firstly proposed by Cukier and Markus [Cukier 1973] and specially mentioned here, is one of the most efficient GSA algorithms. It can calculate Sensitivity Indices (SIs) based on a unique analytical expansion of ANOVA (ANalysis Of VAriance). Some recent case of its applications in vibroacoustics can be found [Christen 2016]. In general, GSA methods help to indicate the variables who have priority to get fixed or paid on attention for model optimization and condensation.

While as GSA mainly serves for metamodelling, data mining models themselves are metamodels, based on great number of samples. As other metamodels, they can do estimations and predictions (classifiers and regressioners), and are also capable for some extra functions such as clustering. But the application of these models generally don't relies on preliminary studies such as GSA, they often regards the uncertainty of inputs as part of the models themselves. And for some algorithms, Random Forest (RF) for example, it can further rank the importance of inputs after the constructions of metamodels, based on how easily the estimation will get wrong if some certain inputs get disturbed. With the explosion of data size on the Internet, these data-based methods become highly recommended. Instead of traditional mathematical tools, data mining and deep learning have become the main tools for data analysts either in industry or for research. Not only in informational industries, the use of RF can be found everywhere: geography [Belgiu 2016], biology [Jia 2016], sociology [Khan 2017] and so many others. The feature importance selection function of RF don't really have any analytical basis such as a formula, but it gives some most direct indications on how serious problem the uncertainty of the inputs can result in.

Got the point that both the analytical GSA methods and data-based Deep Learning methods can do the job of uncertainty identification, some interesting comparison can then be launched. Regarding to the acoustic background of the datasets in this paper, some publications can be referred to: application of FAST on analytical models of sound transmission [Christen 2017] and application of RF on numerical datasets of sound emission [Morizet 2016] for example. Conducted from these research cases, some impressional properties can be drawn on FAST and RF. In the aspect of theoretical basis, FAST seems to be more analytically solid while RF gives a more practical definition of sensitivity indicator. In the aspect of scientific applications, FAST is a tool of preliminary study and RF is a metamodeller. And in the aspect of advantage/disadvantage, FAST is fast yet too statistical, and RF is functionally strong but without a convincing theoretical basis. So somehow a comparison between these two algorithms can give researchers a bit of inspiration

of how to cover each others' weakness as well as to maintain their advantages.

4.2 Special properties of Random Forest

Random Forest (RF) is a machine learning algorithm proposed by Breiman [Breiman 2001], mainly to solve classification and regression problems. The basic structure of this method is to construct multiple different decision trees and to get them voting for a most reasonable estimation, as presented in Figure 4.1. This kind of design is proposed to avoid at best effort the 'over-fitting'

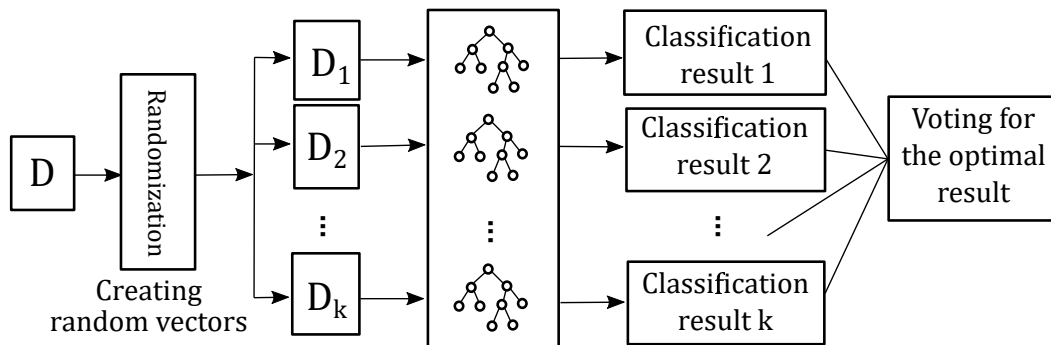


Figure 4.1: A simple illustration of Random Forest given by Wang et al. [Wang 2015].

phenomena when generating single decision trees, usually being Classification And Regression Trees (CARTs). The key point of generating an effective 'Random' Forest is to randomly pick training data and flag variables for the construction of trees, making each of them a unique decisioner. This kind of data operation is called 'bagging', thus its specific cross-validation algorithm got named as Out-Of-'Bag' (OOB) validation. The OOB validation can not only estimate the error rate of RF estimation, but also evaluate the relative importance of the inputs concerning their influence on the outputs.

Both the variance-based sensitivity indices and this OOB validation based variable importance selection results can represent how the uncertainty of each inputs can disturb the output value. One based on theoretical decomposition and another based on numerical experimental observations. Thus it can be quite interesting to get them compared for a deeper inspect.

4.2.1 Classification And Regression Trees

CART is a kind of decision tree capable to treat continuous inputs and outputs for regression problems. In an RF model, several dozens of trees are required in order to get convergent results. Thus for the 'Random' purpose, each CART are randomly parametrized.

Firstly, each CART randomly picks about 60% the total training data as its own training data, and the rest part will later be used in OOB validation phase. Such

convention of taking about 60% of the total training data for each CART actually has a statistical explanation. For a dataset S with n elements, if we take n randomly drawn with replacement, the expectation of total unique elements to be drawn when n become great enough is:

$$(1 - (1 - 1/n)^n)n \approx (1 - e^{-1})n \approx 0.632n. \quad (4.1)$$

Thus it is also called 0.632 rule in bootstrapping. The fact that different trees use different training samples makes a good basis of generating trees within different 'backgrounds'.

Secondly, for the efficiency purpose, the CARTs used in RF are all binary trees, which means at each nodes the training data will be divided into two parts satisfying the least square criteria. Normally, all the input datasets need to be screened in order to determine the split on which input's which value. While for RF, in order to avoid local optimums, only limited randomly picked inputs are chosen to be screened for each split. Normally for a dataset with K features, \sqrt{K} features will be chosen for a classification case and $K/3$ features will be chosen for a regression case. Like this the trees can have a much larger variety of 'personalities' without being dominated by some influential variables.

Thirdly, in case of continuous output, the nodes are considered to be enough converged and become a leaf node when split training samples already meet the convergency criteria. The criteria can either be a certain amount of depth of the tree, a small margin of value bounds, or a rather low threshold of group variance. All these criterions have been proved to be statistically stable and capable to reduce the total variance. Logically each CART will take average of leaf node sample values as a single-tree estimation value, then the whole RF will again take average of all these estimation values as the final estimation. These procedures makes an RF with 'democratic' semi-continuous outputs.

4.2.2 Out-Of-Bag validation and its variable importance selection

The OOB validation refers to the techniques of using unbagged samples as validation sets for each CART, giving an all-over percentage of correct estimation P , where higher value generally means better approximation. Then to the input importance selection phase, each time all the sampling values of a certain feature x_i will be randomly permuted, so that this value would become some irrelative noise value. The difference $SOOB_i = P - P(x_i \text{ randomly permuted})$ is defined in this case the importance factor of x_i . Or it can also be called 'OOB-based sensitivity index'. A greater value of this index means more serious estimation error would be made if this input gets disturbed, so more importance should be given to quantify its uncertainty.

This 'sensitivity index' has very direct practical meaning as the potential of causing error in RF estimation when facing uncertainty. After normalization, each $SOOB_i$ represents the percentage of wrong estimations caused by the uncertainty

of x_i . It does not have a very rigorous analytical definition, which in reverse helps to make its value more interpretable in industrial meanings.

OOB validation is an essential component of RF, while rarely it gets directly applied as an uncertainty indicator, maybe because of the calculation efficiency. But theoretically it works on all kinds of samples that FAST is capable to treat, and may have a better performance on correlated datasets and strongly non-linear models. Different from ANOVA and FFT, the logistic binary trees don't really care about sampling continuity.

4.3 Experimental design

The datasets being used in this research is retrieved from a former study on acoustic sandwich materials. As a model with 13 inputs and 1 output, each dataset contains 20 000 samples in form of $y = f(x_1, x_2, \dots, x_{13})$.

For an acoustic model, it may not only be studied under a certain frequency, but be evaluated on a continuous frequency bounds, which results 100 frequencies taken to fit a curve. Under each frequency, the 20 000 $\{x_1, x_2, \dots, x_3\}$ vectors are the same while their corresponding y values are different.

And in addition, for this simple acoustic models, the y value can be obtained either by analytical model or Wave Finite-Element (WFE) model. These two models give slightly different results and are also taken into comparison in this research. So in total there are two $20000 \times 13 \times 100$ 3d-matrix of input values x and two 20000×100 matrix of output values y .

4.3.1 Acoustic transmission loss of sandwich panels

The Transmission Loss (TL) is a very important criteria of material's sound isolation capacity. This value generally represents how much the power of the sound wave can be decreased after travelling through the piece of material. In this research, TL is y as model outputs and estimation objective.

And for the input vector $\{x_1, x_2, \dots, x_3\}$, it is composed with 13 variables concerning mechanical and geometrical properties of honeycomb sandwich composite materials. For the sake of simplicity, all the inputs are set to be uniformly distributed with a 20% variance around their mean values, seeing Table 5.1:

The mean values of these variables are mostly obtained from experiments while some other parameters such as air sound speed are fixed as constant.

4.3.2 Choice between analytical models

In traditional case of sandwich panels with isotropic and homogenous core material, analytical models [Mead 1969] can give a fast and accurate estimation of its vibroacoustic properties. But with fast development of manufacturing techniques, more and more delicate core meso-structures have been developed [Zhang 2015], Finite-

Table 4.1: Table of variables and their values

Notation	Variable	Value distribution	Unit
Inputs			
E_c	Core material Young's modulus	$U[13.6, 20.4]$	GPa
E_s	Face-plate Young's modulus	$U[56, 84]$	GPa
h_c	Core layer thickness	$U[16, 24]$	mm
h_s	Face-plate thickness	$U[0.8, 1.2]$	mm
l	Non-vertical meso-structural length	$U[2.08, 3.12]$	mm
l_h	Vertical meso-structural length	$U[2.08, 3.12]$	mm
t	Meso-structural wall thickness	$U[0.08, 0.12]$	mm
η	Structural damping factor	$U[0.004, 0.006]$	-
θ	Meso-structural angle	$U[24, 36]$	deg
ν_c	Core material Poisson's ratio	$U[0.272, 0.408]$	-
ν_s	Face-plate Poisson's ratio	$U[0.16, 0.24]$	-
ρ_c	Core material density	$U[2160, 3240]$	kg/m ³
ρ_s	Face-plate density	$U[2440, 3760]$	kg/m ³
Output			
TL	Acoustic Transmission Loss	-	dB
Parameter			
f	Frequency	$Exp[100, 10000]$	Hz

Element models[[Yang 2017](#)] are required to avoid the error generated in the homogenization.

Their relation is very like the one between FAST and RF. The analytical one is robust and computationally faster while the numerical one is sometimes more powerful and easier in presentation

4.4 Results comparison and discussion

Before comparing the results of the two methods, some parametric details of the algorithms need to be detailed first.

FAST is a non-parametric distribution-based method and RF is a parametric sample-based method. So the methodology is to generate the samples by FAST, getting the sensitivity indices, and then reuse these samples in RF.

Some important parameters of RF: percentage of samples used in construction of each tree: 65%; number of trees: 260 (20 trees per input); number of variables to be screened at each node: 4; number of split points to be tested for each variables: 20; largest error from exact value to be considered as correct: 5%.

Last point to be mentioned is that S_i is theoretically normalized with a sum smaller than one but $SOOB_i$ has no mathematical restrictions. So in order to get them visually easier to be compared, the values of $SOOB_i$ are also normalized by $\sum S_i$.

4.4.1 Analytical model dataset

Concerning the honeycomb sandwich composite material's sound transmission properties evaluated using analytical methods, the frequency-based sensitivity indices obtained by FAST is shown in Figure 4.2, and the variable importance sorted by RF OOB validation is shown in Figure 4.3 .

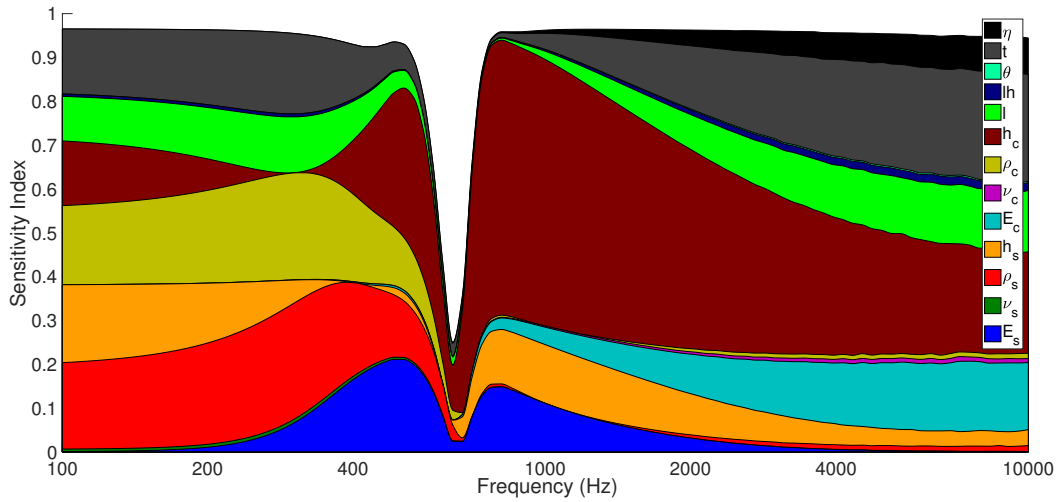


Figure 4.2: Sensitivity indices obtained by FAST, samples from analytical model.

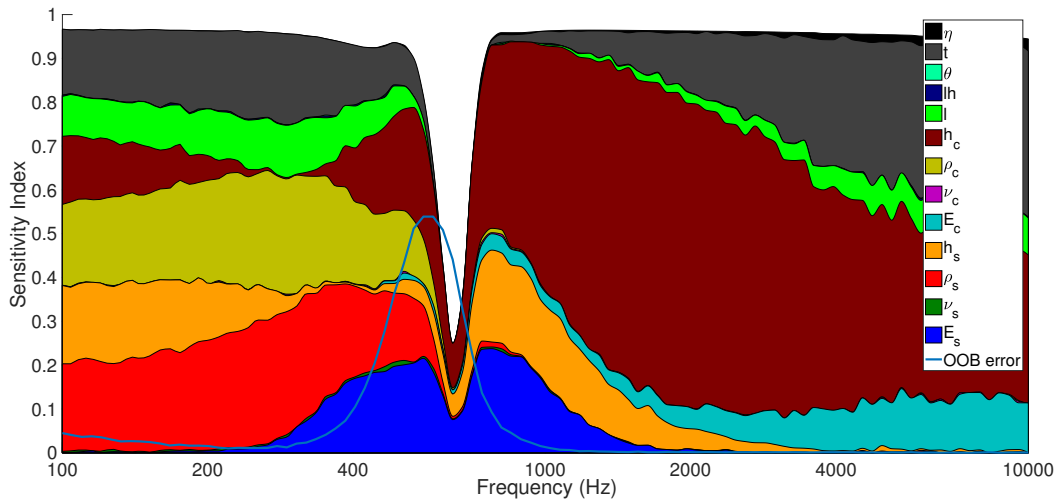


Figure 4.3: Variable importance sorted by RF OOB validation and normalized with the results of FAST, samples from analytical model.

In global view, these two graphs are quite similar to each other, not only because Figure 4.3 is normalized with the value of Figure 4.2, but also the values of each sensitivity indices are in the same trend of evolution along the Frequency axe. In general, both of the graphs represent the fact that the material densities (mass) are quite influential at low frequency while the thickness of the panel become more or

less dominant at mid-high frequency. The order of variables' importance selected by the two methods keeps in agreement at least within this frequency bounds, and is very reasonable when referring to physical facts.

Both of them also represented some details in this model. At around 350Hz, the sensitivity index of h_c gradually get decreased and then regrow into the most influential input, and the similar phenomena can also be observed for h_s at 400Hz. Deeper analyze shows that at 340Hz, TL and h_c transfer from negative correlation to positive correlation. At that point, TL is almost in function irrelevant with h_c . Same reason for h_s , but as h_s has a much smaller value than h_c , its evolution is less evident than the former. Another important point is that at about 700Hz, the sum of variance-based sensitivity indices becomes suddenly very small. This frequency corresponds to the critical frequency of the panel, where the panel get resonated by the acoustic wave and almost non of the input variables can handle this situation. At this point, a small sum of S_i indicates that great error has been observed and FAST can no longer guarantee the effectiveness of these values. At similar frequency a bit smaller than 700Hz, the RF OOB error curve also reaches to a peak higher than 50%, meaning extremely bad approximation by RF, so as well the results of OOB importance selection can neither be trusted.

Some of the only annoying point is that the curve in 4.3 is not as smooth as the one in 4.2, this is probably because of the random permutation of the variables. In real 'random' case, some 1% error and a -20% error will eventually make a difference. The fact that all inputs have taken uniform distribution instead of gaussian distribution may also have an impact on this vibration.

4.4.2 WFE model dataset

And for the samples generated by the WFE model, Figure 4.4 refers to the results obtained by FAST and Figure 4.5 refers to the results obtained by RF OOB validation.

Comparing Figure 4.4 to Figure 4.2, it can be clearly seen that the two models reflect eventually to the same problem, though with a bit difference at the results plot. Most of the particular points mentioned in last part can be refound in these graphs, such as the critical frequency, the point of property transfer and even the fact that E_s is only influential around the critical frequency.

And comparing Figure 4.5 to Figure 4.3, no similar unsmoothed points can be found in common. The fact shows that the unsmoothed curves are likely to be caused by random errors, but not some strange singular points. Some small vibration on the curve can even also be observed in Figure 4.4 at high frequency.

It's very nice to see that the RF OOB results are more graphically similar to the ones of SA results under the same group than the ones in the analytical model group. This gives a solider proof of the numerical similarity between these two sets of values: one from analytical development, another from experimental observation, the two under totally different definition but for the same objective of uncertainty quantification.

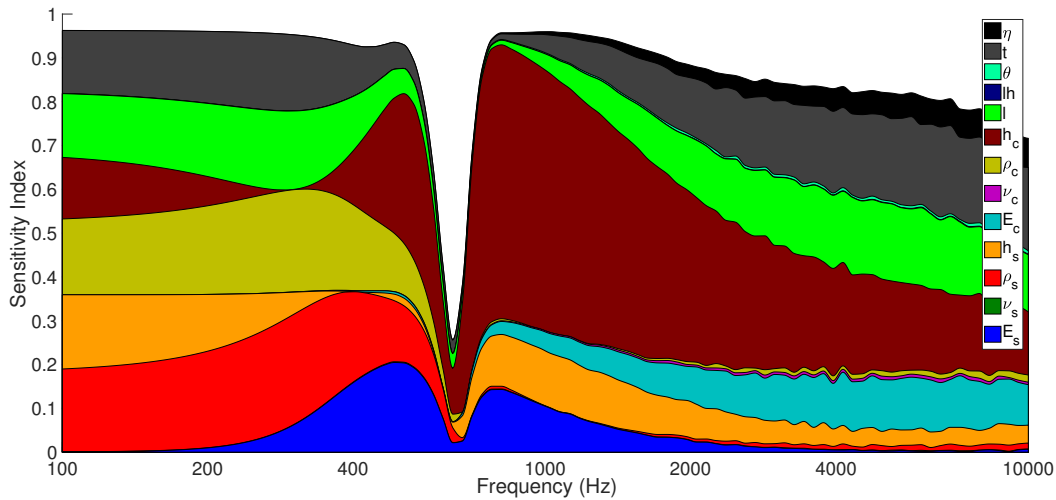


Figure 4.4: Sensitivity indices obtained by FAST, samples from WFE model.

4.4.3 Discussion

Random Forest, like other data mining tools, is quite 'subjective' towards different industrial cases. There are always the samples that it can treat perfectly and the ones that don't really fit the algorithm. In this research, even the OOB error curve keeps very steadily low except at the critical frequency, some imperfect details can be found regarding to Fig. 6.1:

The reason that this kind of biased estimation occurs is obvious: it's an estimation made by a large group of decisioners, so the results will always tend to become closer to the global average value. An example of how this phenomena can ruin the estimation can be seen in Fig. 6.2:

The quasi-continuous output design of the RF and the CARTs makes the estimation tending to vary very smoothly along the variation of some certain inputs. This property in inverse prevents the estimation from fast reaction towards discontinuity.

It is a problem, but regarding to Figure 6.1, the error may be reduced as the values are biased in linear form. It means if a 'rotation' or some kind of correction can be applied towards the bias, there's a good opportunity to improve its estimation.

4.5 Chapter conclusion

This paper presents a step of exploration into the possibility of inter-explanation among uncertainty quantification methods. FAST is a classic statistic global sensitivity analysis method, with well established theory basis and high calculation efficiency, but sometimes its results can be difficult to interpret in industrial cases. Random Forest is an upcoming data mining based regressionier and classifier, capable to construct metamodels based on different kinds of inputs and as well to tell the importance of each variable, but its selection feature is still intuitively defined and can not be recognized when not using RF. These are two different methods

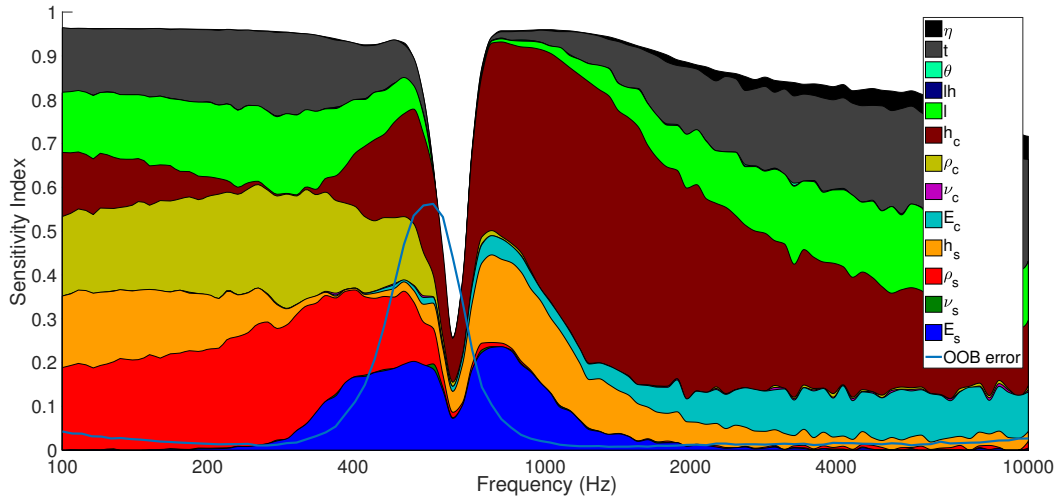


Figure 4.5: Variable importance sorted by RF OOB validation and normalized with the results of FAST, samples from WFE model.

with different theoretical structures but can both achieve the goal of uncertainty quantification.

The two set of numeric experimental results shows that even the two differently defined sensitivity indicators S_i and $SOOB_i$ can numerically reach in great agreement. Such results show a potential of numeric tools being mixed in applications. The variance-based sensitivity indices can hardly be explained in engineering word, but the RF OOB variable importance indicator can help it. A run of constructing and evaluating a RF takes quite long time but FAST can save the time and even give a reasonable proof for the results. The potential of combining the advantages of each tools may worth something for researchers and engineers.

Lastly, in this research with a vibroacoustic background, the special properties of sandwich composite panel also help to find out some weakness of the mentioned algorithms. Some more dive into this problem can possibly make another step of improvement.

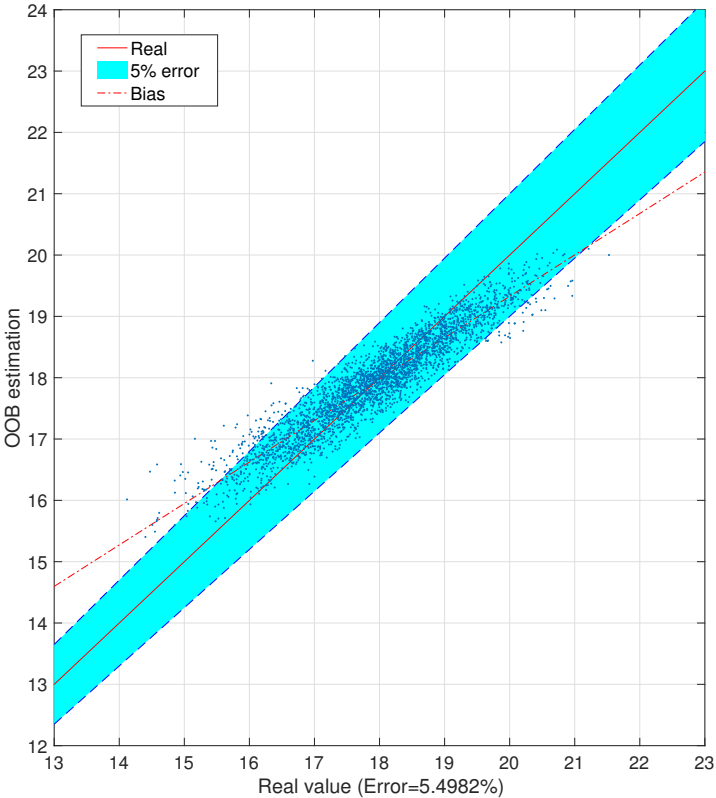


Figure 4.6: A mapping of estimated values (y values) on original sampling values (x values).

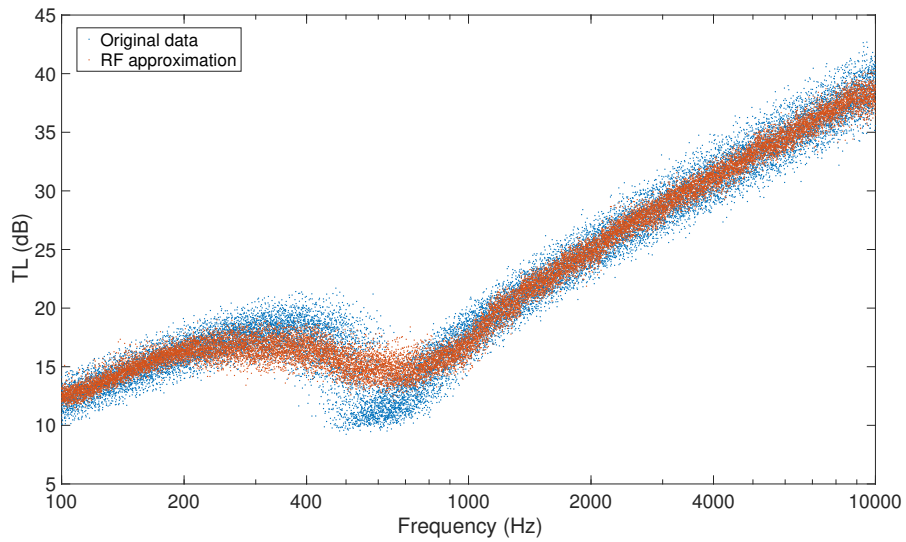


Figure 4.7: An example of how RF mistreat the function discontinuity.

Extended FAST method for GSA on 1D-structural damper arrays

Contents

5.1	Chapter introduction	73
5.2	FAST-pe: multi-sampling curves design and parametric configurations	74
5.2.1	Basic structure of FAST-pe	74
5.2.2	Configurations of the raw algorithm	75
5.3	The occur of random characteristic frequency movement and its essentials	77
5.4	Studies into the problem	78
5.5	Chapter conclusion	81

5.1 Chapter introduction

In previous studies of FAST series Sensitivity Analysis (SA) algorithms, many improvements have been made for their compatibility under various engineering conditions. Correlation and parametric dependency exist universally and is taken into consideration. Data-based sensitivity analysis was only active in traditional statistics field but is becoming quite hot in deep learning, so the data-based FAST got developed and was taken into comparison with random forest algorithm.

In these former studies, periodic structures are always taken as test cases, one is elastic porous material, the other is sandwich composite material. During the modelization of these two different kind of materials, two different methodologies were shown. In case of porous material, as the geometrical parameters are difficult to be measured precisely, homogenized mechanical parameters are thus introduced to replace the geometrical ones. This is like an empirical solution to complex system, extra uncertainty is introduced and can hardly be estimated. In this case, though SA can still be applied on such multi-input single-output model, its results can hardly be directly used for industrial improvements such as structural optimization and uncertainty control. In opposition, for the model of sandwich composite materials, all the meso-geometrical parameters are directly taken into calculation, but with the assumption of perfect periodic structures. So different from the porous material case,

here the SA is applied in a way that makes direct help to engineering decisions, but the main cause of input uncertainties — the deformation of cells is totally ignored.

Of course the two methodologies are not wrong, at least they are supported by mechanics in practical aspects. Both homogenization simplification and uniform hypothesis are like negotiations to insufficient calculation resources in numerical simulations. However, with more and more powerful computers been made, such kind of calculation-saving approaches became less necessary especially for low dimension models. Thus finally it becomes possible to well characterize each unit of some finite periodical structures.

The main purpose of this piece of work is to give a conception of enhanced FAST algorithm that can be used in SA of a system with multiple similar but not uniform units, and to taken this uncertainty among units into consideration of the overall output uncertainty quantification. Some small sampling strategies are modified from traditional FAST methods and then the enhanced FAST algorithm, called FAST-pe, is tested on a vibroacoustic model of 1-D damper array system.

5.2 FAST-pe: multi-sampling curves design and parametric configurations

5.2.1 Basic structure of FAST-pe

For the applications of traditional FAST in a system with N inputs and 1 output, each of the input sampling vector $\mathbf{X}_{i \in N}$ is given a different periodicity of ω_i from each other. After a FFT of the output vector \mathbf{Y} , the sensitivity indices of each input x_i can directly be obtained by regarding to its corresponding amplitudes of ω_i . The mapping of 1 input towards 1 frequency is the core of original FAST method. Figure 5.1 is an example of uniformly distributed periodic sampling curve for \mathbf{X}_i :

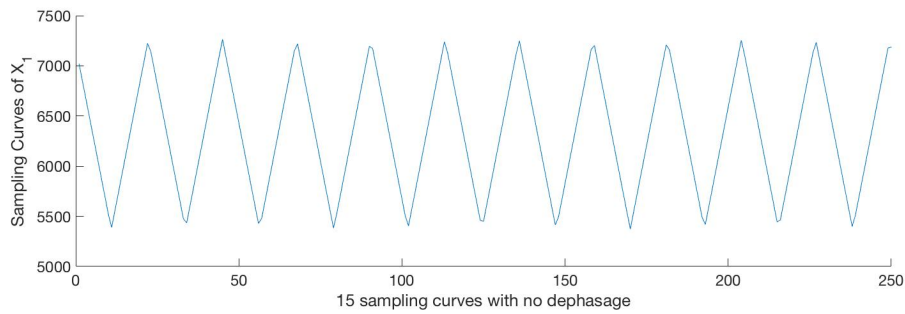


Figure 5.1: Uniform periodic sampling curve for traditional FAST method.

In case of multi-unity systems with U units, the entire entry dataset becomes a 3-D matrix with $\mathbf{X}_{i \in N}^{j \in U}$ representing the input vector of x_i on j th unit. For the objective of estimating the overall sensitivity of x_i for all the units, the input vector - frequency mapping is no longer 1 to 1 but thus set to be U to 1. In practice the frequency of all the U input vectors $\mathbf{X}_i^{j \in U}$ are given the same frequency ω_i . The

after processing of FFT is same as before and this time the amplitude of ω_i does not correspond to a certain input vector, but a series of vectors of a same variable. Figure 5.2 is an example of uniformly distributed periodic sampling curves for $\mathbf{X}_i^{j \in U}$:

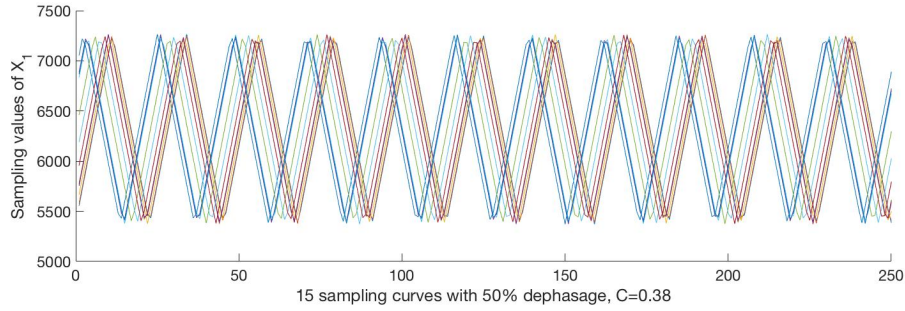


Figure 5.2: Multiple uniform periodic sampling curves for FAST-pe method.

Taking an example, for a system $y = f(x_1^1, x_1^2, \dots, x_1^5, x_2^1, \dots, x_3^4, x_3^5)$, it is treated almost in the same way as $y = f(x_1, x_2, x_3, \dots, x_{14}, x_{15})$, where the only difference is that the sampling curve for each set of inputs $x_i^{j=1,2,\dots,5}$ uses the same given periodicity. This modification generally has two objectives: first, the influence of multiple variables can be measured by one sensitivity index; second, with only 3 frequencies required, the algorithm of FAST may ask for less sampling numbers, thus the calculation can be done with higher efficiency.

As a brief conclusion, the expansion from traditional FAST to FAST-pe takes these following steps:

- 1) Enlarge the original model from $y = f(x_1, x_2, \dots, x_N)$ to $y = f(x_1^1, x_1^2, \dots, x_1^U, x_2^1, \dots, x_N^{U-1}, x_N^U)$, where the model constrains N inputs for each of U similar units.
- 2) Construct sampling curves for all $N \times U$ inputs, where all the vectors of the same parameter $X_i^{j \in U}$ are given the same periodicity ω_i .
- 3) Evaluating the model to obtain the output vector Y .
- 4) Executing FFT on Y and estimating the amplitudes on $\{\omega_1, \omega_2, \dots, \omega_N\}$, where each S_i represents the co-effect of multiple sampling curves $X_i^{j \in U}$ for multiple units.

5.2.2 Configurations of the raw algorithm

Conventionally the FAST algorithms are all no-parametric ones with given datasets, but in case of design or optimization applications where no enough datasets can be obtained, some more parameters on sampling phase can greatly increase the reliability of SA results.

Firstly, the marginal distributions can be freely set as in all the FAST algorithms. Former studies have already shown the importance of properly set marginal distributions in various applications. To be possible for a mathematical profile approximation, boundaries must be set for the values of sampling dataset.

Secondly, the maximum dephasage among sampling curves of the same variables

can be adjusted. This parameter is originally designed for this FAST-pe method, which measures the likelihood among system units. Well known as presented by the 6-omega principle, the error of the outputs is composed by the random distribution and the bias of standard value. In industrial cases, this bias of standard value will mainly be observed as a correlation of parameters for multiple units from a same production line. Here the dephasing has a direct relation with the correlation among units and thus the bias of standard value. Simply, a smaller dephasing interval means higher correlation and greater bias, which means all the units have the similar trend to be a bit greater or lesser at some properties. In practice, such condition may be caused by a aged 3-D printer or any other kind of quality decline. When the dephasing is set to be 0, it means all the units are exactly the same, and the SA results will be the same as the conventional synchronized solution; oppositely when the dephasing is set to 2π (maximum), it means no dependency among units so no bias occurs, thus the SA results will show some homogenized characteristics. A measurement C is taken as an indicator where 0 means non correlated and 1 means fully correlated. Figure 5.3 shows a comparison of sampling curves under different dephasing intervals.

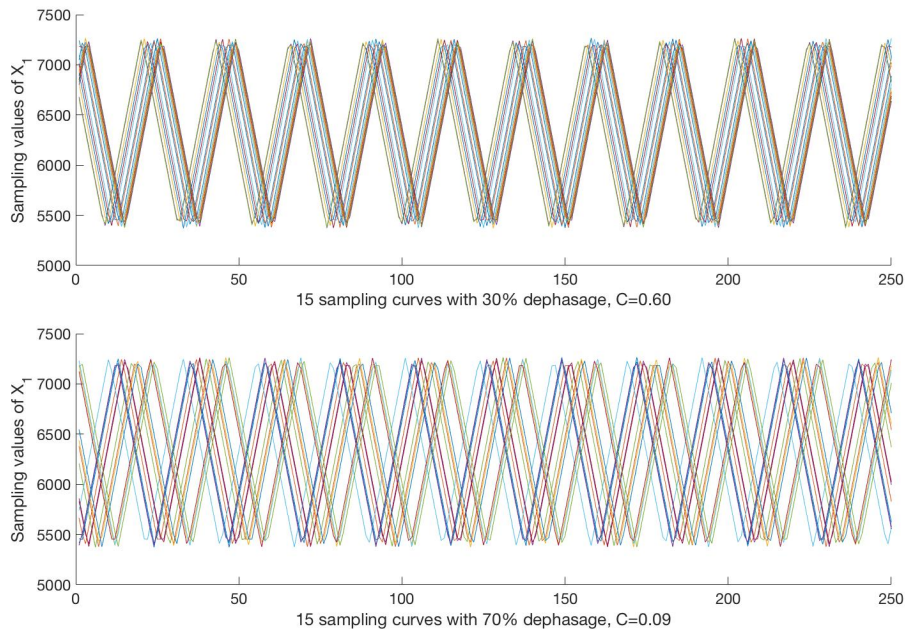


Figure 5.3: Multiple uniform periodic sampling curves for FAST-pe method under different dephasing restrictions.

Lastly, the correlation among variables, as already been proposed by former studies which introduced FAST-C. The correlation among variables exists everywhere in natural datasets and can also be resulted by constraints in multi-objective optimization process. Different from the 2-D sampling matrix in FAST-C, FAST-pe adds another dimension as the number of units U . In order to apply Iman’s transform, the 3-D sampling matrix \mathbf{X} must firstly be divided to 2-D matrices $\mathbf{X}_{i \in N}^{j \in M}(1)$,

$\mathbf{X}(2), \dots, \mathbf{X}(U)$. By applying Iman's transform, the re-ordered sampling matrices with correlation can be obtained by $\mathbf{X}_C(k) = \text{IMAN}_k(\mathbf{X}(k))$, and later in the phase of after process the periodicity can be recovered by $\mathbf{X}(k) = \text{IMAN}_k^{-1}(\mathbf{X}_C(k))$. Then the problem is that the reverse process is not executed once per analysis, so only one reordering process can be chosen as the standard order, traditionally $\text{IMAN}_1()$ and $\text{IMAN}_1^{-1}()$. For this purpose, all the other re-ordered sampling matrices $\mathbf{X}_C(k = 2, \dots, U)$ must be reordered for another time to $\mathbf{X}_{C_1}(k)$ that $\mathbf{X}(k) = \text{IMAN}_1^{-1}(\mathbf{X}_{C_1}(k))$. This second arrangement can be achieved by a composition of two array re-ordering operations.

5.3 The occur of random characteristic frequency movement and its essentials

In this piece of work, a simple multi-resonator model is taken into application. In brief, 15 similar resonators printed by a same 3-D printer are put on a 1-D beam with several configurable parameters including m the mass, k the stiffness and z the distance between each of the resonators. Damping factor is also considered but finally chosen to be proportional to the stiffness matrix, like a constant. The objective output of this model is the width of acoustic band gap created by these resonators, as shown in Figure 5.4.

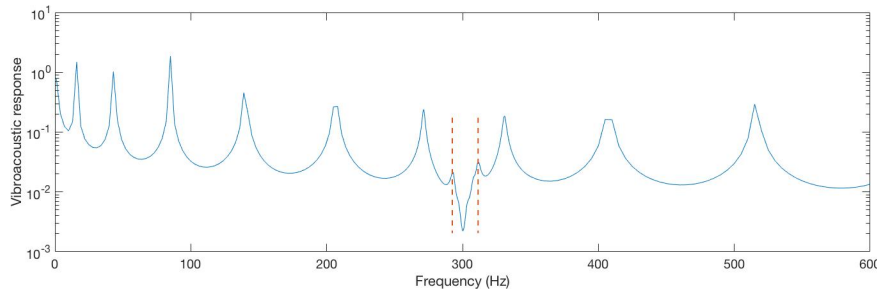


Figure 5.4: Stop band created by the array of resonators.

Considering that this is a conceptional model, and referring to the users' guide of the 3-D printer, uniform distribution with 15% of variance is given to each of these inputs. While some preliminary studies with traditional SA and data mining algorithms show that the unity distance z will only become influential when the variance is lifted above 100%. But some serious bugs such as resonator order reverse may occur under that setting, so finally in this part of work only the influence of m and k are focused.

With only 3 variables, 250 sampling curves are generated where the samples of k are given a periodicity of 11Hz and the samples of m are given a periodicity of 21Hz. Figure 5.5 presents the fourier amplitude given by the traditional FAST algorithm: the two great peak at 11Hz and 21Hz insisted on the dominance of k and m on the uncertainty of output.

Table 5.1: Table of variables and their corresponding sensitivity indices

Notation	Variable	Sampling frequency	SI
$m(x_1)$	Mass	11Hz(ω_1)	S_1
$k(x_2)$	Stiffness	21Hz(ω_2)	S_2
$z(x_3)$	Distance between resonators	27Hz	Ignorable

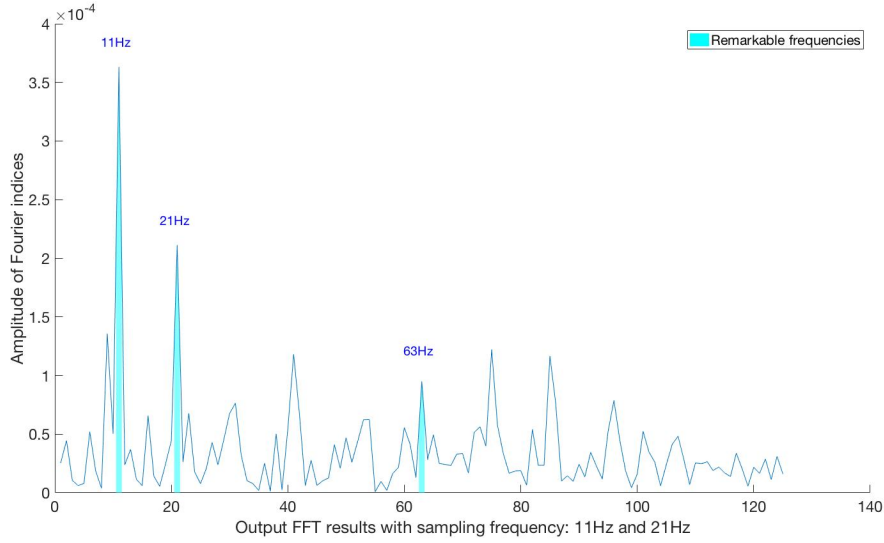


Figure 5.5: Fourier amplitude given by FAST algorithm.

Surprisingly the FAST-pe algorithm with 50% dephasage gives a spectrum a bit different from the FAST one, seeing Figure 5.6. In this graph, the peaks at 21Hz, 22Hz and 42Hz still stand out apparently, while another unexpected peak at 32Hz eventually draws the attention. This peak can only be regarded as an error because there is not a single sampling periodicity as 32Hz or any of its divisor. During multiple SA tests, the value at 32Hz peak seems very unstable, some times higher, some times lower and sometimes even moved to 10Hz. This phenomenon makes the SA results of FAST-pe very unstable and thus no accurate conclusions can be drawn directly using conventional FAST post-proceeding based on FFT.

5.4 Studies into the problem

In order to further investigate into the occurrence of unexpected spectrum, some more simulations under the same configuration have been made. In most of their results the peak of either or both 10Hz and 32Hz can be observed. Til now, no theoretical explanations can be found for this movement of fourier amplitude, but some rules can be found.

Just like the given periodicity 11Hz and 21Hz, the two 'unusual' characteristic

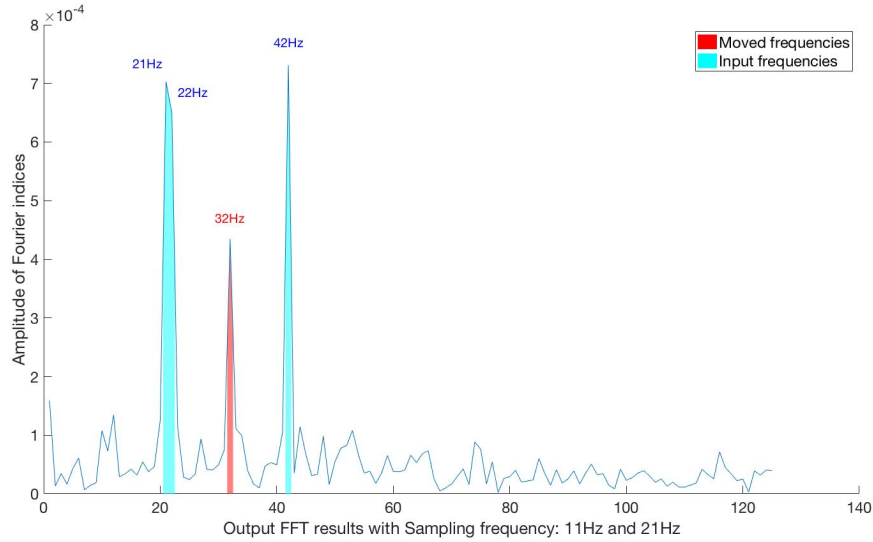


Figure 5.6: Fourier amplitude given by FAST-pe algorithm.

frequencies also have influences on high order spectrums such as 22Hz or 64Hz. Except for these mentioned frequencies, peaks sometimes also appears at like 20Hz or 63Hz as shown in Table 5.2, while usually with a less great amplitude. Looking at all these frequencies, it seems that they are all linear combinations of the given frequencies 11Hz and 21Hz, among which the first order sum 32Hz and the first order difference 10Hz have the biggest proportion and the higher order ones owns less amplitude.

Table 5.2: Table of some most observed spectrums with input frequencies with $\omega_1=11\text{Hz}$ and $\omega_2=21\text{Hz}$

ω	(ω_1, ω_2)	Peak value	Unusual frequency
32Hz	$\omega_1 + \omega_2$	High	Yes
10Hz	$\omega_2 - \omega_1$	High	Yes
42Hz	$2\omega_2$	High	
22Hz	$2\omega_1$	High	
11Hz	ω_1	Medium	
20Hz	$2\omega_2 - 2\omega_1$	Medium	Yes
21Hz	ω_2	Medium	
64Hz	$2\omega_1 + 2\omega_2$	Medium	Yes
63Hz	$3\omega_2$	Low	
52Hz	$3\omega_2 - \omega_1$	Low	Yes
74Hz	$\omega_1 + 3\omega_2$	Low	Yes

So what's the meaning of these spectrums, well they should may be put along with the normal spectrums to see their essence. In Figure 5.7, ten sets of SA results

are put together in proportioned bar graphs, in which S_1 is directly related to 11Hz and its multiples, S_2 related to 21Hz and multiples while other proportion explained by 10Hz and 32Hz.

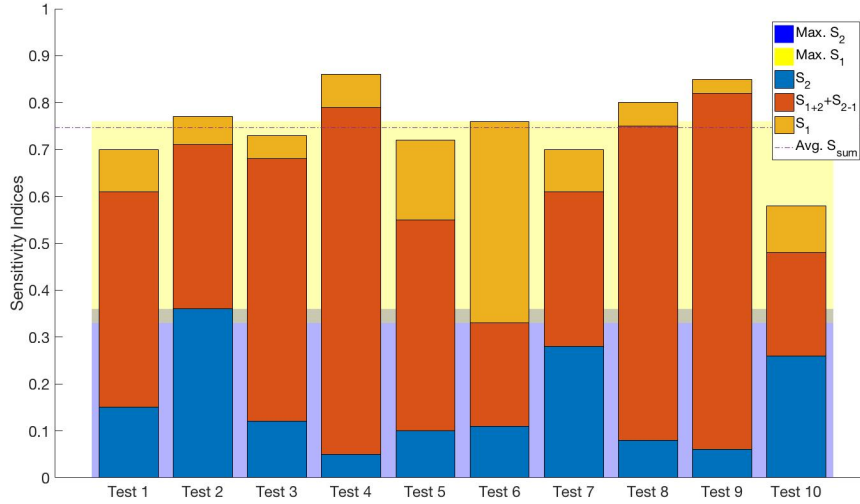


Figure 5.7: SA results of ten simulations accounting the frequencies 10Hz and 32Hz.

Sure in the 10 repetitions not even a single sensitivity index maintains a stable value, but their sum somehow keeps quite near the average value. The test 10 seems a bit away from the general case but it is caused by some important higher order terms not account in this bargram. At the same time the average value of S_{sum} is very close to the sum of S_{1max} and S_{2max} .

With the given statistics, an assumption is made. The sum of sensitivity indices still depends mainly on the value of S_1 and S_2 , but some times their corresponding amplitudes at 11Hz and 21Hz may be partially or completely moved to these new frequencies. Like the amplitude at 43Hz can be partially taken from 22Hz and partially taken from 21Hz, but the proportion seems not certainly to be 50%-50%. No rules have already been discovered to transform these amplitudes back to their original ones. Base on this assumption, it's very likely that the real S_1 is about 0.39 and the real S_2 about 0.36, which means k and m are almost equally influential on the width of band gap created by the resonators.

Remembering that taking SA by using traditional FAST algorithms will not cause this problem, it is very likely that this problem is caused by the newly introduced multiple sampling curve design. In order to prove this, a set of tests with different dephasage limits have been taken, from 0 dephasage to 2π dephasage, where the 0 dephasage case actually equals to the results of traditional FAST.

Quite clearly, the problem of spectrum movement becomes more serious with increasing dephasage interval, with regards to Figure 5.8. The sum of sensitivity indices increases when the dephasage limit increases from 0 to 20%, and stayed

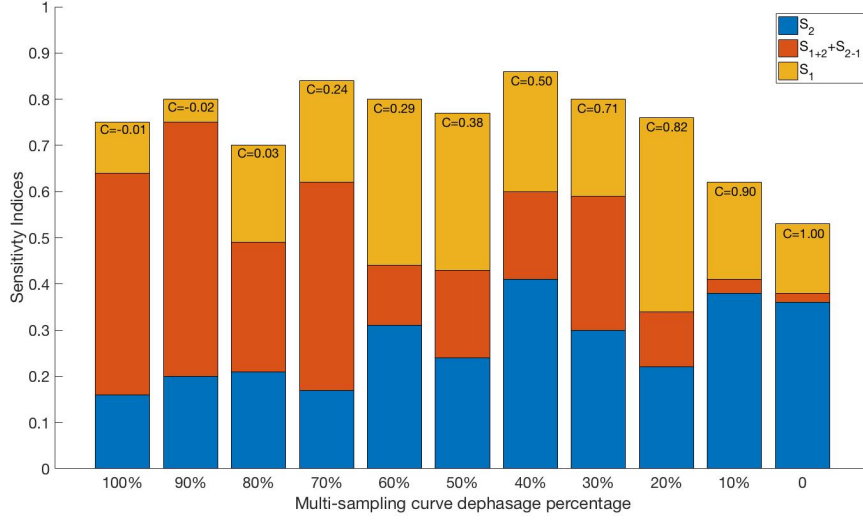


Figure 5.8: FAST-pe test results with different dephasage limits.

around this level. Interestingly, at 0 dephasage m has much larger influence on output uncertainty than k , while with increasing dephasage, which means less similarity among units, the importance of k gradually increases to a similar level as m .

According to the rule of the frequencies to be given to each inputs:

$$\sum_{i=1}^n r_i \omega_i \neq 0; r_i = \text{integer and } \sum_{i=1}^n |r_i| \leq M + 1, \quad (5.1)$$

then linear combination was considered as a kind of interference by early researchers of FAST. While this portion of Fourier amplitude kept always insignificant and thus become no longer taken into the calculation of first-order sensitivity indices. For some reason, this interference get re-discovered with FAST-pe sampling strategies. For the solutions to this problem, actually non has yet been found. Several configurations on sampling curves have been tested, mainly on their beginning phases, but there is not enough evidence to say if the problem really got improved or not.

The next direction of this research might be on the choice of preset frequencies. Before the set of frequencies only consider to avoid low order interferences, but with the phenomenon of linear frequencial combinations, some more criterions should probably be considered.

5.5 Chapter conclusion

In this piece of work a new enhanced FAST algorithm called FAST-pe is proposed to solve the GSA problem of systems with multiple similar units like periodic structures. This algorithm is later applied on a vibroacoustic model of 1-D damper array, though quite big problem still exist, some of the results do worth a discussion.

Though the sensitivity indices obtained by FAST-pe seem to be very unstable with the disturb of unexpected fourier amplitude spectrum, some results can still possibly be read after several repetitive executions. With original FAST method, m the mass has a dominant role on the output uncertainty, k the stiffness has moderate influence and z the geometrical parameter can almost be ignored. While the results obtained by FAST-pe shows that with no commitment of uniform units, k might be able to gain the same level of influence as m , upon the overall structural damping property.

The core part of this work is the occurrence of the unexpected fourier amplitude spectrums. After many tests, it can be recognized that these spectrums are very likely to be portions of the original spectrum on given sampling frequencies, and they locate mainly on the frequencies as linear combinations of the original ones'. The reason of their occurrence can not yet be explained by theoretical analysis, but statistics have shown that the increasing dephasage of sampling curves has a positive correlation with this problem.

Objectively speaking, the FAST-pe is just an intuitive test of algorithm compatibility improvement for new requirements of GSA methods. Actually no new theories is introduced and it is not surprising that FAST-pe doesn't work perfectly. Quite some researches have presented how hard it is to satisfy them conditions of unique ANOVA decomposition. Til now, FAST has already been largely improved, and it's natural to see the path becoming harder and harder. But if the objective of this research can be achieved, maybe not with FAST-pe, that will absolutely become a milestone of this cross-field academic research concerning GSA and vibro-acoustics.

Individual research case and representative FAST applications

Contents

6.1	Chapter introduction	83
6.2	Correction of biased RF estimations	84
6.2.1	Correction and comparison	85
6.2.2	Discussion	87
6.3	FAST sampling strategies in various research cases	88
6.3.1	Case 1: SA on multi-layer honeycomb structure optimization process	89
6.3.2	Case 2: SA on tilting pad journal bearing performance	92
6.4	Chapter conclusion	94

6.1 Chapter introduction

In former chapters, the main roles are the FAST-series SA algorithms, all the studies have the same objective of deeper investigating and improving their performance in various environments. At first FAST has already been proven as an accurate and efficient method, and FAST-c enables it to treat samples with correlations. When coming against the problem of not unique multi-variable distribution generated by Iman's transform, FAST-orig is thus proposed to fit better the cases with given dependent or independent sampling datasets. Considering the essence of the current research institution, FAST-pe is also on its way of development, for the sake of better modelling the multi-units systems where each of them could have independent uncertainties. Some other related researches concerning its comparison with machine learning methods have also been made and the results are quite interesting.

When focused on the algorithms themselves, the vibro-acoustic models taken into tests are generally chosen to be not very complex: elastic porous materials with isotropic and homogenetic hypothesis; sandwich honeycomb panels with perfect periodicity; and a 1-D damper system with limited units of simplest structures. These models are simply analytical and have been very deeply, if not completely studied. It doesn't mean that the SA can only be meaningful when applied to models without preliminary studies, which is actually useless in scientific aspect, but these

models doesn't reach the industrial complexity level in mechanical or acoustical area. So in this chapter, two extra SA application cases will be briefly presented, they both have moderate structural complexity and specific parametric constraints. Some deep analysis will be made in the aspects of the choice of FAST algorithms based on different environmental conditions and of SA experimental design for each cases.

And, if still remembered, there was a discussion left in a previous chapter concerning some observed estimation bias of Random Forest. Here in this chapter a kind of simple correction for the regression trees will also be tested. There were several unsatisfying estimation results left in that chapter and they can potentially be eliminated or recovered with this correction.

So in this chapter, there will be two main sections. The first section mainly introduces a simple correction of RF for its estimation bias problem, comparisons will be made to see if the problems left in previous researches can all be solved. The second section of this chapter will contain some brief introductions of two different SA applications in relative complex models: a multi-layer sandwich honeycomb model and a 5-pad journal bearing model. The focus of sight on these two models is mainly on the experimental design, thus how to choose a proper algorithm and to adopt it correctly on the model in respect of their research objectives.

6.2 Correction of biased RF estimations

In previous RF applications, CART trees have been chosen to fulfill the structure of the forest, for the purpose of treating continuous statistics. Thus as a regression algorithm, this RF algorithm also has similar defects as the others: capable to work only with enough training datasets covering the whole sampling space and value field; conservative estimation results are tend to be given for the points near the edge of sampling space. These weakness have already been observed in its previous application on acoustic transmission model, seeing the mapping of estimated value - real value in Figure 6.1:

The graph shows clearly that the spread of data mapping is in form of spindle, most of the estimations stays near the central value while several points at the two ends poked out of the error limits. And the tendency of conservative estimations also compressed the spindle in vertical direction, which makes the linear regression of the estimated points biased from the original values. Thus the following Figure 6.2 shows more exactly how conservative the estimated values are when compared to original training values.

Apparently the estimated values form a band narrower than the originals, which is a result of value compress at the y-axis. And in another point, the regression algorithm based on weighted average always tend to give continuous results, which causes great error near the acoustic critical frequency where the panel's vibro-acoustic property has a sudden change.

The plan of recovery for the first problem is to give a geometric estimation value

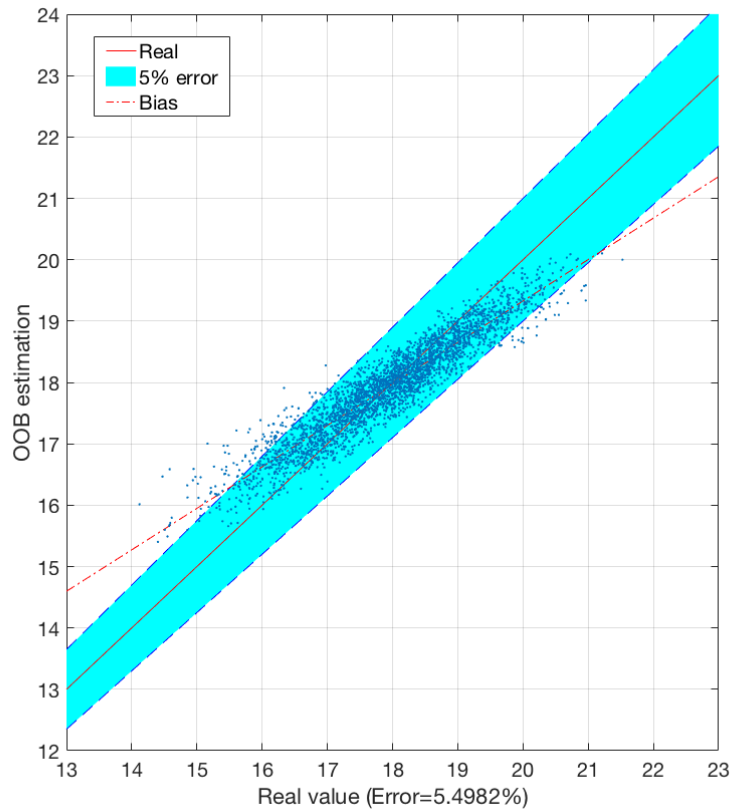


Figure 6.1: Estimated value mapping of RF results based on regression decision trees.

correction based on the angle of bias, all the estimated values will be extended along the y-axis. And for the second problem of continuous estimation, it will exist as long as the algorithm is applied on continuous datasets, but hopefully the case would get better with the solvation of the first problem.

6.2.1 Correction and comparison

As have noticed before, the spindle-like data spread has a linear-like bias and the correction is operated in a simplest geometrical way. Firstly we have the perfect estimation line $L_1 : y = x$, and the actual estimated center value line $L_2 : y = ax + b$ obtained by a linear least square approximation. Then all the estimated value y_0 will then be corrected by a linear relation of $y_{new}/y_0 = y_0/(ay_0 + b)$, thus $y_{new} = y_0^2/(ay_0 + b)$. Though on the data mapping the x value of each point is fixed and can not move, the correction on y value finally realized a rotation-like operation.

In the test of this algorithm correction, another set of statistics is taken from the same vibro-acoustic model. This time the dataset is taken from the points

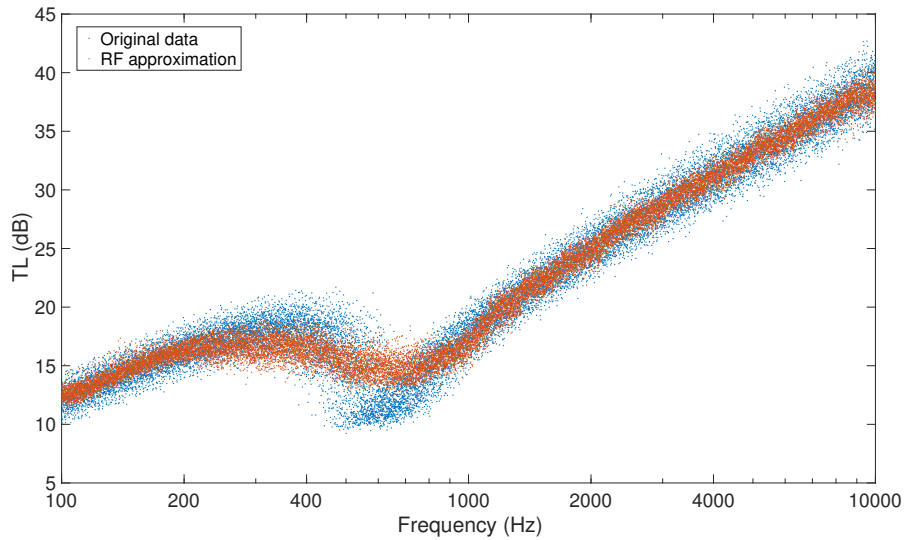


Figure 6.2: RF estimated value mapping along frequency axe.

near 550Hz, where the critical frequency locates. At this frequency, the acoustic characteristics of sandwich panel have a rapid transition which caused a nearly non-continuous performance. The former performance of RF estimation at this correction is not very satisfying, with an OOB error over 50%. The mapping of estimated values is shown in Figure 6.3. The overall spread of these points is like a eclipse but weighted more at the end of smaller values, and with the bias of estimation, these large number of estimated points are all situated out of the 5% safety zone.

Then by applying the anti-bias correction, the new estimated points are mapped in Figure 6.4. In the new results mapping, though the large width of data spread still causes more than 40% of OOB estimations, comparatively about 15% of the points at the bigger end of spindle get well adjusted and become acceptable. And for the ordinary cases with quite low OOB error like in Figure 6.1, using this correction can make the accuracy of estimation over 99%.

For the case of data mapping on the complete frequency band, its corrected version is shown in Figure 6.5. The most direct impression is that the spread of points becomes much wider and can almost cover the training data spread, which means the conservative estimation problem has been mostly recovered. And with this correction, even not exactly for the continuuity problem, the data mapping seems better at around 500Hz, where a clearer separation can be observed. The only annoying point is the visible segmentation at around 2000Hz, which already exists in the pre-correction mapping but becomes really ugly after the correction. The reason for its occurrence is still under investigation.

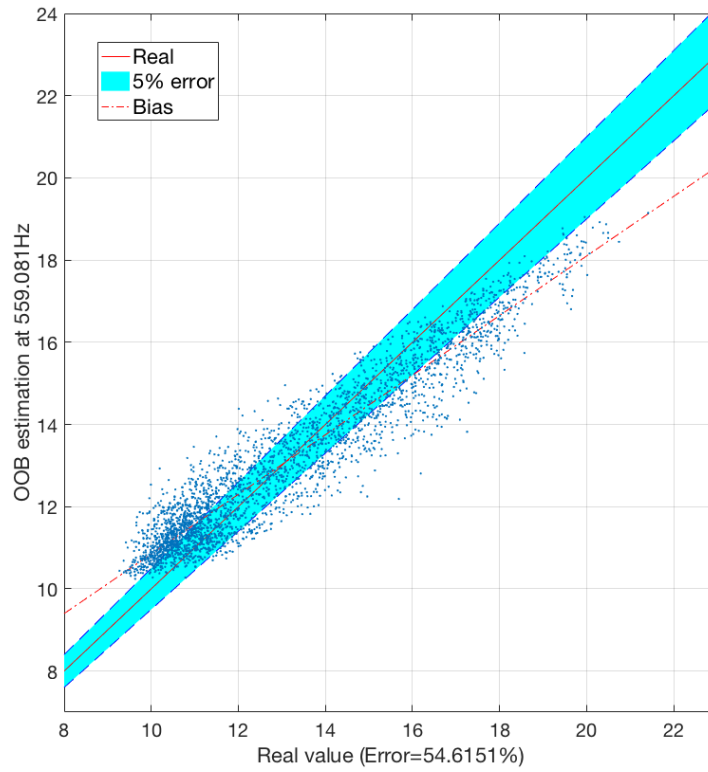


Figure 6.3: OOB error of RF estimation at 550Hz of vibro-acoustic model, before correction.

6.2.2 Discussion

Same as original biased estimation results from similar mathematical models, Figure 6.1 and Figure 6.3 give different degrees of bias, which means the correction parameter determined with the first training dataset can not work perfectly on the second test dataset. Such evidence sets a quite strict condition for the use this correction, where the training datasets and the testing datasets must be generated from exactly the same source under the same environmental conditions. This would be a great challenge for its application in industrial cases where the training sets are mainly empirical observed data and the testing sets come from anywhere possible. Some preliminary studies to ensure the similarities between these two datasets is obligated.

Also it should be mentioned that the two datasets in this study both obey quite regular spread shape, either like a spindle or an eclipse, so the linear least square can properly show the overall bias of statistics. While in common cases some irregular data spread can also be found, taking Figure 6.6 as an example:

This data mapping presents all the RF estimations of the vibro-acoustic model

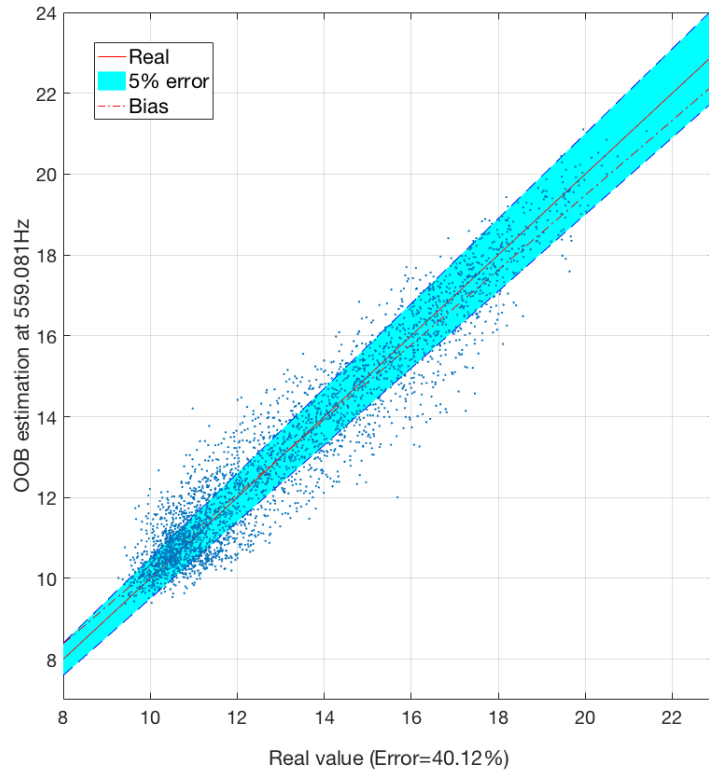


Figure 6.4: OOB error of RF estimation at 550Hz of vibro-acoustic model, after correction.

in the whole frequency band. Yet as have been observed before, these segmentally estimated point don't have a spatial continuous distribution, and a 'tail' at small values can also be observed. This kind of irregular form of mapping spread is physically caused by the rapid transform of sandwich panel's mechanical properties, especially near its critical frequency. Already seen that the linear bias is very small, so a comparably weak effect of correction operation can be expected, as shown in Figure 6.7:

Eventually, 1% more incorrectly estimated statistics are obtained. So as a conclusion, two conditions of applying this correction process have been discovered, one is the reliability of training datasets, and another is a regular form of estimated data mapping.

6.3 FAST sampling strategies in various research cases

Other than the previous applications of FAST series algorithms and RF on porous elastic materials and sandwich composite materials, SA methods have also played an role in some inter-group cooperation. In this section, two cases of meta material

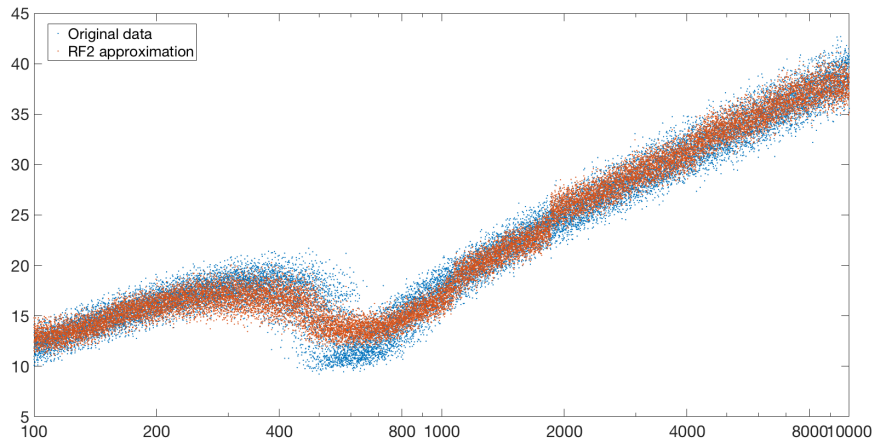


Figure 6.5: Corrected RF estimated value mapping along frequency axe.

and journal bearing are introduced, their SA results could possibly be found elsewhere in some publications so only the preliminary studies would be analyzed in this section.

6.3.1 Case 1: SA on multi-layer honeycomb structure optimization process

Sandwich composite materials with honeycomb meso-structure has been developed and studied for several decades, there are also two chapters in this thesis taking this model as example. While in recent years, with higher and higher performance with required, some more structurally complex, multi-layer sandwich materials are becoming the main roles in industries. So in this subsection, some details of the sampling strategies are discussed in a preliminary study of a double layer honeycomb sandwich design phase. The model of this sandwich panel can be seen in Figure 6.8:

The objective of this study is to optimize the vibro-acoustic performance of the sandwich panel near its critical frequency, where the multi-layer design can work out. Generally speaking the honeycomb structure of each layer is defined with 4 geometrical parameters α, β, a and sh , while the two layers use two different set of parameters so their critical frequencies would not get synchronized. The SA is thus conducted to its numeric model to find out which among the 4 parameters has the greatest influence on the TL curve.

During the preparation and sampling phase of FAST method, some model constraints and characteristic properties should also be firstly verified. First of all, as the two layers are structurally the same with different geometrical parameters, it is economically preferred to estimate only the sensitivity indices of the parameters of the first layer. Secondly, in order to make the optimization convincible, the 4 parameters vary in the sampling space with a constraint of fixed panel mass, as the objective of optimization is to improve the performance without adding extra

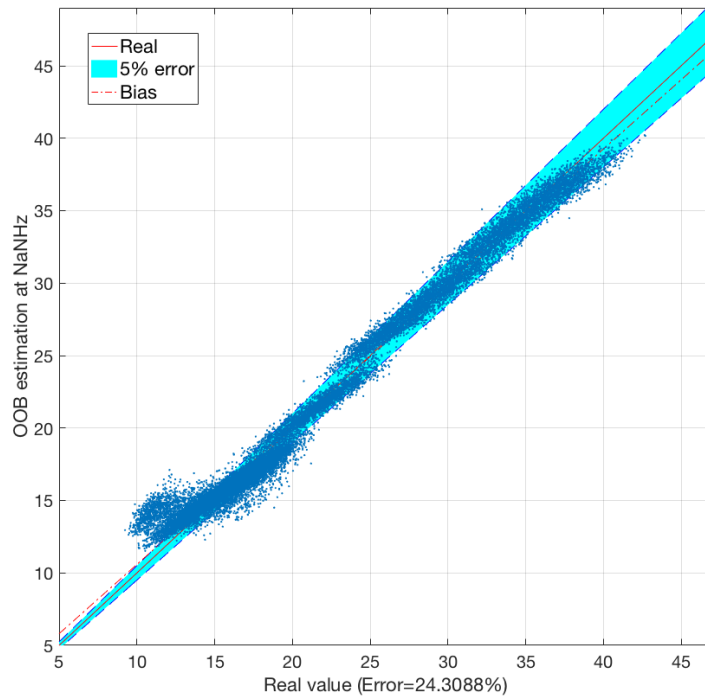


Figure 6.6: OOB error of RF estimation on the whole frequency band of vibro-acoustic model.

weights.

The first request indicate exactly to the advantage of GSA where the 'Global' means a continuous sampling space. Using conventional LSA methods, there's mainly two solutions: either to fix the second layer and vary the parameters of the first layer, not even together, or to set a map between the parameters of the two layers, where the simplest way is to suppose that the two layers are exactly the same. Obviously such approaches can not satisfy the need of research, but with GSA methods, such as FAST, it will be possible to let all the parameters varying together and to only measure the influence of 4 parameters among them. Technically, estimating the sensitivity indices of only part of the variables will cause the sum of sensitivity indices less than 1, but it doesn't matter if only for ranking their importance, and such approach can greatly reduce the number of samples required for this GSA.

As just mentioned, the number of samples is a quite important value to be controlled, mainly because of the fixed mass constraints. According to the model, there is a function to calculate the overall mass with these geometrical parameter given, only the combinations that result to a certain mass with a very small variance are accepted in FAST algorithm, and the marginal distributions of each variable can then be obtained. As the constraint is relatively strong, large amount of samples

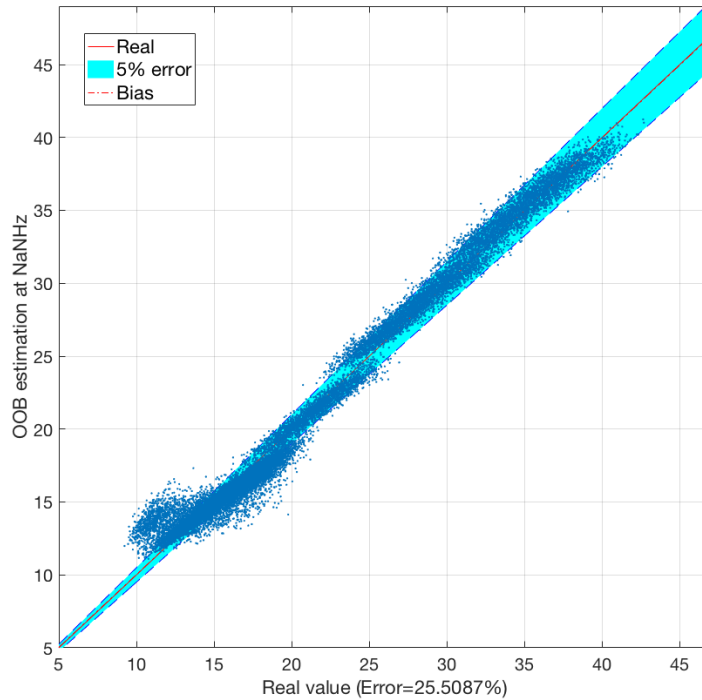


Figure 6.7: OOB error of RF estimation on the whole frequency band of vibro-acoustic model, after correction.

were abandoned before being used in SA algorithm, that explains the reason of insisting on analyzing as less inputs as possible. Thus, as the samples are strongly correlated with irregular distribution rules, FAST-orig is chosen as the best solution, it respects best the original statistics as well as being able to work with a flexible number of samples.

A last technical point to mention in this case is how to generate a sampling curve for the 8 variables of sandwich material's two layers. As these two layers are totally independently designed, the sampling curves must not contain the correlation between them. A common solution is to generate a sampling curve firstly for a single layer and to calculate the acoustic properties of all possible combinations. But the traversal of all combinations is so computational heavy that it is actually even less efficient than making a SA of all 8 parameters. The solution proposed in this study is to make a 2-D Latin Hypercube sampling of the two layers, which at the same time eliminated the requirement of extra samples and simulations, and satisfied the need of non-correlated sampling strategy.

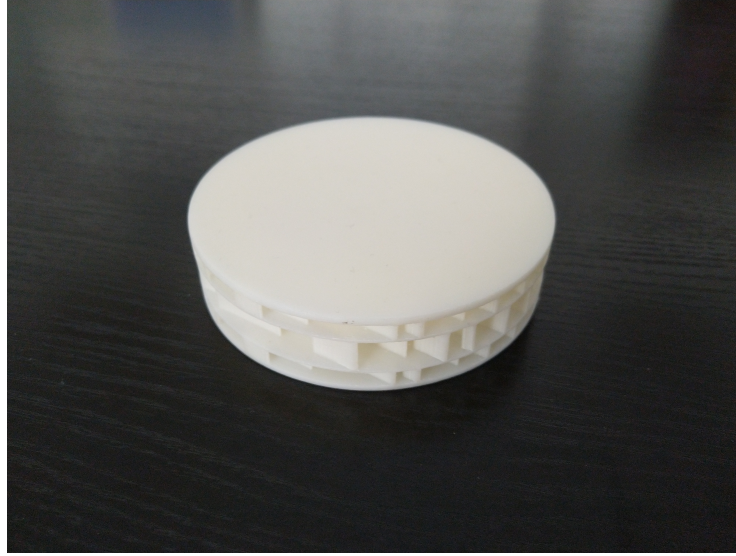


Figure 6.8: A photo of a double-layer sandwich sample made by 3D-printing.

6.3.2 Case 2: SA on tilting pad journal bearing performance

Known that meta-materials are very hot as SA research topics in recent years, in traditional mechanical systems there are also occasions where SA can play its role, such as this multi-pad journal bearing model. Journal bearing with rotative pads is a kind of advanced design which has better compatibility and stability under various working conditions. The only obvious disadvantage of this kind of journal bearing is its structural complexity, where a lot of parameters must be controlled during production and assemblage phase. So this is how SA is required in this research.

Figure 6.9 presents a clear illustration of the whole journal bearing and the pad in photo stands for the main object of this SA. In this research, the uncertainty at the inputs of the system mainly focuses on the geometrical error induced to the pads during fabrication. Five among all these geometrical parameters are studied, seeing Figure 6.10:

Unlike the former case of double layer sandwich panel, this time the uncertainties are generated during fabrication, some more realistic sampling curves would be used in this SA. As the experimental basis is in China and the pads are also produced there, some chinese standards of material proceeding have been referred. According to that quite old standard, Gaussian distributions with $3\text{-}\sigma$ accuracy is confirmed. Compared to former cases where very large uncertainty interval with uniform distribution is common used, the errors identified in industrial cases is rather small.

Still this is not the end, as the oil film in bearing structure must keep extremely thin, which means very small space between the pads and other parts of the bearing. Thus, even with very small input uncertainties, there still will be rare cases of structural bugs during simulations, thus these bugged sampling sets need to be

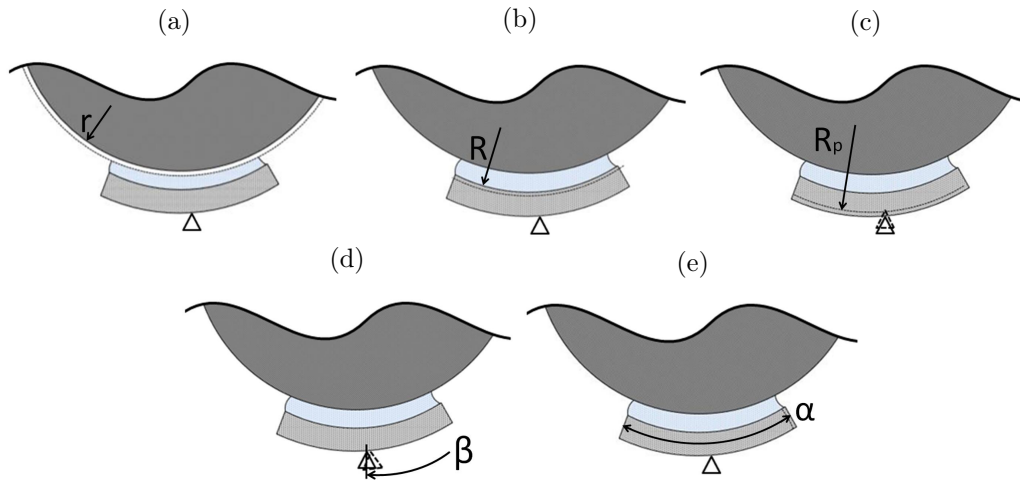


Figure 6.10: Five geometrical parameters of the tilting pad journal to be studied: (a): r the shaft radius, (b): R the pad internal radius, (c): R_p the pivot radius, (d): β the pivot location, (e): α the pad extent angle.

didn't work well in previous tests and some key problems have not been solved; secondly, though these five pads are structurally similar, their working conditions are totally different, the bottom pad actually hold the main load and the upper ones just helps to keep the stability. So at last in this research, only the uncertainty of the bottom pad is evaluated while the others are considered to be constants without uncertainty.

6.4 Chapter conclusion

The first section of this chapter is an additional research following the former study of SA and deep learning comparison. This section is the only section which hasn't any relation with sensitivity analysis or FAST methods. Briefly speaking, the bias of estimation is a kind of common error for Random Forest with regression trees, some direct correction is applied and the results becomes thus more reasonable.

The second section of this chapter presented two more application cases of FAST series algorithms on models of multi-layers sandwich panel and moving pad journal bearing. In both cases, the choices of the exact FAST algorithm are quite interesting. In former chapters, the traditional FAST and FAST-c methods are regarded as standard solution for optimization problems and FAST-orig is more suitable in industrial cases. But in this chapter, FAST-orig become the only choice when there's a strong non-linear constraint in optimization problem, while FAST is considered more efficient in industrial cases with precise documentation.

Many researchers have expressed the fact that researches based on statistical or deep learning methods can only become scientific when enough comprehension of the objective models have been achieved. Such comprehension reflected in a SA is not only in the conclusion part but more on how the sampling curves are generated

and thus can work perfectly with a properly chosen SA algorithm. Also, one of the former chapters has presented how statistic based methods and deep learning based methods can give similar results upon the same case, the pre-proceeding part has yet become the critical part of tell the effectiveness of one uncertainty quantification process.

As for the exact SA results these two models, they are not included in this chapter but some related publications might be able to be found recently or in near future. Simply concluded, the SA conducted to the multi-layer sandwich panel model confirmed many theoretical predictions and is now guiding the design of experiments using 3-D printed sandwich samples; and the other one on the 5-pad journal bearing gives several new aspects of how influential are the inputs with extremely small sampling space.

Part 2: Conclusions

The main contents of this part 2, chapter 4 and 5 are both original researches and thus the concepts seem to be a bit futuristic. In one aspect, till now we can not imagine one uncertainty quantification application using both machine learning and GSA methods; and in another aspect, the FAST-pe algorithm does not yet work and can not even be proven to be robust. They both are steps forward to the universe of uncertainty, one in a macroscopic view of common similarity, other in a microscopic view of precision in a certain industrial case. These steps might, and are very likely to be, not on the right path of technology development, but at least enriched our experience and broadened the horizon of possibility.

Based on the experience of FAST, FAST-c and FAST-orig, and under the need of multi-units correlation identification, a prototype of FAST-pe is developed. In the technical point of sampling and post proceeding, FAST-pe can theoretically replace all these algorithms above, except for the problem that its results don't converge. Compared to other ANOVA-based SA algorithms like CRM or Sobol'-Jensen, the FAST-series algorithms seem to have bigger potentials in compatibility developments. Thanks to the design of periodic sampling and FFT, most of the current data-based algorithm are much slower than FAST. Thus, if the objective of certain application is uncertainty quantification without constructing a meta-model, FAST is potentially a competitive algorithm.

For me, the chapter 6 is my favorite in this thesis, not only because I can choose to only write the most essential part of applications, but also it reminds me of the joy of teamwork. Throughout these years, I'm nearly always the only one working on statistics in our group, digging alone the codes of FAST can not be very interesting but cooperating with other mechanics are real enjoyments. One characteristic of generation sampling curves from physical models is that the variables always have different constraints, commonly presented by their co-distributions. This means the correlation always exists, and way different from the form of correlation matrix. In chapter 5 and 6, actually three different solutions are presented: add compatibility modules onto GSA algorithms; fix on the main objective of GSA and simplify the model; transfer a distribution-based design into a data-based design. When treating problems with concrete objectives, except for the case of very high sampling cost, data-based solutions are generally recommended.

Conclusions and perspectives

General conclusions

This thesis is mainly addressed to the development of FAST-series algorithms, categorized as ANOVA-based global sensitivity analysis methods, along with their applications on multiple mathematical models of periodic acoustic materials. The FAST series algorithms, including FAST, FAST-c, FAST-orig and FAST-pe, and several other GSA algorithms, for the purpose of comparison, have been applied respectively to three mathematical models of vibro-acoustic materials: porous elastic material, sandwich composite material and 1-D multiple damper structure. The context of these applications raised several requirements for the compatibility of FAST algorithms, such as correlation and dependency among input variables, not unique HDMR expansion and the bias of normal distribution for multiple units. Thus based on the traditional FAST algorithm, improvements were applied to its later versions: FAST-c introduced Iman's transform to manually construct correlated sampling curves; FAST-orig transformed from distribution-based algorithm to data-based algorithm; FAST-pe introduced a second level correlation design among multiple units with the compatibility to the two former algorithms. In these algorithms, FAST-orig and FAST-pe are completely original in this thesis. Though these mathematical models are mainly analytical and not very complex, the great agreement between their empirical observations and GSA results has well proved the effectiveness of these algorithms.

These ANOVA-based GSA algorithms has always been an essential part of uncertainty quantification tools, though never entered the most popular ones. Since very long time, GSA can barely compete with LSA methods, for the great disadvantage at computational complexity and at its relatively complicated theoretical basis. Since the end of last century, the rapid development of computers helped to solve the computational problem of many GSA algorithms and the publications of GSA has greatly increased. While unfortunately the new coming machine learning methods finally took the biggest piece of cake. Thus in order to figure out the difference between GSA and machine learning, a Random Forest algorithm, which is also capable for uncertainty quantification, was chosen to make a direct comparison with FAST on the sandwich honeycomb panel. Generally both of them can roughly give similar SA results and are capable to self-evaluate the quality of test. In one aspect RF has a better compatibility as it's a data-based algorithm and can generate a meta-model, while in another aspect FAST has a much better calculation efficiency with a clearer analytical basis. Generally machine learning methods are exactly suitable in this era of big data but GSA can still compete in some professional areas.

The three GSA applications mentioned above in Chapter 2, 3 and 5 presented a complete and standard process of ANOVA-based GSA applications, especially for these distribution-based FAST algorithms. But in these big cases, algorithms were pre-determined and the datasets were just perfectly generated for these algorithms. While in real industrial or research cases, such perfect combo can hardly exist: special sampling strategies need to be designed under various constraints; existing data-sets need to be pretreated to respect the condition of GSA application; even sometimes the task of uncertainty quantification might have to be splitted and get completed by two different algorithms. These are exactly what we overcame during the cooperations of other laboratory research projects. Yet these cases were interesting experiences and contains some details of FAST coding mechanisms.

Perspectives

With the trend of automatization in industrial, the need of uncertainty quantification will absolutely continue to increase. Concerning the complexity of industrial models, data-based GSA algorithms might be the best choice in the aspect of efficiency. But rarely the ultimate objective of its application will stop at uncertainty quantification, parametric optimization and meta-model construction are common objectives that sensitivity analysis can not achieve by itself. That's why data-mining and machine learning tools are much more popular than GSA in these years. But it should be mentioned that almost all these big-data-based algorithms are both parametric and computationally intensive. Which means it usually takes heavy labour and time consumption to achieve their best results. Thus, in most cases where not enough preliminary study results are accumulated, some high efficiency non-parametric algorithms, such as FAST, are recommended. So, as GSA methods generally can only work together with other data-based parametric algorithms, some more improvements can potentially be made on their compatibility. Most of these machine learning algorithms don't really have any relation with ANOVA-HDMR, then how to translate the SA results based on variance proportion to their definition of sensitivity can be a valuable engineering topic.

The core problem of my thesis begins with correlation and also breaks at correlation. For an analytic tool based on ANOVA-HDMR, the common existence of correlation in real world is actually catastrophic and at the same time inevitable. Almost all these GSA algorithms mentioned in this thesis, except for the traditionally ones, are either propose to or originally capable to treat correlated datasets. But neither FAST-c towards normally correlated datasets nor FAST-pe towards double correlated datasets are perfect perfect solutions in each case. Observation has confirmed that FAST-c does not give a unique SA result and FAST-pe can not even converge. Well the basis is still the problem of not unique decomposition for

ANOVA-HDMR, thus copula seems to be the only theoretical possible solution in this case. But former studies have already shown that to find a set of orthogonal functions in a randomly distributed high-dimensional space is not as easy as to say. So FAST-orig might be the best approximation at its precision and compatibility up to now, but the research for an ultimate solution will absolutely continue.

Actually when we mentioned GSA, its main opponent in the market has never been machine learning and data-mining, but actually the LSA that statisticians always criticize. In common thought, with the development of computer processors, the difference of computational intensity between GSA and LSA should be shorten and GSA should have a total advantage towards LSA in performance. However, there has never been a signal that the publications on GSA can reach 1% of those on LSA. In my opinion, institutional research on statistics are becoming more and more social directed. Publications of analysis results are more and more specifically organized for common public and the social medias are normally eager to dig out more numbers to draw people's attention. For me this is not a problem or something, at least the easy accessibility of LSA results actually make generates more social value than these complex formulas of GSA.

Publications during the thesis

International Journals

- **W. Chai**, J.-L. Christen, A.-M. Zine, M. Ichchou. *Sensitivity analysis of a sound absorption model with correlated inputs*. Journal of Sound and Vibration, vol. 394, pages 75-89, 2017.
- **W. Chai**, M. Ichchou, Z. Zergoune, A.M. Zine. *Sensitivity analysis for sound transmission models of sandwich composite structures with correlated inputs*. Submitted to Journal of Theoretical and Computational Acoustics, in process.
- **W. Chai**, A. Saidi, AM. Zine, C. Droz, M. Ichchou. *Comparison of uncertainty quantification process using statistical and data mining algorithms*.

International Conferences

- **W. Chai**, Z. Zergoune, A.-M. Zine, M. Ichchou. *Sensitivity analysis on acoustic characteristic properties of sandwich composite materials with various core meso-structures*. 20th International Conference on Composite Structures, Paris, France, 2017.
- **W. Chai**, Z. Zergoune, A. Zine, M. Ichchou. *Global sensitivity analysis on sandwich panel's acoustic characteristics with correlated inputs*. MEDYNA 2017: 2nd Euro-Mediterranean Conference on Structural Dynamics and Vibroacoustics, Marrakech, Morocco, 2017.

National/ Regional Conferences

- **CHAI W.**, M. N. Ichchou, A-M. Zine. *Sensitivity analysis on analytical models of porous acoustic materials with correlated inputs*. Journée des doctorant CeLyA, Lyon, France, 2017.

Appendix A: Details of FAST post-proceeding based on FFT

Details of portional and total variance estimation for FAST post-proceeding given by [Saltelli 1999]:

For a model $y = f(\mathbf{x}) = (x_1, x_2, \dots, x_n)$ whose inputs vary in a unit hyper cube $K^n = (\mathbf{x} | 0 \leq x_i \leq 1; i = 1, 2, \dots, n)$ with their pdf $P(\mathbf{x}) = P(x_1, x_2, \dots, x_n)$. The fomula of direct calculation of the r th moment of y is:

$$\langle y^{(r)} \rangle = \int_{K^n} f^r(x_1, x_2, \dots, x_n) P(x_1, x_2, \dots, x_n) d\mathbf{x}. \quad (\text{A.1})$$

Based on $P(\mathbf{x})$, the sampling curves of each input x_i can be written in the form of:

$$x_i(s) = G_i(\sin \omega_i s), \quad i = 1, 2, \dots, n, \quad (\text{A.2})$$

where s is a scalar varying over $-\infty < s < +\infty$, and G_i is a transformation function corresponding to the pdf of x_i . And the most important parameter is ω_i which donates different periodicity to input variables. Under the strict condition of non-interference:

$$\sum_{i=1}^n r_i \omega_i \neq 0, \quad -\infty < r_i < +\infty, r_i = \text{integer}. \quad (\text{A.3})$$

It means that none of these frequency can be obtained as linear combination of others, and thus these searching curves can fullfill the whole sampling space. Under this condition, the ergodic theorem (Weyl 1938) indicates that:

$$\langle y^{(r)} \rangle \equiv \bar{y}^{(r)} = \lim_{T \rightarrow \infty} \frac{1}{2T} \int_{-T}^T f^r(x_1(s), x_2(s), \dots, x_n(s)) ds. \quad (\text{A.4})$$

Thus the variance D of the model can be obtained by:

$$D = \langle y_{(2)} \rangle - \langle y^{(1)} \rangle^2 \equiv \bar{y}^{(2)} - (\bar{y}^{(1)})^2. \quad (\text{A.5})$$

Regarding to Equation A.2, with ω_i as positive integers, we can take 2π as the value of T . Noting $f(x_1(s), x_2(s), \dots, x_n(s))$ as $f(s)$, Equations A.4 and A.5 become:

$$\bar{y}^r = \frac{1}{2\pi} \int_{-\pi}^{\pi} f^r(s) ds, \quad (\text{A.6})$$

and

$$\hat{D} = \frac{1}{2\pi} \int_{-\pi}^{\pi} f^2(s) ds - \left[\frac{1}{2\pi} \int_{-\pi}^{\pi} f(s) ds \right]^2. \quad (\text{A.7})$$

Then $f(s)$ can be expanded in Fourier series:

$$y = f(s) = \sum_{j=-\infty}^{+\infty} \{A_j \cos js + B_j \sin js\}, \quad (\text{A.8})$$

where the Fourier coefficients A_j and B_j are defined as:

$$A_j = \frac{1}{2\pi} \int_{-\pi}^{\pi} f(s) \cos js ds, B_j = \frac{1}{2\pi} \int_{-\pi}^{\pi} f(s) \sin js ds, \quad (\text{A.9})$$

over the domain of integer frequencies $j \in \mathcal{Z} = \{-\infty, \dots, -1, 0, 1, \dots, +\infty\}$. The spectrum of each frequency is thus defined as $\Lambda_j = A_j^2 + B_j^2$ with $j \in \mathcal{Z}$. Based on their definitions, the Fourier coefficients and the spectrum have following properties: $A_{-j} = A_j, B_{-j} = -B_j, \Lambda_{-j} = \Lambda_j$. By evaluating the spectrum for the harmonic frequencies $p\omega_i$, the portional variance D_i corresponding to the input x_i can then be estimated:

$$\hat{D}_i = \sum_{p \in \mathcal{Z}'} \Lambda_{p\omega_i} = 2 \sum_{p=1}^{+\infty} \Lambda_{p\omega_i}, \quad (\text{A.10})$$

where $\mathcal{Z}' = \mathcal{Z} - \{0\}$. By summing up all the $\Lambda_j, j \in \mathcal{Z}'$, the total variance can also be estimated:

$$\hat{D} = \sum_{j \in \mathcal{Z}'} \Lambda_j = 2 \sum_{j=1}^{+\infty} \Lambda_j. \quad (\text{A.11})$$

Formulas A.7 and A.11 provide the same quantity based on Parseval's theorem:

$$\sum_{j \in \mathcal{Z}} \Lambda_j = \frac{1}{2\pi} \int_{-\pi}^{\pi} f^2(s) ds = \bar{y}^{(2)}. \quad (\text{A.12})$$

S_i , given by \hat{D}_i / \hat{D} , is the first-order sensitivity index that estimates the main portion of uncertainty on y explained by the input x_i .

Appendix B: Dataset reordering procedure for correlation design in FAST-pe algorithm

A brief process of sampling re-ordering to generate correlation for the sampling curves of multiple units in FAST-pe algorithm.

Taking the mathematical model of $y = f(x_1, x_2, \dots, x_n)$, $\mathbf{x}_i = [x_i^1, x_i^2, \dots, x_i^u]$, $1 \leq i \leq n$, in this model u indicates the number of similar units in this multi-units system and n indicates the number of input variables for each unit. For the execution of FAST-pe algorithm, multiple sampling matrices are generated for each of these units, noted as $\{\mathbf{X}^1, \mathbf{X}^2, \dots, \mathbf{X}^u\}$, the matrices are in this form:

$$\mathbf{X}^j = \begin{bmatrix} x_1^j(1) & x_2^j(1) & \cdots & x_n^j(1) \\ x_1^j(2) & x_2^j(2) & \cdots & x_n^j(2) \\ \vdots & \vdots & \ddots & \vdots \\ x_1^j(m) & x_2^j(m) & \cdots & x_n^j(m) \end{bmatrix}, \quad 1 \leq j \leq u, \quad (\text{B.1})$$

in which m represents the number of samples for model evaluation. In the sampling matrix, the values of each column are noted as $\mathbf{x}_i^j = [x_i^j(1), x_i^j(2), \dots, x_i^j(m)]^T$, representing the actual periodical sampling datasets for the i -th input of the j -th unit. Based on Appendix A, all these sampling vectors are generated periodic where all the vectors of the i -th input are donated with the same frequency ω_i . For example, \mathbf{x}_1^2 and \mathbf{x}_1^3 are both periodically sampled with the characteristic frequency of 11Hz and with the same marginal distribution profile, but having different original phase, as shown in Figure 5.2 of Chapter 5.

Iman's transform gives an matrix elements re-ordering process of constructing a new matrix with a given correlation matrix \mathbf{C} , noted as:

$$\mathbf{X}^{j(\mathbf{C})} = \text{IMAN}^j(\mathbf{X}^j, \mathbf{C}), \quad \text{corr}(\mathbf{X}^{j(\mathbf{C})}) \approx \mathbf{C}. \quad (\text{B.2})$$

For the expression conveniency, the correlation matrix is set to \mathbf{C} as default in this appendix and Equation B.2 can be shortened as $\mathbf{X}^{j(\mathbf{C})} = \text{IMAN}^j(\mathbf{X}^j)$. Similarly, the vector re-ordering process can be noted as:

$$\mathbf{x}_i^{j(\mathbf{C})} = \text{IMAN}_i^j(\mathbf{x}_i^j). \quad (\text{B.3})$$

Well known that Iman's transform makes the re-ordering based on the rank of real value array elements, where the function $\text{rank}(\cdot)$ gives the position of each elements in a row or column vector when reordering them in ascendent order, which means 1 for the minimum and the biggest integer, notably the number of elements in the vector, for the maximum element. For example:

$$[2, 4, 3, 1] = \text{rank}([-1, 3, 2, -2.2]).$$

Take \mathbf{I} as the identical rank operator in column vector, where $\mathbf{I}_m = [1, 2, \dots, m]^T$. Thus there is a relation between \mathbf{x}_i^j and its rank:

$$\mathbf{x}_i^j \equiv \mathbf{I}_m[\text{rank}(\mathbf{x}_i^j)]. \quad (\text{B.4})$$

As m is a constant, the vector \mathbf{I}_m will be noted as \mathbf{I} and the rank vector $\text{rank}(\mathbf{x}_i^j)$ will be noted as \mathbf{r}_i^j . With the definition of rank function and vector reordering operation clarified, Equation B.3 can be rewritten in the way of:

$$\mathbf{x}_i^{j(\text{C})} = \mathbf{x}_i^j[\mathbf{IMAN}_i^j]. \quad (\text{B.5})$$

According to the post-proceeding design of FAST-C, after model evaluations, the output vector $\mathbf{y} = [y(1), y(2), \dots, y(m)]$ will be reordered:

$$\mathbf{y}_i = \mathbf{y}[\mathbf{IMAN}_i^{1'}], \quad (\text{B.6})$$

so that \mathbf{y}_i will contain the periodical information of \mathbf{x}_i^j which got eliminated after the operation of Equation B.3. The reverse vector $\mathbf{IMAN}_i^{j'}$ of \mathbf{IMAN}_i^j is defined as:

$$\mathbf{IMAN}_i^j[\mathbf{IMAN}_i^{j'}] \equiv \mathbf{IMAN}_i^{j'}[\mathbf{IMAN}_i^j] \equiv \mathbf{I}. \quad (\text{B.7})$$

By this post process, the periodicity of input x_i^1 is restored and can thus be refelcted in FFT results of \mathbf{y}_i , but for other units of the system, the periodicity of $x_i^j, 2 \leq j \leq u$, are not restored as all the units used different re-ordering operators \mathbf{IMAN}_i^j .

In order to make the FFT post-process valide for all the input datasets, the solution is to find a second re-ordering vector \mathbf{tbl}_i for all the sampling curves so that :

$$\mathbf{x}_i^j = \tilde{\mathbf{x}}_i^j[\mathbf{IMAN}_i^1], \text{ with } \tilde{\mathbf{x}}_i^j = \mathbf{x}_i^{j(\text{C})}[\mathbf{tbl}_i]. \quad (\text{B.8})$$

Taking the equations B.4 and B.5 into the Fomula B.8, we can obtain:

$$\mathbf{I} = \mathbf{IMAN}_i^j[\mathbf{tbl}_i[\mathbf{IMAN}_i^1]]. \quad (\text{B.9})$$

Thus with the definition of Equation B.7:

$$\mathbf{tbl}_i[\mathbf{IMAN}_i^1] = \mathbf{IMAN}_i^{j'}, \quad (\text{B.10})$$

so finally the secondary re-ordring vector for periodicity correction can be obtained as:

$$\mathbf{tbl}_i = \mathbf{IMAN}_i^{j'}[\mathbf{IMAN}_i^{1'}], \quad (\text{B.11})$$

with both **IMAN** vectors directly accessible from Iman's transform.

It should be mentioned that the restorage of periodicity using \mathbf{tbl}_i re-ordering process only works for the estimation of i -th input's sensitivity index, thus for the other inputs, the whole process of 're-ordering, evaluation, post-proceeding and FFT estimation' must be repeated completely.

Bibliography

- [Allard 2009] Jean Allard and Noureddine Atalla. Propagation of sound in porous media: modelling sound absorbing materials 2e. John Wiley & Sons, 2009. (Cited on pages 11 and 26.)
- [Amico 2013] R D Amico, A Pratellesi, N Baldanzini and M Pierini. *Reformulation of the Stochastic BEM to improve the computational efficiency in the prediction of the vibro-acoustic behaviour of structures with uncertainties*. Journal of Sound and Vibration, vol. 332, no. 9, pages 2132–2148, 2013. (Cited on page 30.)
- [Baho 2016] O. Baho, Z. Zergoune, M. Ichchou, B. Harras, R. Benamar, B. Troclet and O. Bareille. *On global bending-shear core transition effects for the vibroacoustic of sandwich structures: Analytical and numerical investigations*. Composite Structures, vol. 154, pages 453–463, 2016. (Cited on pages 31, 33 and 40.)
- [Belgiu 2016] Mariana Belgiu and Lucian Draguc. *Random forest in remote sensing: A review of applications and future directions*. ISPRS Journal of Photogrammetry and Remote Sensing, vol. 114, pages 24–31, 2016. (Cited on page 62.)
- [Bellman 1957] R. Bellman and Rand Corporation. Dynamic programming. Rand Corporation research study. Princeton University Press, 1957. (Cited on page 62.)
- [Biot 1956] Maurice A Biot. *Theory of propagation of elastic waves in a fluid-saturated porous solid. II. Higher frequency range*. The Journal of the Acoustical Society of America, vol. 28, no. 2, pages 179–191, 1956. (Cited on page 11.)
- [Borgonovo 2003] Emanuele Borgonovo, George E Apostolakis, Stefano Tarantola and Andrea Saltelli. *Comparison of global sensitivity analysis techniques and importance measures in PSA*. Reliability Engineering & System Safety, vol. 79, no. 2, pages 175–185, 2003. (Cited on pages 9 and 62.)
- [Breiman 2001] L E O Breiman. *Random Forests*. Machine Learning, vol. 45, pages 5–32, 2001. (Cited on page 63.)
- [Chai 2017] W Chai, J-L Christen, A-M Zine and M Ichchou. *Sensitivity analysis of a sound absorption model with correlated inputs*. Journal of Sound and Vibration, vol. 394, pages 75–89, 2017. (Cited on pages 30 and 39.)
- [Chastaing 2012] Gaelle Chastaing, Fabrice Gamboa and Clementine Prieur. *Generalized hoeffding-sobol decomposition for dependent variables-application to sensitivity analysis*. Electronic Journal of Statistics, vol. 6, pages 2420–2448, 2012. (Cited on pages 9 and 10.)

- [Christen 2016] Jean-Loup Christen, Mohamed Ichchou, Olivier Bareille and Bernard Troclet. *Global sensitivity analysis of analytical vibroacoustic transmission models*. Journal of Sound and Vibration, vol. 368, pages 121–134, 2016. (Cited on pages 13, 30, 33, 40 and 62.)
- [Christen 2017] Jean-Loup Christen, Mohamed Ichchou, Bernard Troclet, Olivier Bareille and Morvan Ouisse. *Global sensitivity analysis and uncertainties in SEA models of vibroacoustic systems*. Mechanical Systems and Signal Processing, vol. 90, pages 365–377, 2017. (Cited on page 62.)
- [Cicirello 2013] Alice Cicirello and Robin S Langley. *The vibro-acoustic analysis of built-up systems using a hybrid method with parametric and non-parametric uncertainties*. Journal of Sound and Vibration, vol. 332, no. 9, pages 2165–2178, 2013. (Cited on page 30.)
- [Clarkson 1983] B. L. Clarkson and M. F. Ranky. *Modal density of honeycomb plates*. Journal of Sound and Vibration, vol. 91, pages 103–118, 1983. (Cited on pages 31 and 32.)
- [Cukier 1973] RI Cukier, CM Fortuin, Kurt E Shuler, AG Petschek and JH Schaibly. *Study of the sensitivity of coupled reaction systems to uncertainties in rate coefficients. I Theory*. The Journal of Chemical Physics, vol. 59, no. 8, pages 3873–3878, 1973. (Cited on pages xiii, 8, 9 and 62.)
- [Doutres 2011] Olivier Doutres, Nouredine Atalla and Kevin Dong. *Effect of the microstructure closed pore content on the acoustic behavior of polyurethane foams*. Journal of Applied Physics, vol. 110, no. 6, page 064901, 2011. (Cited on pages 13, 15 and 19.)
- [Doutres 2014] Olivier Doutres, Morvan Ouisse, Nouredine Atalla and Mohamed Ichchou. *Impact of the irregular microgeometry of polyurethane foam on the macroscopic acoustic behavior predicted by a unit-cell model*. The Journal of the Acoustical Society of America, vol. 136, no. 4, pages 1666–1681, 2014. (Cited on pages 20, 21, 24 and 30.)
- [Doutres 2015] Olivier Doutres, Morvan Ouisse, Nouredine Atalla and Mohamed Ichchou. *Unit-cell variability and micro-macro modeling of polyurethane acoustic foams*. In Euronoise 2015, pages 2467–2472, 2015. (Cited on page 24.)
- [Ferretti 2016] Federico Ferretti, Andrea Saltelli and Stefano Tarantola. *Trends in sensitivity analysis practice in the last decade*. Science of the Total Environment, vol. 568, pages 666–670, 2016. (Cited on pages xiii and 6.)
- [Fisher 1918] Ronald Fisher. *Studies in Corp Variation. I. An examination of the yield of dressed grain from Broadbalk*. Journal of Agricultural Science, vol. 11, no. 2, pages 107–135, 1918. (Cited on page 6.)

- [Funtowicz 1990] Silvio O Funtowicz and Jerome R Ravetz. Uncertainty and quality in science for policy, volume 15. Springer Science & Business Media, 1990. (Cited on pages [xiii](#) and [xix](#).)
- [Gaspar 2014] Ana Gaspar and Fernando Lopez-caballero. *Methodology for a probabilistic analysis of an RCC gravity dam construction. Modelling of temperature, hydration degree and ageing degree fields*. Engineering Structures, vol. 65, pages 99–110, 2014. (Cited on pages [39](#) and [62](#).)
- [Gatelli 2009] Debora Gatelli, Sergei Kucherenko, Marco Ratto and Stefano Tarantola. *Calculating first-order sensitivity measures: A benchmark of some recent methodologies*. Reliability Engineering & System Safety, vol. 94, no. 7, pages 1212–1219, 2009. (Cited on page [8](#).)
- [Gibson 1997] L. J. Gibson and M. F. Ashby. Cellular solids: structure and properties. Cambridge university press, 1997. (Cited on pages [11](#) and [34](#).)
- [Guillaumie 2015] L. Guillaumie. *Vibroacoustic flexural properties of symmetric honeycomb sandwich panels with composite faces*. Journal of Sound and Vibration, vol. 343, pages 71–103, 2015. (Cited on pages [31](#) and [33](#).)
- [Iman 1982] Ronald L Iman and WJ Conover. *A distribution-free approach to inducing rank correlation among input variables*. Communications in Statistics-Simulation and Computation, vol. 11, no. 3, pages 311–334, 1982. (Cited on pages [17](#), [37](#) and [39](#).)
- [Jacques 2006] Julien Jacques, Christian Lavergne and Nicolas Devictor. *Sensitivity analysis in presence of model uncertainty and correlated inputs*. Reliability Engineering & System Safety, vol. 91, no. 10, pages 1126–1134, 2006. (Cited on page [9](#).)
- [Jia 2016] Jianhua Jia, Zi Liu, Xuan Xiao, Bingxiang Liu and Kuo-Chen Chou. *pSuc-Lys: predict lysine succinylation sites in proteins with PseAAC and ensemble random forest approach*. Journal of theoretical biology, vol. 394, pages 223–230, 2016. (Cited on page [62](#).)
- [Khan 2017] Alaptagin Khan, Hannah McCormack, Elizabeth Bolger, Cynthia McGreenery and Martin Teicher. *Childhood Maltreatment and Normal Adult Personality Traits: Evidence for Developmental Sensitive Periods of Exposure*. Biological Psychiatry, vol. 81, no. 10, pages S197–S198, 2017. (Cited on page [62](#).)
- [Kucherenko 2012] Sergei Kucherenko, Stefano Tarantola and Paola Annoni. *Estimation of global sensitivity indices for models with dependent variables*. Computer Physics Communications, vol. 183, no. 4, pages 937–946, 2012. (Cited on pages [10](#) and [37](#).)

- [Malek 2015] S. Malek and L. Gibson. *Effective elastic properties of periodic hexagonal honeycombs*. *Mechanics of Materials*, vol. 91, no. P1, pages 226–240, 2015. (Cited on page 34.)
- [Mara 2015] Thierry A Mara, Stefano Tarantola and Paola Annoni. *Non-parametric methods for global sensitivity analysis of model output with dependent inputs*. *Environmental Modelling & Software*, vol. 72, pages 173–183, 2015. (Cited on page 10.)
- [McKay 1997] Michael D McKay. *Nonparametric variance-based methods of assessing uncertainty importance*. *Reliability engineering & system safety*, vol. 57, no. 3, pages 267–279, 1997. (Cited on page 10.)
- [McRae 1982] Gregory J McRae, James W Tilden and John H Seinfeld. *Global sensitivity analysis - a computational implementation of the Fourier amplitude sensitivity test (FAST)*. *Computers & Chemical Engineering*, vol. 6, no. 1, pages 15–25, 1982. (Cited on page 8.)
- [Mead 1969] D. J. Mead and S. Markus. *The forced vibration of a three-layer, damped sandwich beam with arbitrary boundary conditions*. *Journal of Sound and Vibration*, vol. 10, pages 163–175, 1969. (Cited on pages 11, 31, 32 and 65.)
- [Mead 1972] D. J. Mead. *The damping properties of elastically supported sandwich plates*. *Journal of Sound and Vibration*, vol. 24, no. 3, pages 275–295, 1972. (Cited on page 32.)
- [Morizet 2016] Nicolas Morizet, Nathalie Godin, J Tang, E Maillet, M Fregonese and B Normand. *Classification of acoustic emission signals using wavelets and Random Forests: Application to localized corrosion*. *Mechanical Systems and Signal Processing*, vol. 70, pages 1026–1037, 2016. (Cited on page 62.)
- [Narayanan 1982] S. Narayanan and R. L. Shanbhag. *Sound transmission through a damped sandwich panel*. *Journal of Sound and Vibration*, vol. 80, no. 3, pages 315–327, 1982. (Cited on page 32.)
- [Ohayon 2014] Roger Ohayon and Christian Soize. *Advanced computational vibroacoustics: reduced-order models and uncertainty quantification*. Cambridge University Press, 2014. (Cited on page 30.)
- [Ouisse 2012] Morvan Ouisse, Mohamed Ichchou, Slaheddine Chedly and Manuel Collet. *On the sensitivity analysis of porous material models*. *Journal of Sound and Vibration*, vol. 331, no. 24, pages 5292–5308, 2012. (Cited on pages 13, 20, 22 and 30.)
- [Pacala 1996] Stephen W Pacala, Charles D Canham, John Saponara, John A Silander Jr, Richard K Kobe and Eric Ribbens. *Forest models defined by field*

- measurements: estimation, error analysis and dynamics*. Ecological monographs, vol. 66, no. 1, pages 1–43, 1996. (Cited on page 9.)
- [Renji 2005] K. Renji. *Sound transmission loss of unbounded panels in bending vibration considering transverse shear deformation*. Journal of Sound and Vibration, vol. 283, no. 1-2, pages 478–486, 2005. (Cited on pages 11, 31 and 33.)
- [Reynders 2014] Edwin Reynders. *Parametric uncertainty quantification of sound insulation values*. The Journal of the Acoustical Society of America, vol. 135, pages 1907–1918, 2014. (Cited on page 30.)
- [Saltelli 1998] Andrea Saltelli and Ricardo Bolado. *An alternative way to compute Fourier amplitude sensitivity test (FAST)*. Computational Statistics & Data Analysis, vol. 26, no. 4, pages 445–460, 1998. (Cited on page 9.)
- [Saltelli 1999] Andrea Saltelli, Stefano Tarantola and KP-S Chan. *A quantitative model-independent method for global sensitivity analysis of model output*. Technometrics, vol. 41, no. 1, pages 39–56, 1999. (Cited on page 105.)
- [Saltelli 2001] Andrea Saltelli, Marco Ratto and Stefano Tarantola. *Model-free importance indicators for dependent input*. In International symposium on sensitivity analysis of model output, pages 21–25, 2001. (Cited on page 10.)
- [Saltelli 2004] Andrea Saltelli, Stefano Tarantola, Francesca Campolongo and Marco Ratto. *Sensitivity analysis in practice: a guide to assessing scientific models*. John Wiley & Sons, 2004. (Cited on page 10.)
- [Saltelli 2005] Andrea Saltelli, Marco Ratto, Stefano Tarantola and Francesca Campolongo. *Sensitivity analysis for chemical models*. Chemical reviews, vol. 105, no. 7, pages 2811–2828, 2005. (Cited on page 62.)
- [Saltelli 2008] Andrea Saltelli, Marco Ratto, Terry Andres, Francesca Campolongo, Jessica Cariboni, Debora Gatelli, Michaela Saisana and Stefano Tarantola. *Global sensitivity analysis: the primer*. John Wiley & Sons, 2008. (Cited on pages xiii and 6.)
- [Saltelli 2010] Andrea Saltelli, Paola Annoni, Ivano Azzini, Francesca Campolongo, Marco Ratto and Stefano Tarantola. *Variance based sensitivity analysis of model output. Design and estimator for the total sensitivity index*. Computer Physics Communications, vol. 181, no. 2, pages 259–270, 2010. (Cited on page 10.)
- [Sobol’ 1990] Il’ya Meerovich Sobol’. *On sensitivity estimation for nonlinear mathematical models*. Matematicheskoe Modelirovanie, vol. 2, no. 1, pages 112–118, 1990. (Cited on page 7.)

- [Sobol 2001] Ilya M Sobol. *Global sensitivity indices for nonlinear mathematical models and their Monte Carlo estimates*. Mathematics and computers in simulation, vol. 55, no. 1, pages 271–280, 2001. (Cited on page 62.)
- [Wang 2015] Zhaoli Wang, Chengguang Lai, Xiaohong Chen, Bing Yang, Shiwei Zhao and Xiaoyan Bai. *Flood hazard risk assessment model based on random forest*. Journal of Hydrology, vol. 527, pages 1130–1141, 2015. (Cited on pages xv and 63.)
- [Xu 2008] Chonggang Xu and George Zdzislaw Gertner. *A general first-order global sensitivity analysis method*. Reliability Engineering & System Safety, vol. 93, no. 7, pages 1060–1071, 2008. (Cited on pages 14 and 17.)
- [Yang 2017] Yi Yang, Brian R Mace, Michael J Kingan, Yi Yang, Brian R Mace and Michael J Kingan. *Finite element method Prediction of sound transmission through , and radiation from , panels using a wave and finite element method a).* The Journal of the Acoustical Society of America, vol. 141, pages 2452–2460, 2017. (Cited on pages 11 and 66.)
- [Zhang 2015] Q. Zhang, X. Yang, P. Li, G. Huang, S. Feng, C. Shen, B. Han, X. Zhang, F. Jin, F. Xu and T. Lu. *Bioinspired engineering of honeycomb structure - Using nature to inspire human innovation*. Progress in Materials Science, vol. 74, pages 332–400, 2015. (Cited on page 65.)
- [Zheng 2015] Chaolei Zheng and Quan Wang. *Spatiotemporal pattern of the global sensitivity of the reference evapotranspiration to climatic variables in recent five decades over China*. Stochastic Environmental Research and Risk Assessment, vol. 29, no. 8, pages 1937–1947, 2015. (Cited on pages 39 and 62.)
- [Zielinski 2015] TG Zielinski. *Microstructure generation for design of sound absorbing foams with spherical pores*. The Journal of the Acoustical Society of America, vol. 137, no. 4, pages 1790–1801, 2015. (Cited on page 14.)